공학박사학위논문

차량 조종성과 횡방향 안정성 향상을 위한 타이어-노면 정보 독립적 후륜 조향 제어

Rear-Wheel Steering Control for Vehicle Maneuverability and Lateral Stability without Tire-Road Information

2021년 2월

서울대학교 대학원

기계항공공학부

박 관 우

차량 조종성과 횡방향 안정성 향상을 위한 타이어-노면 정보 독립적 후륜 조향 제어

Rear-Wheel Steering Control for Vehicle Maneuverability and Lateral Stability without Tire-Road Information

지도교수 이 경 수

이 논문을 공학박사 학위논문으로 제출함

2020 년 10 월

서울대학교 대학원
기계항공공학부
박 관 우

박관우의 공학박사 학위논문을 인준함

2020 년 12 월

위 원 장 : 차 석 원 (인)

부위원장 : 이 경 수 (인)

위 원 : 이 동 준 (인)

위 원 : 박 용 래 (인)

위 원 : 임 성 진 (인)

Abstract

Rear-Wheel Steering Control for Vehicle Maneuverability and Lateral Stability without Tire-Road Information

PARK Kwanwoo

Department of Mechanical and Aerospace Engineering

The Graduate School

Seoul National University

Active steering systems have been developed over the past few decades to improve vehicle handling performance. Through the development from the previous mechanical system to the enhanced electronic control system, the rear-wheel steering (RWS) system, which can significantly improve the maneuverability and stability, has recently come into the spotlight. Steering the rear wheels offers control of rear lateral tire forces, and RWS systems offer great advantages in various maneuvers. At low speeds, RWS is controlled in the opposite direction to the front-wheels for increasing the vehicle maneuverability and agility. At high speeds, RWS is controlled in the same direction to the front-wheels for improved vehicle lateral stability. The most widely used control technique is the model-based controller to track the desired motion of reference models. However, the performance can deteriorate if the information on tires and vehicle models are not accurate.

This paper presents a rear-wheel steering control algorithm to enhance vehicle handling performance without prior knowledge of tire characteristics. RWS system is a chassis control module that can effectively improve vehicle maneuverability and lateral stability. Since the tire-road friction coefficient is difficult to obtain in real world application, the proposed RWS control

algorithm is designed so that it can be implemented without any tire-road information.

The proposed RWS control algorithm consists of steady-state and transient control inputs. The steady-state control input is proportional to the driver's steering input for achieving the desired yaw rate gain. The desired yaw rate gain is obtained through an offline numerical optimization that is aimed to minimize the vehicle sideslip angle, which is evaluated the most effective active steering system in terms of handling performance and actuator cost. The transient control input consists of feedforward and feedback control inputs. The feedforward input is designed to improve transient responses of the yaw rate and lateral acceleration. Computer simulation studies have shown that a trade-off relationship between overshoot and response time exists when the RWS control input is a sum of the steady-state and feedforward inputs. To compromise this conflict, a feedback input has been designed. The overshoot can be significantly reduced while the response time is slightly changed via the feedback input.

The proposed algorithm has been investigated via computer simulations. The simulation has been conducted for step steer and sine with dwell scenarios under various road friction conditions. The performance of RWS vehicle was evaluated using objective indices. Simulation results of the step steer scenario show that the proposed algorithm enhances vehicle handling performance and emulates the performance of the optimal control. It is also validated that the proposed RWS algorithm, which is tuned based on the optimal control of step steer, enhances vehicle lateral stability in the sine with dwell test scenario under low friction road condition.

Keywords: Rear-Wheel Steering Control, Vehicle Handling, Maneuverability, Agility, Lateral Stability, Lateral Transient Response, Offline Numerical Optimization, Performance Evaluation

Student Number: 2017-35813

Contents

List of Figures

Chapter 1

Introduction

1.1. Background and Motivation

Rear-wheel steering (RWS) control has been developed for decades with the aim of improving vehicle handling performance and stability. With the vigorous development of high-performance vehicles recently, new chassis control modules such as rear-wheel steering and torque vectoring have begun to be offered as options. Among them, rear-wheel steering is known as the most effective single control module in improving the handling performance and lateral stability of vehicles (Nah & Yim, 2019; Yim, 2020; Yim, Kim, & Yun, 2016). In the 1970-80s, there have been attempts to lead the market trend with rear-wheel steering. Rear-wheel steering module was developed and mounted on passenger cars such as Nissan Sky-line and Hyundai Sonata. However, the control module was deemed to be too much for commercialization at that time in terms of actuator costs, and then it was subsequently buried. Today, with the

advancement of the vehicle's electronic systems, the rear-wheel steering has begun to be re-spotlighted again.

Steering the rear wheels offers control of rear lateral tire forces, and RWS systems offer great advantages in urban driving situations and on the highway. In the urban driving situations such as cornering in a narrow alley, the driver's burden to exert steering wheel angle can be reduced when the curvature changes suddenly because the RWS system increases the vehicle's yaw rate gain by steering the rear wheels in the opposite direction to the front wheels. In the highway driving situations, the vehicle's lateral stability can be improved throughout the driving range from mild handling to limit handling maneuvers because the RWS system decreases yaw rate gain by rear wheels in the same direction as the front wheels.

Such rear-wheel steering system, which can greatly improve vehicle maneuverability and lateral stability, has been developed with the aim of being mounted on high-performance vehicles (hyper cars), large sedans and Sport Utility Vehicles (SUV). Actually, many automakers are developing rear-wheel steering systems and selling the vehicles equipped with them.

Audi calls it "All-Wheel Steering" system (Wimmer, Meurle, Sacher, & Siedersberger, 2015), and the steering system with an electric spindle drive turns the rear wheels inward by as much as 5 degrees depending on the situation. This is fitted in high-performance SUV models such as Audi Q7 and RS Q8.

Lexus calls it "Lexus Dynamic Handling (LDH)" system as a products name, and technically called "Dynamic Rear Steering (DRS)" (Akita, 2019; Zhang,

Khajepour, & Goodarzi, 2017). It is an independent system that makes handling and agility sharper. So, it is mounted on top-spec vehicles of Lexus, GS range.

Mercedes-Benz calls it “Rear-Axle Steering” and is scheduled to be fitted in its S-Class vehicles in 2021. Depending on the speed and the steering angle, the rear wheels are turned in the same or the opposite direction as the front wheels (Steffen Wagner, Weiskircher, Ammon, & Prokop, 2018). In the S-Class, the full steering angle of ten degrees is especially used during parking maneuvers. The turning circle radius of long wheelbase vehicles can be reduced by up to 2 meters. The environmental data of the vehicle sensors (radar, camera, ultrasonic) are used to adapt the maximum angle to the relevant situation.

In Porsche, it is called “Rear-Axle Steering” system too, and it is steered in the opposite direction to the front wheels up to 50kph, and it is steered in the same direction at higher speeds. This system is aimed at changing the handling characteristics through the effect of reducing/increasing the virtual wheelbase of vehicles. This system is available on Porsche 911 GTS models (Harrer, Görich, Reuter, & Wahl, 2013; Schäfer, Wahl, & Harrer, 2012).

In BMW, called “Integral Active Steering”, the rear wheels are steering within a range of up to 3 degrees through the electric motor in the steering column (Treichel, 2016). The precise angle of lock is determined by a control device after measuring factors like speed, steering wheel angle, etc. As with the preceding companies, the direction of steering is determined by vehicle speeds. Especially when changing lanes at high speeds, the vehicle practically ‘glides’ in an even sideways motion, which extremely comfortable for all the vehicle’s occupants and especially so for those in the rear.

Hyundai Motor Group is currently developing a rear-wheel steering control module and is in the process of developing and mass-producing electronic gear train and electronic limited-slip differential (e-LSD) systems to enable stable operation. This new component will be applied to the Genesis GV 80 and new G80 sports.

1.2. Previous Researches

The purposes of RWS control broadly fall into two categories: 1) minimize vehicle side slip angle, and 2) track the desired yaw rate. Early rear-wheel steering control methods have been used to enhance vehicle stability and maneuverability by regulating the side slip angle (Abe, 1999; Eguchi et al., 1989; Furukawa, Yuhara, Sano, Takeda, & Matsushita, 1989; S.-H. Lee, Lee, Ha, & Han, 1999; Nagai, Hirano, & Yamanaka, 1997). Nagai et al. designed a state feedback controller to maintain the zero-side slip angle by constructing the model-following RWS control (Nagai et al., 1997). Lee et al. proposed a control strategy, i.e., 'four-wheel independent steering.' (S.-H. Lee et al., 1999) This control strategy aimed to reduce not only the side slip angle but also the actuating power. Eguchi et al. considered both vehicle lateral dynamics and suspension dynamics such as roll steer and compliance steer to make the side slip angle equal to zero (Eguchi et al., 1989).

A number of studies have been proposed to enhance the vehicle's stability and maneuverability by tracking the output of the reference vehicle model. Lv et al. proposed a yaw rate tracking four-wheel steering (4WS) by means of multi-objective H optimal control (Lv, Chen, & Li, 2004). This proposed algorithm accomplishes desired handling characteristics with fewer state variables than conventional model-following control methods. Wagner et al. performed and compared the performance of active steering controllers through

the optimization (S Wagner, Schilling, Braun, & Prokop, 2017). Concretely, Wagner et al. evaluated front-wheel steering (FWS), rear-wheel steering (RWS), and all-wheel steering (AWS) for the tracking performance of the desired vehicle yaw rate and lateral speed. They concluded that RWS control shows the best performance in terms of actuator costs and vehicle lateral behavior. However, these model-based methods need to pinpoint parameters between the tire and road surface as well as the vehicle parameters.

Most model-based RWS control methods utilize a model that consists of vehicle lateral dynamics and tire dynamics. Based on such models, the RWS or 4WS control inputs are obtained by assuming that the correct vehicle model and parameters are known. Therefore, the performance of control methods can deteriorate when the uncertainties of the vehicle modeling and parameters are presented. For instance, when the driver negotiates a corner with high lateral acceleration conditions, the tire characteristics enter the nonlinear region. In this case, there are differences between nominal and actual parameters, and such parameter errors deteriorate the algorithm's performance (Abe, 1999; Ogaji, Sampath, Singh, & Probert, 2002; Rissanen, 1966; Zarco & Exposito, 2000). Therefore, practitioners often have laborious tasks such as adjusting control gains and parameters. To resolve this inconvenience, there are some methods to design a robust controller in consideration of uncertainties. Russell and Gerdes proposed a state feedback controller to track a reference model and demonstrated stability and robustness to the model uncertainties (Russell & Gerdes, 2015). Akar proposed a sliding mode controller to track both zero-side slip angle and reference yaw rate, which showed robustness against parameter

variations (Akar, 2006). Yim proposed a coordinated control with ESC and active steering modules to track reference model by sliding mode control (Yim, 2015).

In contrast to the model-based control methods that are widely researched, many car manufacturers have adopted a simple proportional RWS control algorithm for application in mass production process (Sano, Furukawa, & Shiraishi, 1986). In the proportional RWS control, the proportional gain is the ratio of the rear-wheel steering angle to the front wheel steering angle as a function of vehicle speed. This gain is designed to minimize the steady-state side slip angle. At low speeds, RWS is controlled in the opposite direction (i.e. reverse-phase) to the front wheels for increasing the yaw rate gain while at high speeds RWS is controlled in the same direction (i.e. in-phase) for enhancing the vehicle stability. However, such simple proportional RWS control has some problems via vehicle tests (Bredthauer & Lynch, 2018). Bredthauer and Lynch investigated the simple proportional RWS control with respect to various tire types such as winter tires and racing tires. Many test drivers suggest that unpleasant vehicle behavior could occur with respect to quick steering inputs and rear-wheel steering calibrations for tires. This is because the simple proportional RWS control does not consider the vehicle's transient response. There are more advanced control methods that consider the transient response in RWS control input to resolve this unnatural vehicle lateral behavior. Cho and Kim designed a delayed RWS whereby the time delay between the front-wheel and rear-wheel is extracted from the responses of the optimal 4WS control (Cho & Kim, 1995). Nissan's phase reversal control considers the suspension

characteristics and demonstrated significantly improved vehicle response at high speeds compared to proportional control and first-order delay control (Irie & Kuroki, 1990). However, Nissan's control logic requires tire and suspension parameters, and errors can degrade the performance of the control algorithm.

1.3. Thesis Objectives

This paper proposes a new RWS control design framework that can modify the vehicle handling characteristics using measurable vehicle signals, and, more importantly, without any information from the tire. By first analyzing offline numerical optimization, the optimal rear-wheel steering control input and physical insights of vehicle behavior are obtained. And design rear-wheel steering control inputs by introducing new parameters that can reflect optimal results.

The proposed RWS control law is a sum of steady-state and transient control inputs. The steady-state part of the proposed algorithm is designed to be proportional to the driver's steering wheel angle input. This steady-state input modifies steady-state handling characteristics according to vehicle speeds. At low speeds, RWS is controlled in the opposite direction (reversed-phase) to the front-wheels for increasing the vehicle agility (increase yaw rate gain). At high speeds, RWS is controlled in the same direction (in-phase) to the front-wheels for improved vehicle stability (reduced yaw rate gain). The transient control input adjusts the vehicle's transient response without any information from the tire. To design such transient control input, new vehicle dynamic models and new design parameters are proposed to exclude such tire parameters. Transient responses such as overshoot, rise time, and peak response time are a function of vehicle and tire parameters, and the transient control input can be designed without tire parameters via the proposed control design framework.

1.4. Thesis Outline

This dissertation is structured in the following manner. An overall research flow of the proposed rear-wheel steering algorithm is described in Chapter 2. In Chapter 3, vehicle dynamics with active steering system is described. This chapter consists of 3D full-car modeling for offline numerical optimization and simplified vehicle lateral dynamics for control design. In Chapter 4, Offline numerical optimization is described. The optimal rear-wheel steering control input, which has best performance in both actuator cost and vehicle handling performance, is calculated and evaluated. In Chapter 5, the proposed control design in this paper is introduced. The proposed RWS control algorithm consists of steady-state and transient control inputs. The steady-state control input is proportional to the driver's steering input for achieving the desired yaw rate gain. The transient control input consists of feedforward and feedback control inputs. The feedforward input is designed to improve transient responses of the yaw rate and lateral acceleration. The overshoot can be significantly reduced while the response time is slightly changed via the feedback input. Chapter 6 shows the simulation results for the evaluation of the performance of the proposed algorithm. Then the conclusion with describes the summary and contribution of the proposed RWS control algorithm and future works is presented in Chapter 7.

Chapter 2

Overall Research Flow of the Proposed Rear-Wheel Steering Control Algorithm

With the vigorous development of high-performance vehicles recently, new chassis control modules such as rear-wheel steering and torque vectoring have begun to be offered as options. Among them, rear-wheel steering is known as the most effective single control module in improving the handling performance and lateral stability of vehicles.

This paper analyzes the behavior of vehicles equipped with rear-wheel steering systems to obtain physical insight, and proposes control design that can improve handling performance based on it. Figure 2.1 shows the overall research flow of the proposed rear-wheel steering control algorithm, which is designed based on offline numerical optimization results. The flow in which the

proposed logic is designed as follows: 1) offline numerical optimization; 2) analysis; 3) control logic design; and 4) validation. First of all, offline numerical optimization is made to analyze the optimum rear-wheel steering control input and lateral behavior that can most effectively improve the handling performance based on the full-car model. Based on optimal results, the best handling performance that rear-wheel steering can produce is analyzed to gain physical insight. And based on these, we develop real-time control logic that can emulate the optimal performance. This developed control logic is validated through comparative evaluation with the optimal results. Through this process, the proposed rear-wheel steering control logic is designed.

The proposed rear-wheel steering control logic is designed separately according to the handling characteristics area. That is, the proposed logic is the sum of the steady-state and transient control inputs. The steady-state control input is designed to reflect the vehicle maneuverability (=yaw rate response) of the optimal rear-wheel steering control. The transient control input is designed to improve the transient response of yaw rate and lateral acceleration. In terms of the yaw rate transient response, the aim of controller is to reduce the overshoot and response time. And in terms of lateral acceleration, the aim is to linearly improve the unnatural nonlinear transient response.

The proposed control logic has been evaluated through open-loop test scenarios that did not involve the driver's intention. In addition to overshoot and response time, performance comparison with optimal controller were made through objective indicators such as TB factor and yaw rate gain. It has been confirmed that the proposed logic has greatly improved the vehicle lateral

stability for friction changes and has expanded the stability area through integration with conventional ESC.

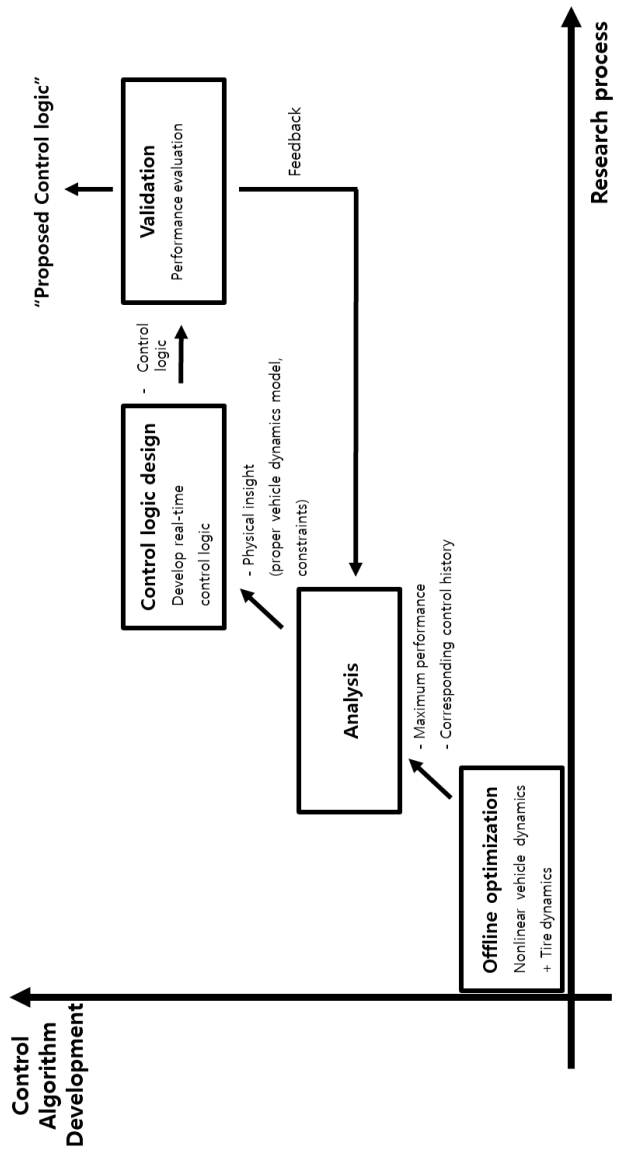

Figure 2.1. Research Flow of the Proposed Rear-Wheel Steering Control Algorithm based on Offline Optimization.

Chapter 3

An Active Steering System Model

Vehicle dynamics model must be defined to analyze how the driver's input and control input affect vehicle handling characteristics and behavior.

Various vehicle models have been proposed and employed for the vehicle control. A kinematic bicycle model describes the lateral motion of a vehicle without considering the external forces. The kinematic model is purely based on geometric relationship. The slip angle at both the front and rear wheel is assumed to be zero. The zero side slip angle assumption is reasonable at low speeds because, the total lateral force from each tire varies quadratically with the vehicle speed for the lateral motion of the vehicle. Typically, it is known that the kinematic model is applicable for the vehicle speed less than $5m/s$ (Rajamani, 2011).

A planar single-track model is the most popular model for the lateral vehicle control in tremendous previous research. There have been diverse variants that varies with the tire model.

However, the tire model parameters are difficult to be identified in practice, because the parameters are unmeasurable directly. Furthermore, the characteristics of the tire is time-varying due to wear, weather, friction coefficient of road, etc. Therefore, the parameters are considered as one of the design parameters in some cases.

In this paper, to analyze the improvement of vehicle handling performance through rear-wheel steer, offline numerical optimization is carried out using the advanced vehicle model (14dof, 3D model) (Setiawan, Safarudin, & Singh, 2009) and non-linear tire model (H. Pacejka & Besselink, 1997; H. B. Pacejka & Bakker, 1992). In addition, the control design phase for actual application is constructed by introducing new design parameters that can adjust vehicle handling characteristics based on planar single-track model (bicycle model).

3.1. 3D Vehicle Model for Offline Optimization

As you can see in Figure 3.1, 14 degree-of-freedom (DOF) Full car model is designed to analyze the handling characteristics of the rear-wheel steering vehicle. This vehicle model includes a nonlinear pacejka tire model. In addition, including the relaxation length tire (RLT) model (Rill, 2006) and the compliance of each wheel, the vehicle behavior is similar to the real vehicle motion.

14 DOF Full car model is applied for the offline numerical optimization.

$$\begin{aligned} I_x \cdot \ddot{\phi} &= M_x - (I_z - I_y) \cdot \dot{\theta} \cdot \dot{\psi} \\ I_y \cdot \ddot{\theta} &= M_y - (I_x - I_z) \cdot \dot{\psi} \cdot \dot{\phi} \\ I_z \cdot \ddot{\psi} &= M_z - (I_y - I_x) \cdot \dot{\phi} \cdot \dot{\theta} \end{aligned} \tag{3.1}$$

$$\begin{aligned} ma_y = \quad & \left(F_{y,fl} + F_{y,fr}\right) \cdot \cos\left(\delta_f\right) + \left(F_{x,fl} + F_{x,fr}\right) \cdot \sin\left(\delta_f\right) \\ & + \left(F_{y,rl} + F_{y,rr}\right) \cdot \cos\left(\delta_r\right) + \left(F_{x,rl} + F_{x,rr}\right) \cdot \sin\left(\delta_r\right) \end{aligned} \tag{3.2}$$

The lateral motion of the vehicle in the 3D model is derived as above. I is the moment of inertia, M is the torque, and ϕ, θ, ψ are the pitch angle, roll angle, and yaw angle, respectively. Assuming that the longitudinal velocity is equal to the velocity of the vehicle, the lateral acceleration is defined as follows.

$$a_y = v_x \cdot \left(\dot{\psi} + \dot{\beta}\right) = v_x \cdot \dot{\psi} + \dot{v}_y \tag{3.3}$$

The addition of rear wheel steer affects the lateral motion of the vehicle.

$$\begin{aligned} \delta_f &= \delta_{f0} - k_f \cdot F_{yf} \\ \delta_r &= \delta_{r0} - k_r \cdot F_{yr} \end{aligned} \tag{3.4}$$

where k_f and k_r is the compliance gain of front and rear tire, respectively. is the lateral force applied to the vehicle, and $\delta_i \{i = f, r\}$ is the steering angle without regard to compliance of wheels. The lateral force of the vehicle affects the roll angle of the vehicle, which affects the force of each suspension and tire. The equation between sprung mass and unsprung mass can be obtained as follows:

$$F_{si} = -k_s(z_s - z_{ui} \pm \frac{l_w}{2}\sin\phi) - c_s(\dot{z}_s - \dot{z}_{ui} \pm \frac{l_w}{2}\dot{\phi}\cos\phi), \quad \{i = ff, fr, rl, rr\} \tag{3.5}$$

$$F_t = k_t(z_r - z_u) + \frac{k_t\phi}{l_w/2} - F_s - m_u g \tag{3.6}$$

where k_s and c_s is the spring coefficient of suspension and damping coefficient of suspension, respectively. And m_u is unsprung mass of vehicle. For convenience in developing suspension dynamics, the damping coefficient is approximated by a constant. In addition, different constants of anti-roll bars are applied to the front and rear axles respectively. At this time, the vertical force applied to each wheel is as follows:

$$
\begin{aligned}
F_{z,fl} &= F_{t,fl} + m_{u,fl} \cdot g + m_s \cdot \left(\frac{l_r}{l_f + l_r} \right) \\
F_{z,fr} &= F_{t,fr} + m_{u,fr} \cdot g + m_s \cdot \left(\frac{l_r}{l_f + l_r} \right) \\
F_{z,rl} &= F_{t,rl} + m_{u,rl} \cdot g + m_s \cdot \left(\frac{l_f}{l_f + l_r} \right) \\
F_{z,rr} &= F_{t,rr} + m_{u,rr} \cdot g + m_s \cdot \left(\frac{l_f}{l_f + l_r} \right)
\end{aligned}
\tag{3.7}
$$

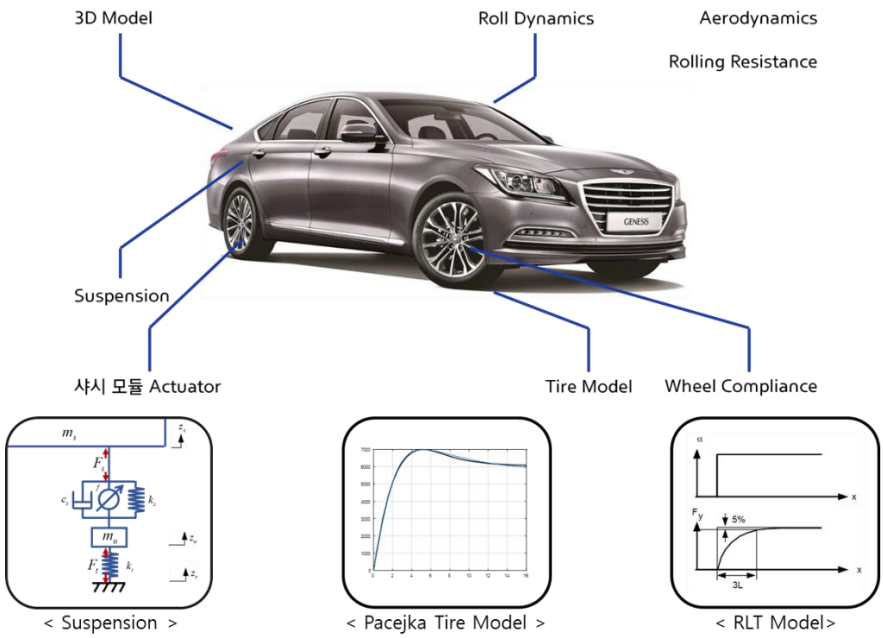

Figure 3.1. 3D vehicle model based on Genesis DH.

The slip angle $\alpha_i\{i = f, r\}$ of each axis is defined as follows. The front wheel steer angle δ_f and the rear wheel steer angle δ_r directly affect the slip angle.

$$\alpha_{fl} = \delta_f - \arctan\left(\frac{v_y + l_f \cdot \dot{\psi}}{v_x - (tw_f / 2) \cdot \dot{\psi}}\right)$$
$$\alpha_{fr} = \delta_f - \arctan\left(\frac{v_y + l_f \cdot \dot{\psi}}{v_x + (tw_f / 2) \cdot \dot{\psi}}\right)$$
$$\alpha_{rl} = \delta_r - \arctan\left(\frac{v_y - l_f \cdot \dot{\psi}}{v_x - (tw_r / 2) \cdot \dot{\psi}}\right) \quad (3.8)$$
$$\alpha_{rr} = \delta_r - \arctan\left(\frac{v_y - l_f \cdot \dot{\psi}}{v_x + (tw_r / 2) \cdot \dot{\psi}}\right)$$

Applying the Pacejka tire model, the lateral force of the tire obtained from the slip angle is as follows:

$$F_{y,i} = \mu \cdot F_{z,i} \cdot D \cdot \sin\left(C \cdot \arctan\left(B \cdot \alpha_i\right)\right) \quad (3.9)$$

Where B, C, and D determine the shape of the tire curve. The μ is the friction coefficient of the road, and $F_{z,i}\{i = fl, fr, rl, rr\}$ is the vertical force applied to the tire. The lateral force of tire is affected by longitudinal force. The lateral force of tire is as follows:

$$F_y = F_{y0} \cdot \frac{\sqrt{\left(\mu F_z\right)^2 - F_x^2}}{\mu F_z} \quad (3.10)$$

Where F_{y0} is lateral force when there is no longitudinal force. Even though the tire slip angle is the same, the lateral force decreases as the longitudinal force increases. The slip angle of the tire is applied to the relaxation length tire (RLT) mode. The formula of the tire slip angle using the RLT model is as follows:

$$\begin{aligned}
\dot{\alpha}_{fl} &= \frac{v_x}{L_y}\cdot\left(\left(\delta_f - \arctan\left(\frac{v_y + l_f\cdot\dot{\psi}}{v_x - \left(tw_f/2\right)\cdot\dot{\psi}}\right)\right) - \alpha_{fl}\right) \\
\dot{\alpha}_{fr} &= \frac{v_x}{L_y}\cdot\left(\left(\delta_f - \arctan\left(\frac{v_y + l_f\cdot\dot{\psi}}{v_x + \left(tw_f/2\right)\cdot\dot{\psi}}\right)\right) - \alpha_{fl}\right) \\
\dot{\alpha}_{rl} &= \frac{v_x}{L_y}\cdot\left(\left(\delta_r - \arctan\left(\frac{v_y - l_f\cdot\dot{\psi}}{v_x - \left(tw_f/2\right)\cdot\dot{\psi}}\right)\right) - \alpha_{fl}\right) \\
\dot{\alpha}_{rr} &= \frac{v_x}{L_y}\cdot\left(\left(\delta_r - \arctan\left(\frac{v_y - l_f\cdot\dot{\psi}}{v_x + \left(tw_f/2\right)\cdot\dot{\psi}}\right)\right) - \alpha_{fl}\right)
\end{aligned} \tag{3.11}$$

where L_y is relaxation length of tire. Compliance is considered for each tire, and the compliance gain of the front wheel and rear wheel are different.

Compliance is considered for each tire, and the compliance gain of the front wheel and rear wheel are different.

$$\begin{aligned}\delta_f &= \delta_{f0} - c_f \cdot F_{fy} \\ \delta_r &= \delta_{r0} - c_r \cdot F_{ry}\end{aligned} \tag{3.12}$$

F_y is the lateral force applied to the vehicle, and $\delta_{i,0}\{i = f, r\}$ is the steering angle without regard to compliance of wheels.

3.2. Simplified Single-Track Model for Control Design

A single-track (bicycle) vehicle model has been used to describe the vehicle lateral dynamics with RWS control input (Abe, 1999, 2015; Rajamani, 2011). The equation of motion can be derived from the bicycle model in Figure 3.2:

$$\begin{aligned} \Sigma F_y &= F_{yf} + F_{yr} = mV_x\left(\dot{\beta} + \gamma\right) \\ \Sigma M_z &= F_{yf} l_f - F_{yr} l_r = I_z \dot{\gamma} \end{aligned} \tag{3.13}$$

The state equation is organized with the two vehicle state variables: 1) side slip angle β; and 2) yaw rate γ.

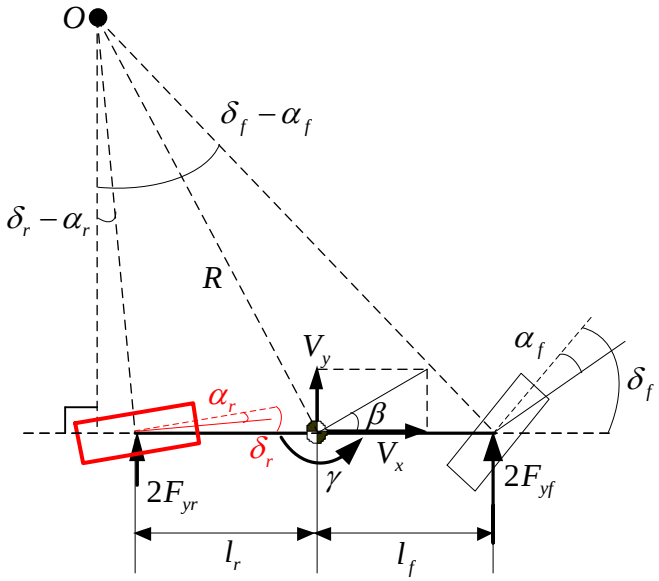

Figure 3.2. A single-track vehicle model for the 4WS vehicle.

Assuming that linear behavior of lateral tire forces the tire slip angles, the tire forces can be described as:

$$F_{yf} = C_f \cdot \left(\underbrace{\delta_f - \beta - \frac{l_f \gamma}{V_x}}_{\alpha_f} \right)$$
$$F_{yr} = C_r \cdot \left(\underbrace{\delta_r - \beta + \frac{l_r \gamma}{V_x}}_{\alpha_r} \right) \tag{3.14}$$

where αf and αr are the slip angles of the front and rear tire, respectively. The tire slip angles are defined by the kinematic relationship with steer angles

and vehicle states. The tire lateral forces are actually calculated as Fy,(f /r)(k) =C(f /r)(k)·α(f /r)(k), and the tire cornering stiffness Cf and Cr are the nonlinear coefficients that well represent the vehicle lateral behavior at k step.

From (3.13) and (3.14), the state equation of the bicycle model with RWS can be written as:

$$\dot{x}(t) = A \cdot x(t) + B \cdot \delta_f(t) + C \cdot \delta_r(t)$$

$$A = \begin{bmatrix} -\dfrac{\left(C_f + C_r\right)}{mV_x} & -\dfrac{\left(C_f l_f - C_r l_r\right)}{mV_x^2} - 1 \\ -\dfrac{\left(C_f l_f - C_r l_r\right)}{I_z} & -\dfrac{\left(C_f l_f^2 + C_r l_r^2\right)}{I_z V_x} \end{bmatrix}, \quad (3.15)$$

$$B = \begin{bmatrix} \dfrac{C_f}{mV_x} \\ \dfrac{C_f l_f}{I_z} \end{bmatrix}, \quad C = \begin{bmatrix} \dfrac{C_r}{mV_x} \\ -\dfrac{C_r l_r}{I_z} \end{bmatrix}$$

where, the vehicle state x(t) is $[\beta \quad \gamma]^T$.

At steady-state, the derivative terms in (3.15) are zero ($\dot{\beta} = 0$, $\dot{\gamma} = 0$), and the vehicle dynamics in (3.15) shrinks to the vehicle cornering kinematics as follows:

$$\delta_f - \delta_r = \frac{L}{V_x}\gamma_{ss} + \underbrace{\frac{m}{L}\left(\frac{l_r}{C_f} - \frac{l_f}{C_r}\right)}_{K_{us}} \cdot V_x \gamma_{ss} \quad (3.16)$$

where γss is the yaw rate in the steady-state, and Kus is the understeer gradient that shows the steering characteristic of the vehicle. The rear-wheel steering angle δr affects vehicle cornering kinematics as follows:

$$\delta_f = \left(\frac{L}{V_x} + K_{us} V_x \right) \cdot \gamma_{ss} \tag{3.17}$$

$$G^{\gamma}_{ss,FWS} = \frac{\gamma_{ss}}{\delta_f} = \frac{V_x}{L + K_{us} V_x^2} \tag{3.18}$$

For vehicles with the rear wheel system (δr ≠ 0) case, the steady-state yaw rate gain for the RWS vehicle $G^{\gamma}_{ss,RWS}$ can be written as follows:

$$\begin{aligned} G^{\gamma}{}_{ss,RWS} &= \frac{\gamma_{ss,RWS}}{\delta_f} = \frac{V_x}{L + K_{us} \cdot V_x^2} \cdot \left(1 - \frac{\delta_{r,ss}}{\delta_f} \right) \\ &= G^{\gamma}{}_{ss,FWS} \cdot \left(1 - \frac{\delta_{r,ss}}{\delta_f} \right) \end{aligned} \tag{3.19}$$

where $\gamma_{ss,RWS}$ is the steady-state yaw rate of RWS vehicle, and δr,ss is the rear-wheel steering input in the steady-state. The steady-state yaw rate gain for RWS vehicle is proportional to that for FWS vehicle as described in (3.18) and (3.19). Moreover, the ratio between two steady-state gains is a function of front and rear steering wheel angles. Therefore, the steady-state cornering characteristics can be modified by controlling the rear-wheel steering angle proportional to the front-wheel steering angle (the driver's input). The details

of modifying the steady-state cornering characteristics are elucidated in the next chapter.

This paper uses values the vehicle parameters from Table 1. These vehicle parameters were tuned to show similar dynamic characteristics of the given test vehicle—an F-segment vehicle with Rear-Wheel Drive (RWD).

Table 1. Nominal values of vehicle parameter

Parameter (Notation)	**Value [Units]**
Total mass (m)	2055.14 [kg]
Yaw moment inertia (I_z)	4551 [$\mathrm{kg} \cdot m^2$]
Wheel base (L)	3.009 [m]
Distance from C.G to front wheels (l_f)	1.477 [m]
Distance from C.G to rear wheels (l_r)	1.532 [m]
Steering gear ratio (N_r)	15.221
Understeer Gradient (K_{us})	0.0063 [$\mathrm{rad} \cdot s^2/\mathrm{m}$]

Chapter 4

Offline Numerical Optimization

This chapter presents an optimal control of rear-wheel steering vehicle for analyzing optimal vehicle handling characteristics. The control inputs of the vehicle are front wheel steer angle, rear wheel steer angle and throttle. The front wheel steer angle and throttle, except the rear wheel steer angle, are determined according to the scenario, i.e. step steer scenario. And then, the optimal control performance is analyzed by comparing with the conventional control method.

An optimization program, GPOPS-2, was used to optimize the rear-wheel steer angle to minimize the cost function for a given scenario (Patterson & Rao, 2014). The process of overall optimization is illustrated in the following figure:

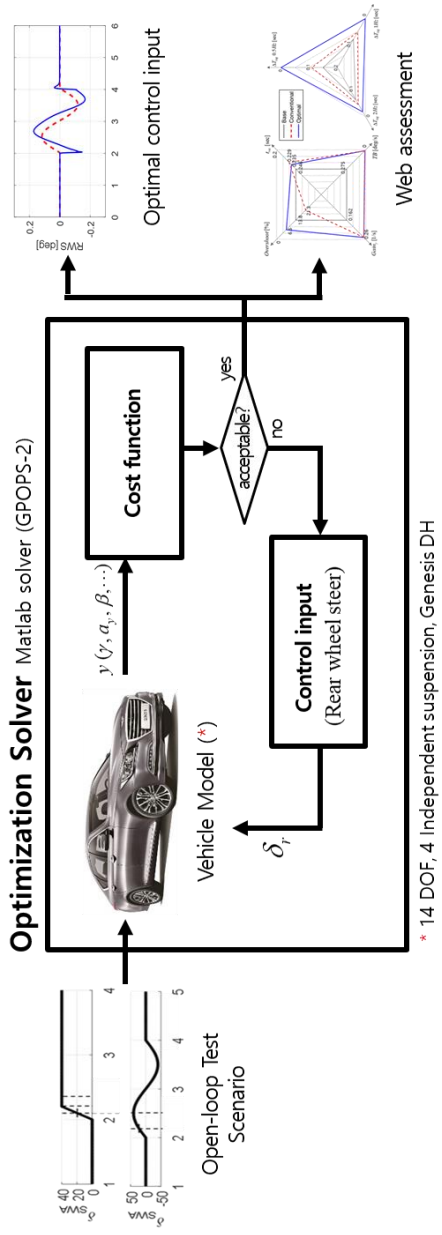

Figure 4.1. Offline optimization configuration for performance analysis of rear-wheel steering vehicle.

4.1. Optimal Problem Statement

The control objective of the optimization is selected based on (S Wagner et al., 2017). Wagner et al. conducted a performance comparison by configuring various active steering controls to track the reference trajectory. The active steering configurations are the passive vehicle (Base), single-actuation configurations for reference yaw rate tracking (FWS^{γ}, RWS^{γ}), and for lateral velocity minimization (FWS^{Vy}, RWS^{Vy}), and all-wheel steering (AWS) for tracking both references. Wagner et al. concluded that RWS^{Vy} shows the best performance when comparing the actuator cost and objective assessments with the various criteria. Therefore, in this paper, RWS^{Vy} control based on the optimization plant in (S Wagner et al., 2017) has been adopted for the offline numerical optimization.

The cost function is set as follow:

$$J = \int_{t_i}^{t_f} \left(\tilde{y}^T Q_y \tilde{y} \right) \cdot dt = \int_{t_i}^{t_f} \left(w_\beta {e_\beta}^2 + w_\gamma {e_\gamma}^2 \right) \cdot dt \tag{4.1}$$

$$\begin{aligned} s.t. \quad & \dot{x}(t) = f\left(x(t), \delta_f(t), \delta_r(t - T_{act,r})\right), \\ & x(0) = x_0,\ u(0) = u_0, \\ & \left[\left|\delta_f(t)\right| \quad \left|\delta_r(t)\right| \right]^T \le \left[\delta_{f,\max} \quad \delta_{r,\max} \right]^T, \\ & \left[\left|\dot{\delta}_f(t)\right| \quad \left|\dot{\delta}_r(t)\right| \right]^T \le \left[\dot{\delta}_{f,\max} \quad \dot{\delta}_{r,\max} \right]^T \end{aligned}$$

Where, $\tilde{y}$ is the output error, matrix Q_y and w_β, w_γ are the weighting factors. e_β and e_γ are the error of sideslip angle and yaw rate, respectively.

The constraints to be satisfied is based on 3D vehicle model that is previously defined in Chapter 3.1. Another constraint is to consider the actuator dynamics of the rear-wheel steering system. The target motion (reference model) $(\beta_{des}, \gamma_{des})$ is set to a vehicle model that does not cause sideslip angle. Therefore, the desired sideslip angle β_{des} is 0, and the desired yaw rate γ_{des} is set by calculating the yaw rate gain based on the vehicle model in which rear-wheel steering for making zero sideslip angle is considered.

The actuator constraints of the rear wheel steering system can steer up to 4deg, and the maximum steering speed is 12deg/sec. The actuator constraints are as follow:

$$\begin{aligned} &\left|\delta_{r,\max}\right| = 4\,\text{deg} \\ &\left|\dot{\delta}_{r,\max}\right| = 12\,\text{deg/sec} \\ &\tau = 0.025\,\text{sec} \end{aligned} \tag{4.2}$$

The first order time delay model is applied to the actuator dynamics of the rear-wheel steering system, and the delay time is set to 25ms.

4.2. Performance Evaluation of Optimal Results

To evaluate the performance of the rear wheel steering vehicle for maneuverability, a step steer test was conducted to select performance index. The performance index was selected to evaluate transient response and steady - state response characteristics of the vehicle. To evaluate the rear-wheel steering at various speeds, the same scenario was also conducted for low speed (30 km/h) and high speed (110 km/h).

According to ISO-7401 standards, the scenario proceeds as follows. The steering wheel angle is inputted within 0.15 seconds that generates lateral acceleration of 4m/s² while keeping the throttle of the vehicle maintaining the constant velocity before turning. In order to generate the same lateral acceleration, the steering angle input changes depending on the speed. Four performance indexes were selected to evaluate the maneuverability of the vehicle. Overshoot, response time and gain indexes are measured based on the yaw rate. The response time of yaw rate measures the responsiveness of the vehicle. The TB factor shows the trade-off relationship between responsiveness and body slip angle in steady state.

$$Overshoot = \frac{\gamma_{\max} - \gamma_{ss}}{\gamma_{ss}} \times 100 \ [\%] \tag{4.3}$$

$$t_{\gamma.resp} = t_{\gamma.\max} - t_{\delta_{SWA.50\%}} \ [sec] \tag{4.4}$$

$$\mathrm{TB} = t_{\gamma.resp} \times \beta_{ss} \ [\sec \cdot \deg] \tag{4.5}$$

$$\text{Yaw rate gain} = \frac{\gamma_{\max}}{\delta_f} [1/sec] \tag{4.6}$$

Here, γ_{max} is the maximum value of yaw rate, and βss is the steady-state value of side slip angle. $t_{\gamma,max}$ is the time required for the response to reach the first peak of the overshoot, and $t_{\delta_{SWA.50\%}}$ is the time required for the steering wheel angle rise from 0% to 50%; it serves as a reference point in calculating the peak response time $t_{\gamma,res}$. The primary concern in this section is to assess how well the proposed control algorithm implements the best performance of the numerical optimization based on objective criteria (Manning & Crolla, 2007; Uys, Els, & Thoresson, 2006).

Table 2. Performance Evaluation Indices

Scenario	**Performance index**	**Calculation**
Step steer	Overshoot	$Overshoot = \frac{\gamma_{max} - \gamma_{ss}}{\gamma_{ss}} \times 100$ [%]
	Peak Response Time	$t_{\gamma.resp} = t_{\gamma.max} - t_{\delta_{SWA.50\%}}$ [sec]
	TB Factor	$\mathrm{TB} = t_{\gamma.resp} \times \beta_{ss}$ [sec · deg]
	Yaw rate Gain	$\frac{\gamma_{ss}}{\delta_f}$ [$1/s$]

The comparative target for evaluating optimal control performance is open-loop control input proportional to front-wheel steering.

The rear wheel steer angle of the open-loop control vehicle is controlled based on the optimization result. In the open-loop control rear wheel steer vehicle, the feedforward gain of rear wheel steer angle was tuned to match the optimized based rear wheel steer angle in steady state.

The optimized rear wheel steer angle minimizes the sideslip angle in steady-state behavior. The rear wheel steer angle according to feedforward gain is as follows:

$$\delta_r = K \cdot \delta_f \tag{4.7}$$

The tuned feedforward gain K varies with speed and is shown in Figure 4.2.

If Feedforward gain K is negative, the rear wheel steer angle is opposite to the front wheel steer angle. And if Feedforward gain K is positive, the rear wheel steer angle is in the same direction as the front wheel steer angle. When the speed is lower than 56 km/h, the rear wheel steer angle is controlled in reverse phase, and when the speed is higher, the rear wheel steer angle is controlled in phases.

Thus, the behavior of the open-loop control vehicle is identical to that of an optimized rear wheel steering vehicle under steady state conditions, but there is a difference in behavior in transient response situations.

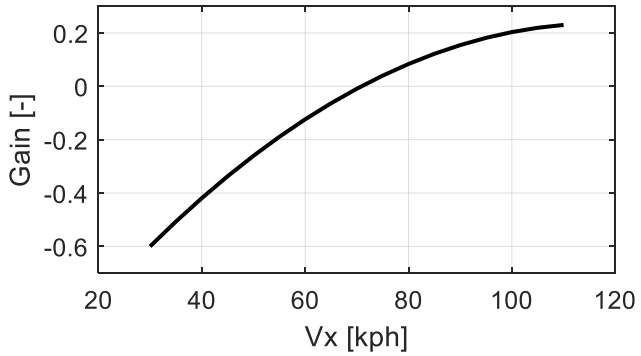

Figure 4.2. Feedforward gain of open-loop controller based on optimization results.

In this section, the simulation is conducted via Matlab and GPOPS-2. The simulation is conducted using the 14 degree-of-freedom Hyundai Genesis DH vehicle model. To compare performance of rear wheel steering vehicle, the base vehicle is compared with the optimization-based rear wheel steering vehicle, and the open-loop controlled rear wheel steering vehicle. The performance of the base vehicle and rear wheel steering vehicles was visualized through the web assessment.

Step steer input test is conducted for low speed (30 km/h) and high speed. (110 km/h). This is to analyze the characteristics of the reverse-phase control and the characteristics of the in-phase control of the rear wheel steering system. Based on the ISO-7401 standard, the throttle input that maintains constant velocity when going straight is maintained until the end of the scenario. Also steering wheel angle is input for 0.15 seconds to generate lateral acceleration of 4m/s². The angular velocity of the steering wheel angle input is constant during steering wheel angle input.

Figure 4.3 shows the vehicle state of the step steer input test at 30 km/h. Figure 4.3 (a) shows that the steering wheel angle input to generate the same lateral acceleration is smaller than that of the base vehicle because the rear wheel steering vehicle has reverse-phase control at low speed. The yaw rate of the Figure 4.3 (b) shows that the overshoot of the rear-wheel steering vehicle decreases with respect to the base. The rear wheel steer angle of the Figure 4.3 (c) shows similar behavior of the conventional vehicle and the optimal vehicle, but the rear wheel steer angle of the optimal vehicle is slightly shaken at the end of the steering angle input. This is estimated to be a computed optimization result to reduce the response time of the yaw rate. In the case of the lateral acceleration of the Figure 4.3 (d), it can be confirmed that the overshoot of the base vehicle is considerably larger than that of the rear wheel steering vehicle.

As the rear wheel steering is involved, the nonlinearity of the lateral acceleration can be improved.

Figure 4.3 (e) shows the body slip angle at this time. As the rear wheel steering is involved, it can be seen that there is almost no body slip angle in the steady state. The Table 3 shows the performance index numerically, and Figure 4.4 is a graph shown on the assessment web. The rear wheel steering vehicle had a slight decrease in the response time compared to the base vehicle, but there was a significant performance improvement in the overshoot and TB factor indexes. In addition, the yaw rate gain was increased by the reverse phase control. Compared with the conventional rear wheel steering vehicle and the optimal vehicle, the performance of the optimal vehicle improved in overshoot and response time.

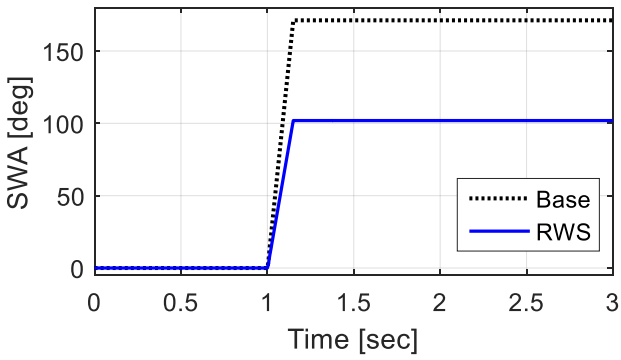

(a) Front steer wheel angle

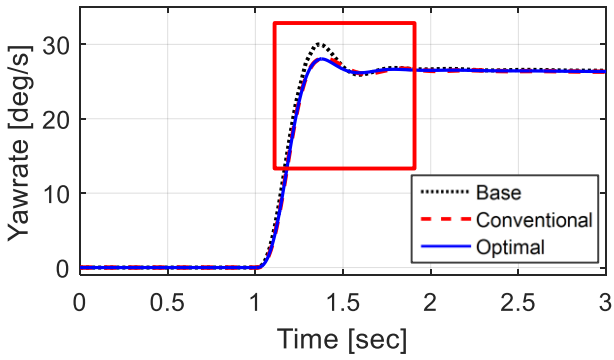

(b) Yaw rate

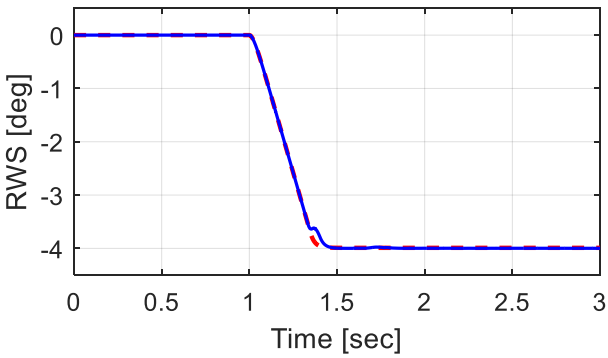

(c) Rear wheel steer

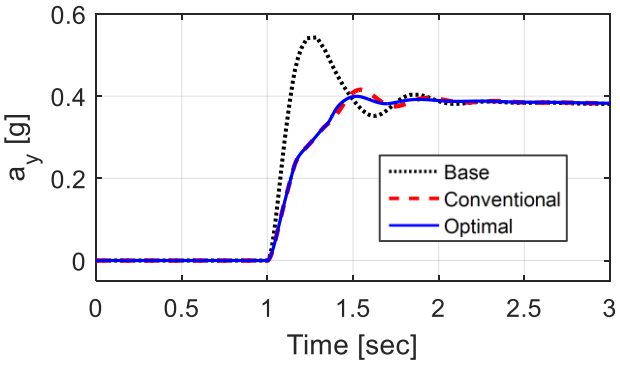

(d) Lateral acceleration

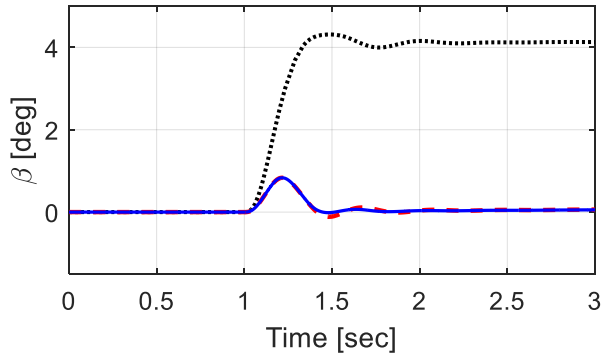

(e) Body slip angle

Figure 4.3. Optimization results: Step steer test @ 30kph

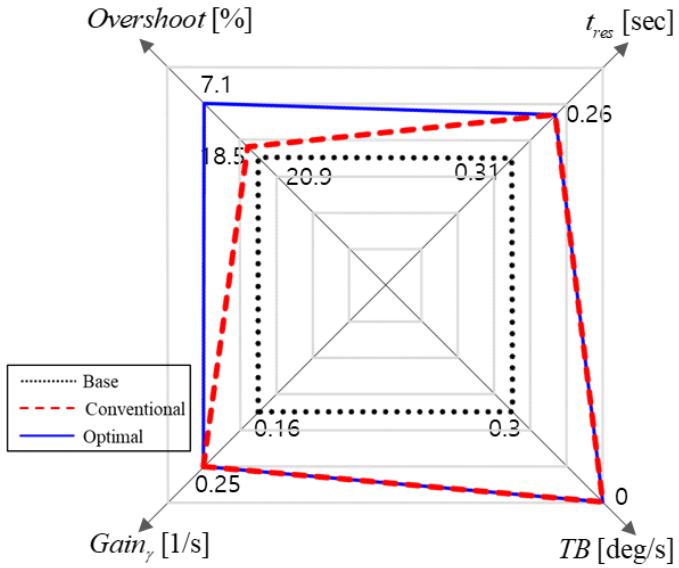

Figure 4.4. Optimization results: Step steer test @ 30kph

Table 3. Performance evaluation indexes: Step steer input test at 30 km/h

	Base	**Conventional**	**Optimal**
Overshoot [%]	13.3	6.7	6.3
Response time [sec]	0.29	0.316	0.303
TB Factor [deg·sec]	1.195	0.0158	0.0152
Yaw rate Gain [1/s]	0.16	0.256	0.256

Figure 4.5 shows the vehicle state of the step steer test at 110 km/h. As shown in Figure 4.5 (a), the steering wheel angle input to generate the same lateral acceleration is larger than that of the base vehicle because the rear wheel steering vehicle performs in-phase control at high speed. The yaw rate of the Figure 4.5 (b) shows that the overshoot of the rear wheel steering vehicle is reduced compared to the base vehicle, and the overshoot of the optimal vehicle is hardly generated. For the rear wheel steer angle of the Figure 4.5 (c), it is seen that the rear wheel steer angle of optimal vehicle is steered in the opposite direction at the beginning due to the occurrence of delay. This improves the response time of the yaw rate and overshoot performance, and generates the lateral acceleration linearly.

Figure 4.5 (e) shows the body slip angle at this time. The Figure 4.5 (e) shows that there is almost no body slip angle in the steady state of the optimal vehicle. In case of conventional rear wheel steering vehicle, it can be seen that the body slip angle occurs somewhat in the transient section. Table 4 shows the performance index numerically, and Figure 4.6 is a graph shown on the assessment web. Optimal vehicle had better performance overshoot, TB factor, and response time than base vehicle. In addition, the yaw rate gain is reduced by the base vehicle.

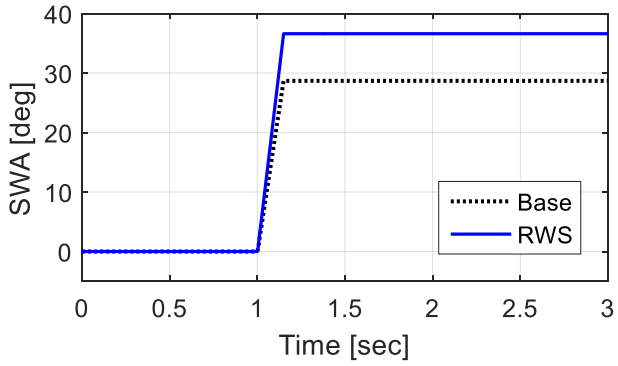

(a) Front steer wheel angle

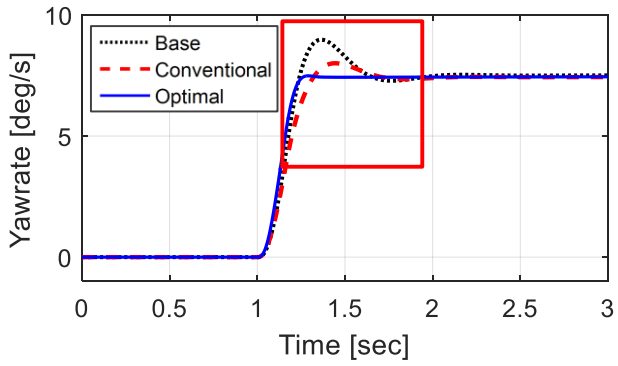

(b) Yaw rate

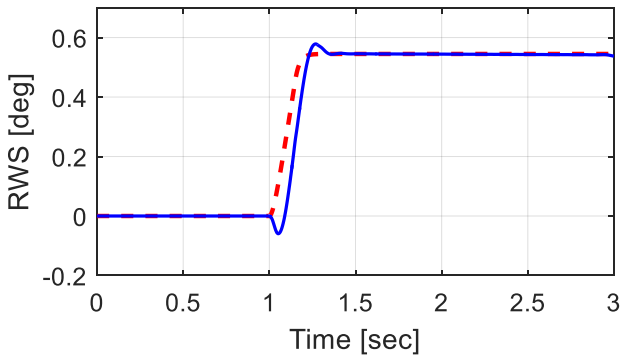

(c) Rear wheel steer

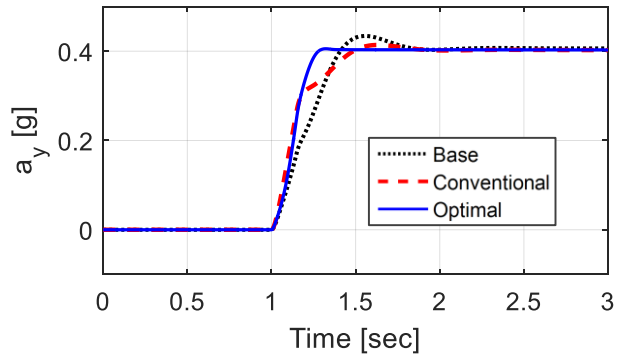

(d) Lateral acceleration

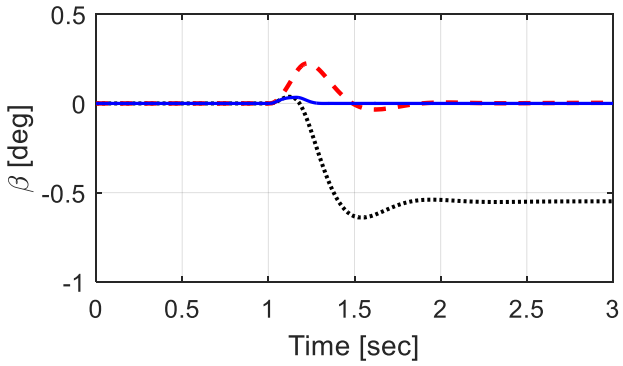

(e) Body slip angle

Figure 4.5. Optimization results: Step steer input test at 110 km/h.

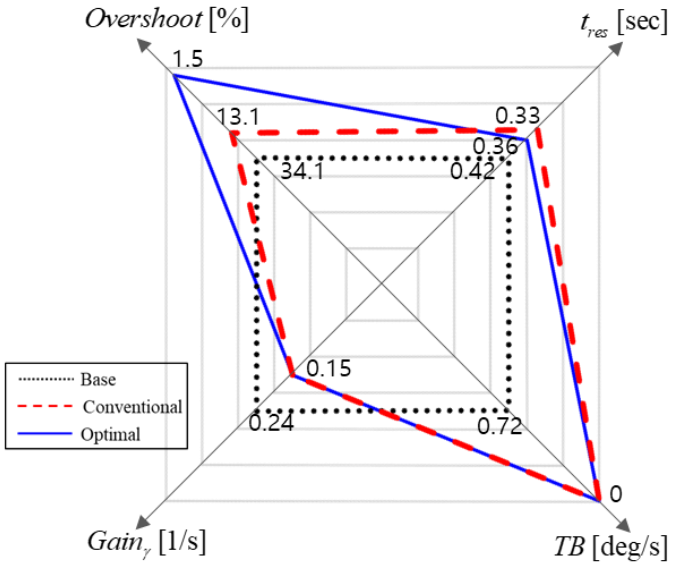

Figure 4.6. Web assessment: Step steer input test at 110 km/h.

Table 4. Performance evaluation indexes: Step steer input test at 110 km/h

	Base	**Conventional**	**Optimal**
Overshoot [%]	27.6	7.71	0.55
Response time [sec]	0.29	0.37	0.215
TB Factor [deg·sec]	-0.160	0	0
Yaw rate Gain [1/s]	0.243	0.201	0.201

Chapter 5

Controller Design

This section details a new rear-wheel steering (RWS) control algorithm. The proposed algorithm is a combination of the steady-state and transient control inputs as shown in Figure 5.1.

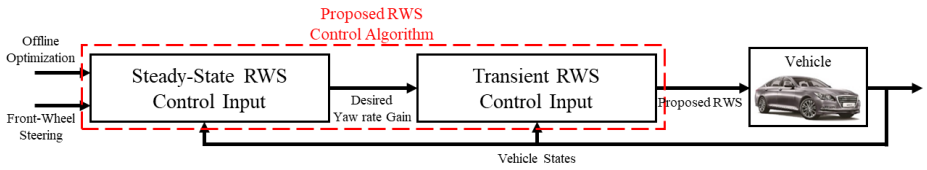

Figure 5.1. Block diagram of the proposed rear-wheel steering control.

The steady-state RWS control input is proportional to the driver's front-wheel steering. The proportional gain is obtained through offline numerical optimization. The transient control input improves the transient handling response such as overshoot, rise time, and peak response. The vehicle transient response can be deteriorated with sole steady-state RWS control (the

proportional control). For example, the lateral acceleration response of the proportional control is unnatural compared to that of the base vehicle (Figure 5.2). Figure 5.2 (a) shows the rear-wheel steering input proportional to the front-wheels, and Figure 5.2 (b) shows lateral acceleration responses. The base is the FWS vehicle with the specification of Table 1. The RWS is a vehicle with the proportional controller. The computed value is the multiplication of the yaw rate and vehicle speed, which means the steady-state lateral acceleration of the RWS vehicle.

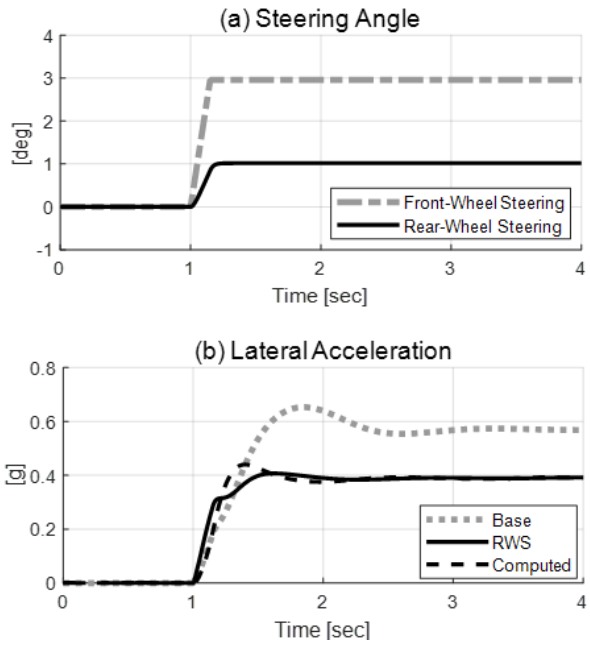

Figure 5.2. A comparison of lateral acceleration of base vehicle and RWS vehicle. 110kph, 45deg(300deg/s) step steer scenario.

The previous research (Bredthauer & Lynch, 2018) showed experimentally that this unnatural lateral jerk makes the driver feel unpleasant. This unnatural lateral jerk results from transient handling characteristics—especially the first-time derivative of the side slip angle. There is a difference between the lateral acceleration and the multiplication of the vehicle speed and yaw rate (Figure 5.2 (b)). Since this difference denotes the first-time derivative of the side slip angle, we conclude that this term is the cause of this unnatural lateral jerk.

To improve this issue, previous studies (Cho & Kim, 1995; Eguchi et al., 1989; Harada, 1995; Irie & Kuroki, 1990; Song & Yoon, 1998) added a 1st-order delay term to the rear wheel steering control algorithm. Adding such a delay term improves the lateral transient response by reducing the phase delay between the yaw rate and the lateral acceleration. Here, the previous approach to add a 1st order delay is expanded. The transient RWS control input consists of two parts: (1) feedforward input to control the delay of the yaw rate response, and (2) feedback input to control the first-time derivative of the side slip angle.

In summary, the proposed RWS control algorithm consists of the steady-state input, the feedforward of transient input (w.r.t. delay of the yaw rate) and the feedback of transient input (w.r.t. the first-time derivative of the side slip angle). The most notable point is that the proposed control algorithm only uses vehicle specifications and measurable vehicle signals instead of the tire cornering stiffness in the vehicle dynamics.

5.1. Steady-State Control Input

The goal of the steady-state RWS control is to minimize the steady-state side slip angle by modifying the vehicle's steady-state yaw rate response. It is well-known that this goal can be accomplished with the RWS input that is proportional to the driver's front steering wheel angle (Bredthauer & Lynch, 2018; Cho & Kim, 1995; Eguchi, 1991; Eguchi et al., 1989; Irie & Kuroki, 1990; Jones, 1989; Marino, Scalzi, & Cinili, 2007; Miki, Sumi, Fukui, Hayashi, & Ishiguro, 1988; Mori, 1993). Therefore, the steady-state control RWS input in this paper is designed to be proportional to front-wheel steering as follows:

$$\delta_{r,ss}(t) = k_{\delta}(V_x) \cdot \delta_f(t) \tag{5.1}$$

where, $\delta_{r,ss}$ is the steady-state control input of the proposed rear-wheel steering, and k_{δ} is the proportional gain to the front-wheel steering.

The steady-state yaw rate response generated by (3.19) can be re-written using (3.18) as follows:

$$\begin{aligned} G^{\gamma}{}_{ss,RWS} &= G^{\gamma}{}_{ss,FWS} \cdot \left(1 - \frac{\delta_{r,ss}}{\delta_f}\right) \\ &= G^{\gamma}{}_{ss,FWS} \cdot \left(1 - k_{\delta}\right) \end{aligned} \tag{5.2}$$

As described in (5.2), the steady-state yaw rate gain of RWS vehicles is a multiple of that of the FWS vehicles, and the proportional gain k_δ is a design variable. As this gain increases (or decreases), the steady-state yaw rate gain of RWS vehicles decreases (or increases) relative to that of FWS vehicles.

Designing the proportional gain kδ is important because the proportional gain kδ is the sole design variable to modify the steady-state response of vehicles. In this paper, a steady state gain is designed through offline numerical optimization results. The control objective of the optimization is selected based on (S Wagner et al., 2017). Wagner et al. conducted a performance comparison by configuring various active steering controls to track the reference trajectory. The active steering configurations are the passive vehicle (Base), single-actuation configurations for reference yaw rate tracking (FWS^{γ}, RWS^{γ}), and for lateral velocity minimization (FWS^{Vy}, RWS^{Vy}), and all-wheel steering (AWS) for tracking both references. Wagner et al. concluded that RWSVy shows the best performance when comparing the actuator cost and objective assessments with the various criteria. Therefore, in this paper, RWS^{Vy} control based on the optimization plant in (S Wagner et al., 2017) has been adopted for the offline numerical optimization.

The optimization results are presented in Figure 5.3. Figure 5.3 (a) represents the ratio of RWS yaw rate gain to FWS gain ($G^{\gamma}_{ss,RWS}/G^{\gamma}_{ss,FWS}$), and (b) shows the proportional gain (k_δ) of steady-state control input. The proportional gain becomes smaller than zero at low speeds to increase the yaw rate gain; as a result, steady-state RWS input is controlled in the reverse-phase as the front-

wheel steering. Conversely, the steady-state RWS input at high speeds reduces the yaw rate gain to improve vehicle stability by steering in the in-phase as the front-wheels. Correspondingly, the proportional gain is bigger than zero, and the control input is set to in-phase to the front-wheel steering. The speed is about 56kph when the steady-state RWS gain is zero. The results are consistent with how practitioners design the RWS control. Typically, RWS is controlled in the reverse-phase to enhance the yaw rate response at low speed while it is controlled in the in-phase to enhance the vehicle stability at high speeds.

In conclusion, the proportional gain kδ from the optimization results and the steady-state control input δr,ss of (5.1) are re-arranged using the yaw rate gains of (5.2):

$$k_{\delta}(V_x) = 1 - \frac{G^{\gamma}_{ss,RWS}}{G^{\gamma}_{ss,FWS}}(V_x) \tag{5.3}$$

$$\delta_{r,ss}(t) = k_{\delta}(V_x) \cdot \delta_f(t) = \left(1 - \frac{G^{\gamma}_{ss,RWS}}{G^{\gamma}_{ss,FWS}}(V_x)\right) \cdot \delta_f(t) \tag{5.4}$$

However, the control input in (5.3) and (5.4) results in an unnatural lateral jerk as illustrated in Figure 3. Therefore, in this paper, the transient control input is designed to compensate for the unnatural lateral jerk.

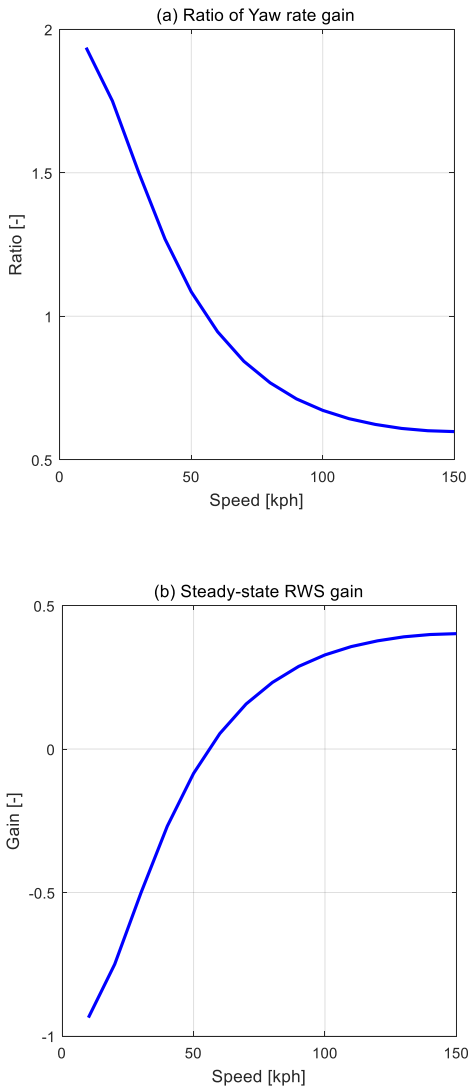

Figure 5.3. Illustration of the ratio of steady-state RWS gain obtained by numerical optimization. (a) Ratio of yaw rate gain $G^{\gamma}_{ss,RWS}/G^{\gamma}_{ss,FWS}$: as vehicle speed increases, the ratio to the base vehicle is reduced vehicle speed increases. (b) Proportional gain k_{δ}: based on about 56 kph, RWS is controlled to be in-phase at high speed and reverse-phase at low speed.

5.2. Transient Control Input - Feedforward

The transient RWS control input consists of model-based feedforward and feedback parts. In this subsection, the model-based feedforward control input is described. The goal of the transient RWS control is to enhance lateral transient response compared to the transient response when only steady-state control in (5.4) is exerted to the vehicle. For example, the goal of the transient control is to reduce yaw rate overshoot and unnatural lateral acceleration response. In this subsection, the proposed feedforward part of the transient control input will be presented first; subsequently, the closed-loop dynamics will be analyzed to investigate how such a control input affects the outcome.

The proposed RWS control input including the steady-state input and the feedforward part of the transient input is represented as follows:

$$\begin{aligned}\delta_r(t) &= \delta_{r,ss}(t) + \delta_{r,tr,ff}(t) \\ &= \underbrace{k_\delta \cdot \delta_f(t)}_{Steady-state} + \underbrace{\left(\frac{1}{\eta} - 1\right) \cdot \left\{ \left(k_\delta - 1\right) \cdot \delta_f(t) + K_{us} \cdot a_y(t) + \frac{L}{V_x(t)} \cdot \gamma(t) \right\}}_{Transient}\end{aligned} \tag{5.5}$$

where, $\delta_{r,tr,ff}$ is the feedforward control to modify transient characteristics of the rear-wheel steering vehicle.

The control law in (5.5) consists of two terms: the steady-state control input for modifying the steady-state yaw rate gain and the feedforward part for

enhancing the vehicle's transient response. Note that the control law in (5.5) is the generalized control input of (5.4). This is because the control input in (5.5) becomes equal to the steady-state RWS of (5.4) when the design parameter becomes 1.

The effects of the control input (5.5) are analyzed. To analyze the effects of the control input in (5.5), the bicycle model in (3.15) is newly formulated in the form of the transfer function as follows:

$$\frac{\gamma(s)}{\delta_f(s)} = \frac{1}{\tau s+1} \cdot \frac{V_x}{L}\left[1 - \frac{\delta_r(s)}{\delta_f(s)} - K_{us} \cdot \frac{a_y(s)}{\delta_f(s)}\right] \tag{5.6}$$

$$\tau = \frac{a_{11}}{a_{21} - |A|} = \frac{I_z V_x \left(C_f + C_r\right)}{C_f C_r L^2} \tag{5.7}$$

Here, aij is the element of matrix A at the i-th row and the j-th column, and |X| is the determinant of matrix X. The derivation of (5.6) and (5.7) are attached in Appendix A. As described in (5.6), the vehicle's yaw rate (or driver's steering angle) is regarded as the sole output (or input) of the system. The rear-wheel steering angle and the lateral acceleration is set as the external input of the system. Note that this system is a first-order delay system with the gain.

In the case of vehicles with the steady-state RWS control input only ($\delta_r = \delta_{r,ss}$), the lateral response can be expressed as follows:

$$\frac{\gamma(s)}{\delta_f(s)} = \frac{1}{\tau s+1} \cdot \frac{V_x}{L}\left[1 - k_\delta - K_{us} \cdot \frac{a_y(s)}{\delta_f(s)}\right] \tag{5.8}$$

As mentioned above, the goal of the feedforward transient input is to enhance the transient response in (5.6). By substituting (5.5) into (5.6), the closed-loop dynamics with the control law in (5.5) can be derived as:

$$\frac{\gamma(s)}{\delta_f(s)} = \frac{1}{\eta\tau s + 1} \cdot \frac{V_x}{L} \cdot \left[1 - k_\delta - K_{us} \cdot \frac{a_y(s)}{\delta_f(s)} \right] \tag{5.9}$$

As described in (5.9), by changing the design parameter η, it is possible to modify the transient response of the vehicle lateral behavior. Since the parameter η is a coefficient of the time constant, the system becomes sluggish or responsive according to the value of such a parameter. We note that the control input in (5.5) can modify the transient response of the vehicle without any information on tire and vehicle parameters.

Analysis of the design parameter η has been conducted via computer simulations. The trade-off relationship between the rise time and the overshoot was discovered via computer simulations. The conceptual figure and the simulation results are presented in Figure 5.4. Figure 5.4 (a) is a schematic diagram of the concept of the design parameter η. When η is bigger than 1, the system becomes sluggish: the rise time of yaw rate response is increased, and overshoot is decreased. On the other hand, the system becomes responsive when η becomes smaller than 1: The rise time in the transient region is improved. Moreover, the notable point in this case is the undershoot response of the rear wheel steering angle command. Figure 5.4 (b) shows the simulation results of changing the design parameter η revealing similarities with the

conceptual diagram. The changes of η also affect the transient response of the lateral acceleration. The design of η is also aimed at modifying such a nonlinear transient response as shown in Figure 5.2. Based on these characteristics, η is tuned with reference to the optimal results in the step steer scenario such as the yaw rate's response time and the lateral acceleration's transient response.

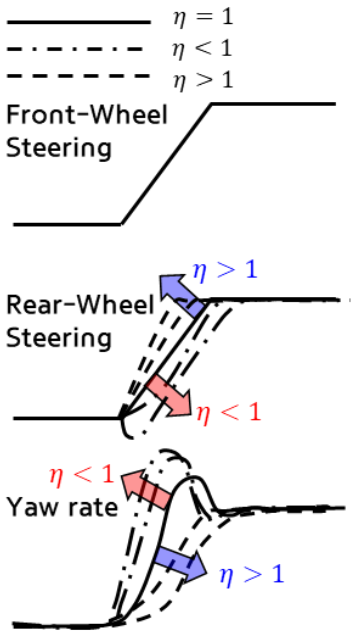

(a) Concepts of design parameter η.

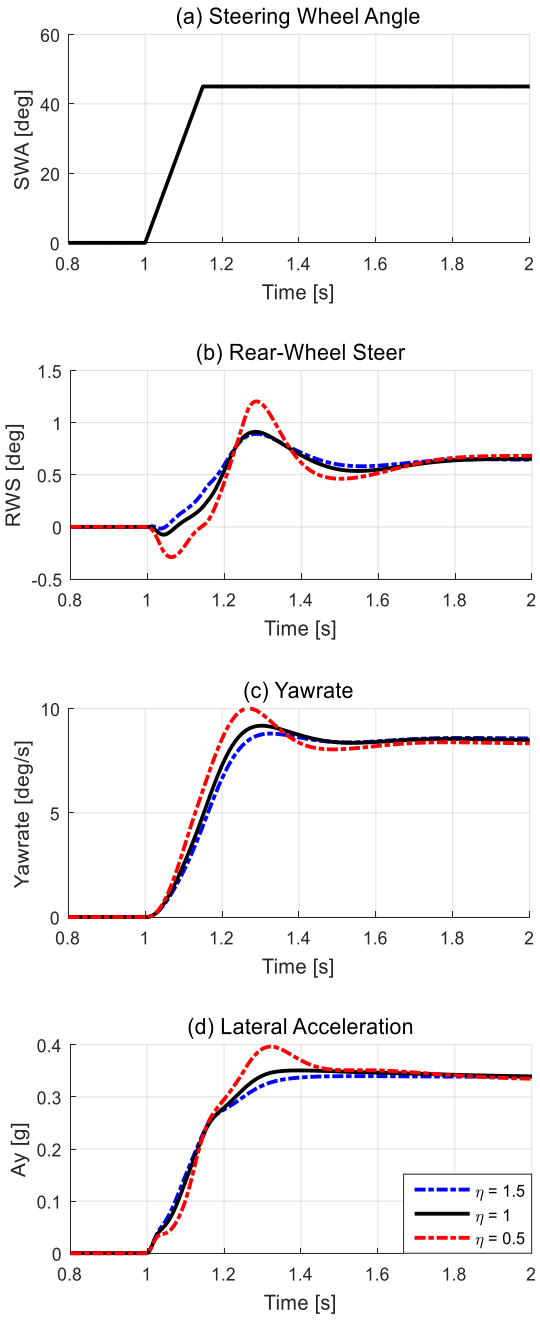

(b) Verification of performance changes through simulation at 80 kph, 45 deg (300

deg/s) step steer scenario.

Figure 5.4. Comparison of vehicle response and rear-wheel steering input with η changes.

Figure 5.5 shows the tuning results using (12) for mimicking the response time of the optimal RWS control's yaw rate. In the case of 30 kph presented in Figure 5.5 (a), the proposed control law (12) can imitate not only the response time but also the overshoot of the optimal yaw rate, by setting the design parameter = 1.3. In the case of 110 kph (Figure 5.5 (b)), the control law (12) can imitate the response time by setting the design parameter = 0.6. However, the overshoot increases noticeably. The overshoot must be reduced since the overshoot of the yaw rate response is related to the lateral instability. Therefore, under high-speed driving, an additional control input is required to minimize the overshoot. The algorithm will be mentioned in detail in Chapter 5.3.

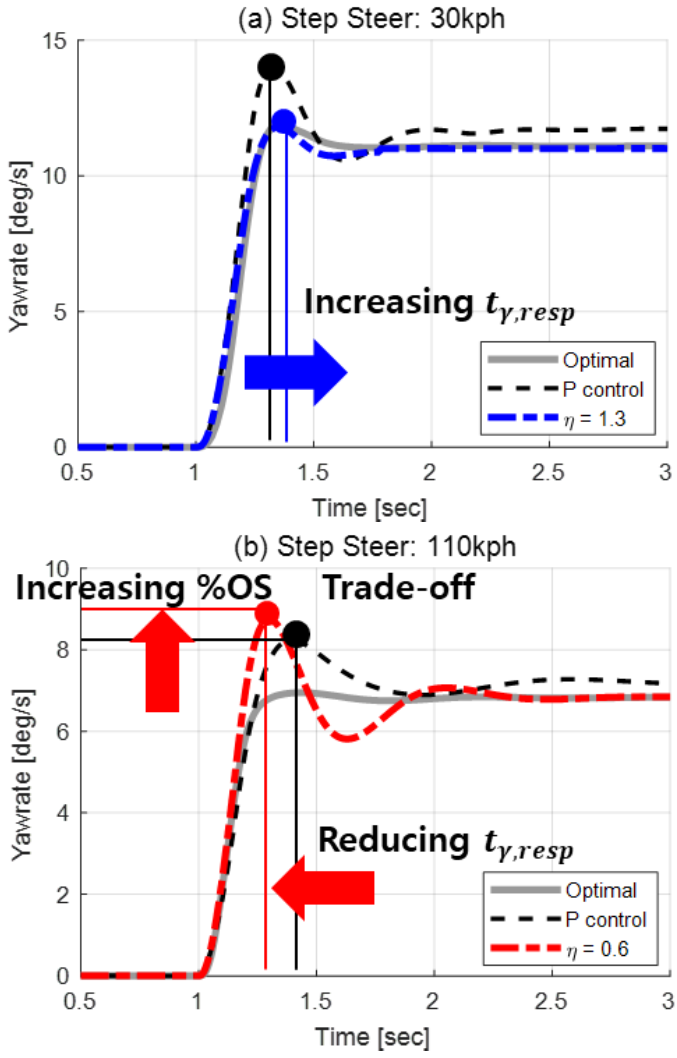

Figure 5.5. Selecting the design parameter η. (a) η=1.3 to imitate the yaw rate's response time of optimal results at 30 kph. (b) η=0.6 to imitate the yaw rate's response time of optimal results at 110 kph.

5.3. Transient Control Input - Feedback

The feedback transient control input is proposed to compensate for the trade-off (Bedner, Fulk, & Hac, 2007; Smith, Tavernini, Claret, Velenis, & Cao, 2016; Zheng & Anwar, 2009) between the overshoot and response time that the feedforward transient control input has illustrated in Figure 5.4 and 5.5. Since the excessive overshoot of the yaw rate response in Figure 5.4-5 results from the side slip rate (the first time derivative of the side slip angle), the proposed feedback control is formulated as follows:

$$\delta_{r,tr,fb}(t) = -K_{fb} \cdot V_x(t) \cdot \left(\dot{\beta}(t) - \dot{\beta}_{des}(t) \right) = -K_{fb} \cdot \left(a_y(t) - V_x(t) \cdot \gamma(t) \right) \quad (5.10)$$

where, $\delta_{r,tr,fb}$ is the feedback control to modify transient characteristics of the rear-wheel steering vehicle, and K_{fb} is the feedback gain that is a positive number. $\dot{\beta}$ is the time-derivative of the side slip angle, and $\dot{\beta}_{des}$is the desired $\dot{\beta}$ that is zero in this paper.

The final form of proposed control algorithm is obtained by adding (5.10) to (5.5) as follows:

$$\delta_{r,proposed}(t) = \delta_{r,ss}(t) + \delta_{r,tr,ff}(t) + \delta_{r,tr,fb}(t)$$
$$= \underbrace{k_\delta \cdot \delta_f(t)}_{Steady-state} + \underbrace{\left(\frac{1}{\eta} - 1\right) \cdot \left\{ \left(k_\delta - 1\right) \cdot \delta_f(t) + K_{us} \cdot a_y(t) + \frac{L}{V_x(t)} \cdot \gamma(t) \right\}}_{Feedforward\ for\ Transient} \quad (5.11)$$
$$\underbrace{-K_{fb} \cdot \left(a_y(t) - V_x(t) \cdot \gamma(t)\right)}_{Feedback\ for\ Transient}$$

The proposed RWS algorithm determines the steady-state response using the yaw rate gain ratio, and modifies the transient response such as overshoot and peak response time by tuning η and Kfb. Yaw rate, lateral acceleration, and steering wheel angle in control law (5.11) are measured from sensors mounted on the vehicle. The vehicle longitudinal speed is estimated using the wheel speed and longitudinal acceleration (Tanelli, Savaresi, & Cantoni, 2006).

Verification is required to ensure that the feedback control reduces the overshoot of the yaw rate without changing the steady-state yaw rate gain. The verification is processed in two parts: (1) the feedback control input does not change the steady-state yaw rate gain, and (2) the feedback control input reduces the overshoot.

First, (5.6) is reformulated by substituting (5.11) to identify whether the feedback gain changes the steady-state yaw rate gain.

$$\frac{\gamma(s)}{\delta_f(s)} = \frac{1}{\underbrace{\frac{\eta}{1+\frac{\eta K_{fb} V_x^2}{L}}}_{\eta_f} \cdot \tau s + 1} \cdot \frac{1}{1+\frac{\eta K_{fb} V_x^2}{L}} \cdot \frac{V_x}{L}\left[1 - k_\delta - \left(K_{us} - \eta K_{fb}\right) \cdot \frac{a_y(s)}{\delta_f(s)}\right]$$
$$= \frac{1}{\eta_f \tau s + 1} \cdot \frac{\eta_f}{\eta} \cdot \frac{V_x}{L}\left[1 - k_\delta - \left(K_{us} - \eta K_{fb}\right) \cdot \frac{a_y(s)}{\delta_f(s)}\right] \tag{5.12}$$

Here, ηf is a function of η and Kfb that can express the yaw rate in the same way of (5.9). The derivation of (5.12) is attached in Appendix B. To obtain the steady-state yaw rate gain, (5.12) can be re-written as follows by applying ay = Vx · γss and the final value theorem (Rasof, 1962):

$$\frac{\gamma_{ss}}{\delta_f} = \underbrace{\frac{V_x}{L + K_{us} \cdot V_x^2}}_{G^{\gamma}_{ss,FWS}} \cdot \left(1 - k_\delta\right) = G^{\gamma}_{ss,RWS} \tag{5.13}$$

The results in (5.13) show that the steady-state yaw rate gain does not change even if the feedback control is added.

Second, this data verified that the feedback control in (5.10) reduces the overshoot. The transfer function of the closed-loop dynamics is derived by substituting (5.9) into (3.15) as follows:

$$\frac{\gamma}{\delta_f}(s) = \frac{ps+q}{s^2+2\zeta\omega_n s+\omega_n^2}$$
$$\frac{\beta}{\delta_f}(s) = \frac{m}{s^2+2\zeta\omega_n s+\omega_n^2} \tag{5.14}$$

$$\textit{where, } p = \frac{\left(k_\delta - 1\right)\left(\frac{1}{\eta}-1\right)c_2}{1-c_1\left(\frac{1}{\eta}-1\right)K_{us}V_x + c_1V_xK_{fb}},$$

$$q = \frac{\left(k_\delta - 1\right)\left(\frac{1}{\eta}-1\right)\left|C \quad A_1\right|}{1-c_1\left(\frac{1}{\eta}-1\right)K_{us}V_x + c_1V_xK_{fb}}$$

$$\omega_n^2 = \frac{\left(\frac{1}{\eta}-1\right)\cdot\frac{|A|}{\left|B \quad A_1\right|}\cdot\left|A_1 \quad C\right|}{1-c_1\left(\frac{1}{\eta}-1\right)K_{us}V_x + c_1V_xK_{fb}}$$

$$2\zeta\omega_n = -\frac{N}{D} \tag{5.15}$$

$$N = tr(A) + \left(\frac{1}{\eta}-1\right)K_{us}V_x\cdot\left|A_2 \quad C\right| + c_2\left(\frac{1}{\eta}-1\right)\frac{|A|}{\left|B \quad A_1\right|} + V_xK_{fb}\left|C \quad A_2\right|,$$

$$D = 1-c_1\left(\frac{1}{\eta}-1\right)K_{us}V_x + c_1V_xK_{fb}$$

Here, ζ is the damping ratio of the system, and ω_n is the natural frequency of the system. Term ci is the elements of the matrix C, and A_i is the i-th column

vector of matrix A. |X| is the determinant of matrix X, and tr(X) is the trace of matrix X.

To verify that the overshoot in the step steer scenario is reduced, the yaw rate response in the step-steer scenario is derived by substituting δf (s) = k/s into (5.14). Term k is the step amplitude of steering command, and the value of k is SWA (45 deg) in this analysis.

$$\gamma(s) = \frac{kps + kq}{s\left(s^2 + 2\zeta\omega_n s + \omega_n^2\right)} = \underset{\gamma_{ss}}{\frac{kq}{\omega_n^2}} \cdot \left[\frac{1}{s} - \frac{s + \zeta\omega_n}{\left(s + \zeta\omega_n\right)^2 + \omega_d^2} - \left(\frac{\zeta\omega_n - \frac{p}{q}\omega_n^2}{\omega_d} \right) \cdot \frac{\omega_d}{\left(s + \zeta\omega_n\right)^2 + \omega_d^2} \right] \quad (5.16)$$

$$\gamma(t) = \gamma_{ss} \cdot \left[1 - e^{-\zeta\omega_n t} \cdot \cos\omega_d t - \left(\frac{\zeta\omega_n - \frac{q}{p}\omega_n^2}{\omega_d} \right) \cdot e^{-\zeta\omega_n t} \cdot \sin\omega_d t \right] \quad (5.17)$$

Here, γ_{ss} is the steady-state yaw rate ($k \cdot G_{ss,RWS}^{\gamma}$) in the step steer scenario, and ω_d is the damped natural frequency of the system ($\omega_n \cdot \sqrt{1-\zeta^2}$). Expression (5.17) is obtained by transforming (5.16) from the s-domain to the t-domain.

For a given step steering input, the overshoot of the yaw rate is calculated as $Overshoot = \frac{\gamma_{max} - \gamma_{ss}}{\gamma_{ss}} \times 100$ [%], and the peak response time is calculated as

$t_{\gamma.resp} = t_{\gamma.max} - t_{\delta_{SWA.50\%}}\,[sec]$. $t_{\delta_{SWA.50\%}}$ denotes the time required for the steering wheel angle rise from 0% to 50%. Reducing overshoot is equivalent to reducing the peak value (i.e. maximum value, γ_{max}) of the yaw rate. Likewise, since $t_{\delta_{SWA.50\%}}$ is fixed, reducing the peak response time $t_{\gamma,res}$ is equivalent to reducing the peak time $t_{\gamma,max}$.

$$\begin{aligned} \text{Reducing } t_{\gamma,res} &\Leftrightarrow \text{Reducing } t_{\gamma,\max} \\ \text{Reducing } \textit{Overshoot} &\Leftrightarrow \text{Reducing } \gamma_{\max} \end{aligned} \tag{5.18}$$

The peak time can be obtained by differentiating (5.17), and the peak value of the yaw rate can be obtained by substituting the peak time again into (5.17).

$$\begin{aligned} &\frac{d\gamma}{dt}(t_{\gamma,\max}) = 0 \\ &\gamma(t_{\gamma,\max}) = \gamma_{\max} \end{aligned} \tag{5.19}$$

The relationship between the peak time/yaw rate and the feedback gain is numerically analyzed. The peak time and the peak yaw rate at 110 kph of vehicle speed were calculated from (5.19). The peak response time and overshoot are shown in Figure 5.6. The yaw rate overshoot monotonically decreases as the feedback gain Kfb increases. However, the relationship between $t_{\gamma,resp}$ and the feedback gain is a convex function, and (K_{fb}, $t_{\gamma,resp}$) = (0.016, 0.17) is a local minimum point. Since decreasing both the overshoot and the peak response time is the goal of the control design, the feedback gain

Kfb is set to 0.016 in the step steer scenario at the 110 kph vehicle speed. The 'X' mark indicates the proposed feedback gain in this case.

Figure 5.7 represents the locus of the closed-loop poles of the transfer function (5.14) and indicates the yaw rate response to the driver's steering input. The feedback gain Kfb varies from 0 to 0.05 under the condition that is dry asphalt ($\mu = 1$) at high-speed (110 kph). Figure 5.7 (a) shows the root-locus plot of the proposed RWS algorithm (Byrnes, Gilliam, & He, 1994; Ogata & Yang, 2002; Phillips & Habor, 1995). Figure 5.7 (b) shows the change of the poles with respect to the change of the feedback gain in the log scale x-axis. As the feedback gain Kfb increases, the pole first moves towards the left-hand plane (LHP; Figure 5.7 (a)) but the poles bifurcate around Kfb = 0.032 as illustrated in Figure 5.7 (a) and (b).

In Figure 5.7 (a), all poles and zeros of the closed-loop system (5.14) exist in the Left-Half Plane (LHP). Especially, since the yaw rate and sideslip angle are based on the same characteristic equation, the poles are the same, and only the yaw rate has a zero. This is what makes both the system and the inverse causal and stable, so by definition it is a minimum phase system (Byrnes, Isidori, & Willems, 1991; X. F. Wang, Chen, & Man, 2001). As the name implies, the "minimum phase system" has a minimum phase-lag. Accordingly, it can be confirmed that the proposed RWS algorithm has good transient response (Qiu & Davison, 1993; J.-S. Wang, Zhang, & Wang, 2006).

The feedback gain of the proposed algorithm is determined by the process shown in Figure 5.6 and places the poles before the bifurcation (Dai & Han, 2004; Gu, Chen, Sparks, & Banda, 1999; Moiola, Colantonio, & Doñate, 1997;

Ono, Hosoe, Tuan, & Doi, 1996; Xu, Chen, Zhang, & Chen, 2019). Figure 5.7 (a) shows that the feedback control increases the yaw damping ratio ζ from 0.16 to 0.6. This means that the feedback control is effective for overshoot reduction. In Figure 5.7 (b), the feedback control places the real part of the poles from -0.1 to -0.3. This means that the feedback control improves the yaw stability of the RWS control system by pole-shifting (Ackermann & Sienel, 1993).

The blue solid line in Figure 5.7 (b) indicates the pole changes when the tire cornering stiffnesses are Cf = 20000 N/rad and Cr = 26800 N/rad, which are the linear cornering stiffnesses of the test vehicle. The linear cornering stiffnesses nicely represent the vehicle's lateral dynamics in mild driving region. However, the tire cornering stiffness can be changed during driving according to vehicle states, tire states, road friction, etc. The closed-loop poles' change under such a condition was investigated to analyze the control performance under varying tire stiffnesses conditions.

Figure 5.8 shows a closed-loop pole change regarding the tire cornering stiffness variation based on (5.14). As illustrated in Figure 5.8, the value of the closed-loop poles increases as the tire cornering stiffnesses increase. This is because increased tire stiffness increases the natural frequency of the closed-loop system. Moreover, the data suggest that the poles are still present on the left-hand plane (stable closed-loop poles) regardless of the tire cornering stiffness.

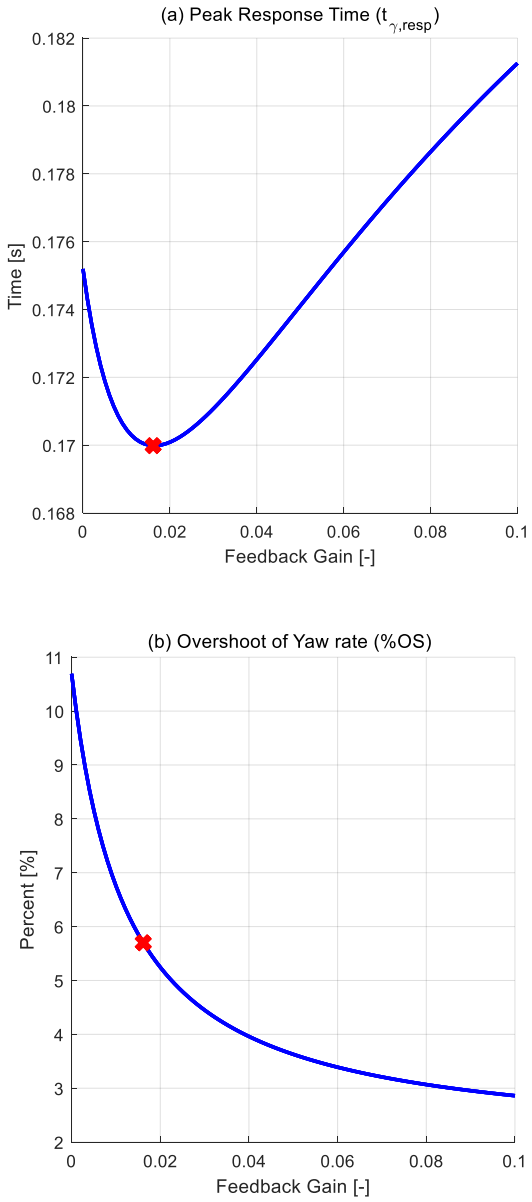

Figure 5.6. Illustration of peak response time and overshoot in step steer scenario at 110 kph, 45 deg (300 deg/s).

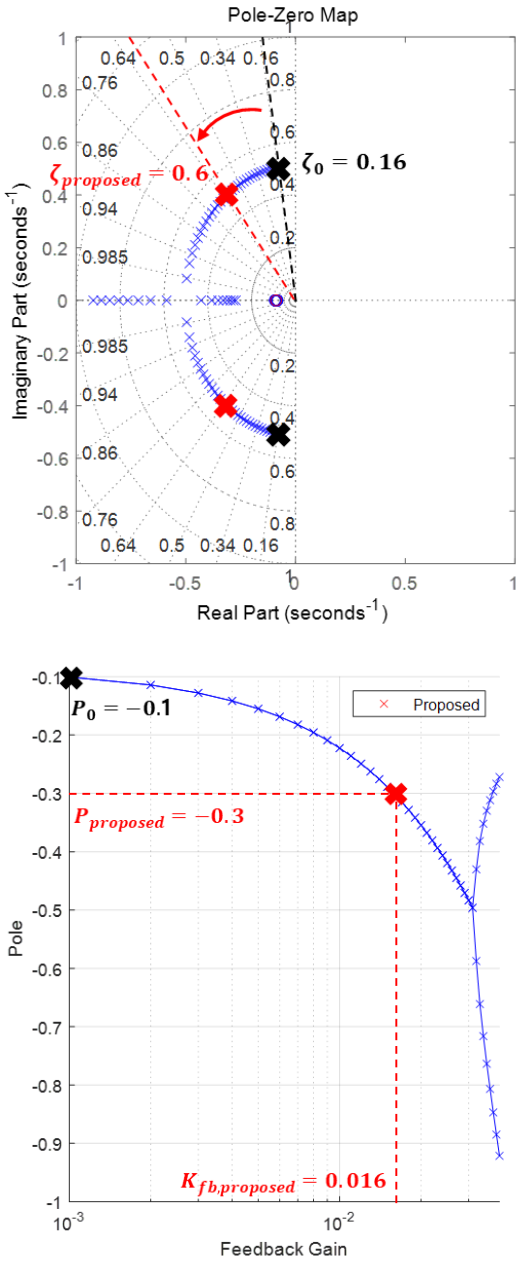

Figure 5.7. Root-Locus of Proposed RWS algorithm at 110 kph, dry asphalt, with vehicle parameters in Table 1.

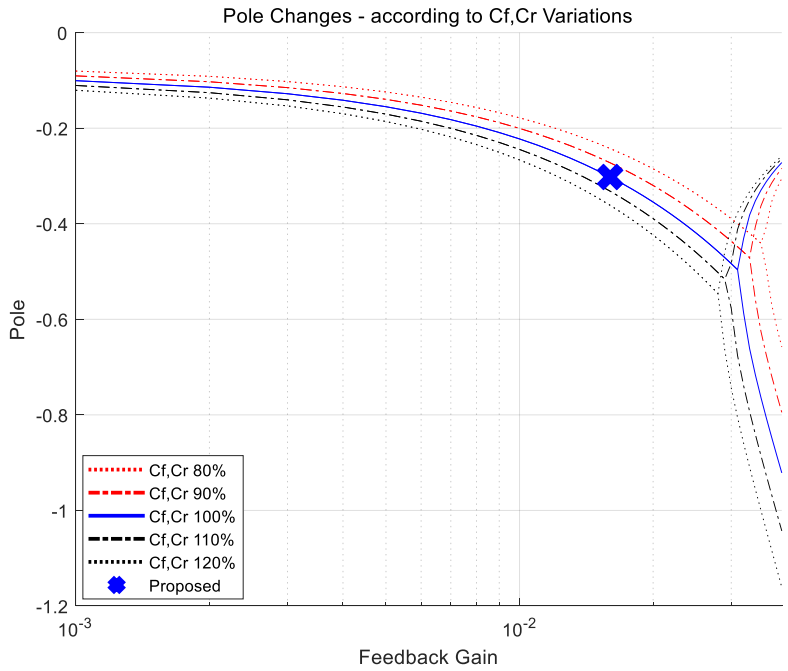

Figure 5.8. Poles versus feedback gain for tire parameter variations. Step steer (45 deg, 300 deg/s) at 110 kph.

The best feedback gain is changed regarding vehicle speed as illustrated in Figure 5.9. Figure 5.8 (a) shows the feedback gain with vehicle speeds obtained via the same process as in Figure 5.6. At low speeds (below 56 kph), the feedback gain is set to 0 because additional feedback control increases the peak yaw rate response time. The feedback gain is increased as vehicle speed increases at high speeds (over 56 kph).

Figure 5.9 (b) displays the value of the design parameter η. Chapter 5.2 shows that in the low speed region, the yaw rate response of the optimal solution can be imitated only by adopting the design parameter η. Therefore, the design

parameter η is adjusted to mimic the optimal solution while the feedback gain is set to zero. However, both the design parameter η and the feedback gain must be tuned to mimic the optimal solution at high speed. At high speeds, η is adjusted to show a similar performance with the optimal solution when the feedback gain is set to Figure 5.9 (a).

Figure 5.10 shows the performance of the proposed algorithm in (18). The proposed algorithm in (5.11) is compared with control inputs in (5.4) and (5.5) and the optimal solution. The simulation scenario is a 45 deg (300 deg/s) step steer at 110 kph vehicle speed on the dry asphalt. 'Feedforward' in Figure 11 stands for the control input in (5.5) with η = 0.6. 'Proposed' is the control input in (5.11) with (η, Kfb) = (0.8, 0.016). Feedback using (η, Kfb) noticeably reduces the overshoot of yaw rate to 13.07%, while feedforward using η changed the results by 40.14%. Moreover, δr,tr,fb in (5.10) acts as a side slip angle feedback control as illustrated in Figure 5.10, and it helps the feedforward control to converge quickly in controlling the steady-state side slip angle to zero. Moreover, the RWS of the proposed algorithm was initially steered to the opposite direction of the front steer angle as shown in Figure 5.10 (a). This initial undershoot command of the proposed algorithm is identical to the RWS command of the optimal solution.

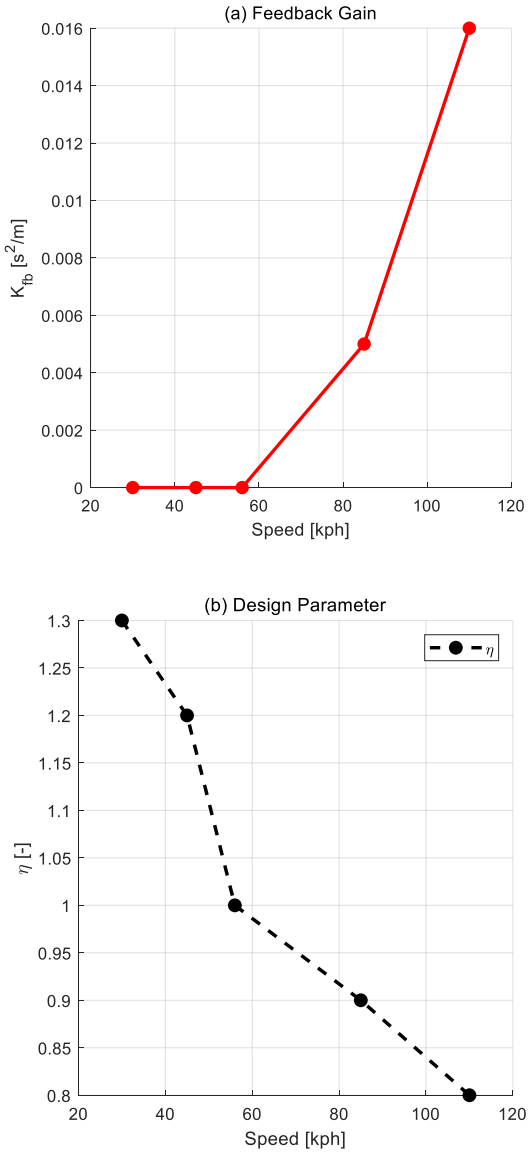

Figure 5.9. Changes of feedback gain and design parameter η with vehicle speed. (a) Feedback gain (K_fb): the feedback gain is increased as vehicle speed increases. (b) Design parameter (η): the design parameters are reduced as vehicle speed increases.

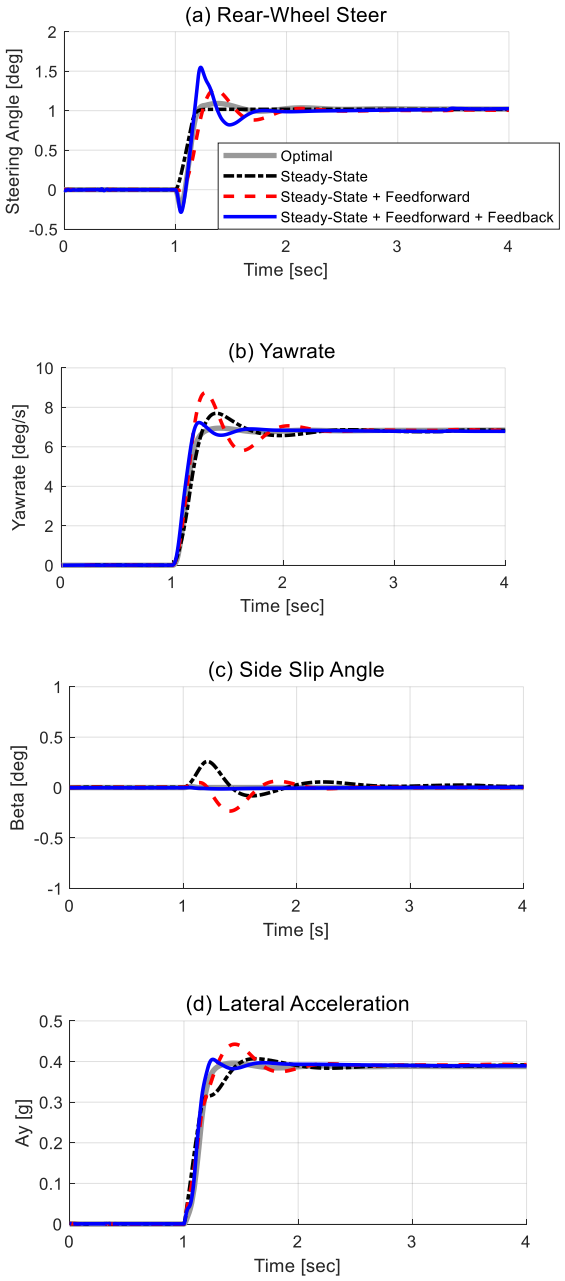

Figure 5.10. Effect of feedback controller with k_δ=0.357, for step steer at 110 kph, 45 deg (300 deg/s), dry asphalt.

5.4. Integration with ESC for Enhanced Lateral Stability

In this chapter, the individual rear-wheel steering control algorithm which is developed in previous chapter and the integrated control algorithm with the conventional electronic stability control algorithm are introduced. And then, the performance verification is carried out. The integrated chassis control algorithm with RWS and ESC is controlled based on the rule-based control strategy as follows:

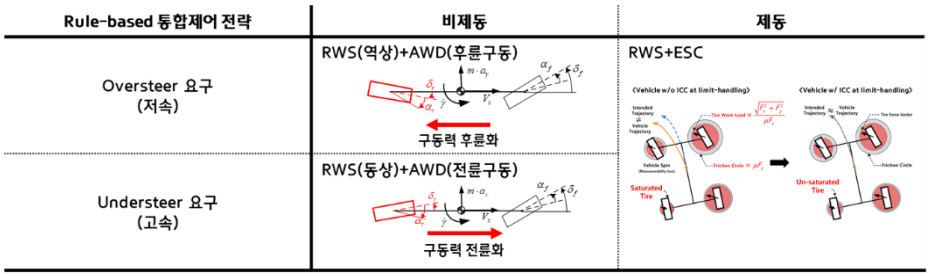

Figure 5.11. Rule-based control strategy for integrated RWS/ESC.

The actuators' intervention is determined by vehicle states and desired motion. Individual rear-wheel steering control which is proposed in this study is always controlled by vehicle speed, yaw rate and lateral acceleration. Integration with ESC chassis module is accomplished by each part that can create synergy for each control purpose. Integration with ESC module is

intended to improve vehicle lateral stability in limit handling driving, so integrated chassis control will operate at the moment of braking is required (Gottmann, Böhm, & Sawodny, 2017; Her, Koh, Joa, Yi, & Kim, 2015; Liberzon, Morse, & Sontag, 2002; Montani et al., 2020; Yim, 2015).

The proposed rear-wheel steering algorithm can adjust and improve vehicle handling performance, excluding tire parameters and road surface friction information. Similarly, ESC algorithm using tire slip angle saturation (Joa, Yi, Sohn, & Bae, 2018) is also a control that can operate in various road conditions without prior tire information. In terms of control that both algorithms can adapt to road friction changes, integrated chassis control also maintains control directionality.

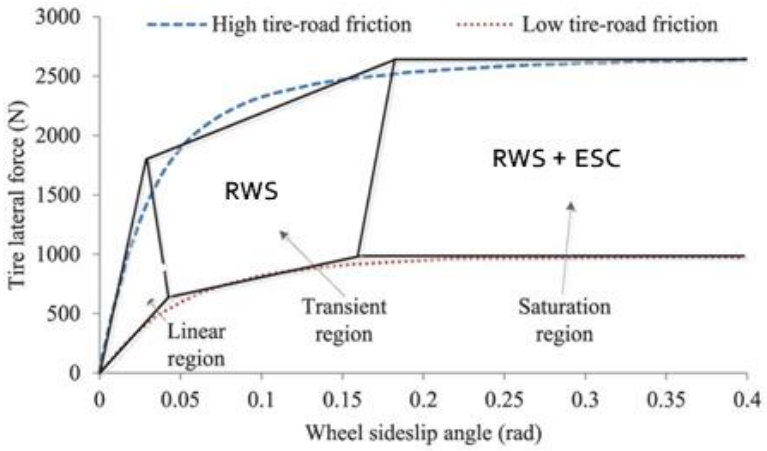

Figure 5.12. Actuators usage with hierarchical algorithm configuration

The integrated chassis control algorithm of RWS and ESC to ensure vehicle stability is conducted to intend to use the actuators hierarchically as shown in

the above figure. From the stability point of view, it is ideal to improve stability through RWS control before rear tire saturation and ensure lateral stability through ESC intervention after saturation (Abe, Ohkubo, & Kano, 1996; Peng, He, & Feng, 2013; J. Zhao, Wong, Ma, & Xie, 2017; S.-e. Zhao, Li, & Qu, 2014). The proposed rear-wheel steering control, which improves maneuverability at low speeds and improves stability at high speeds, is controlled in the form of permanent control, and it is integrated with ESC by considering the additional yaw moment generated through RWS intervention.

To analyze the effect of rear-wheel steering intervention on ESC algorithm, the concept of pre-developed ESC algorithm is used (Joa et al., 2018). To proposed an electronic stability control algorithm that can be controlled without the estimation of road friction coefficient, the normalized cornering stiffness factor is introduced as the following figure below.

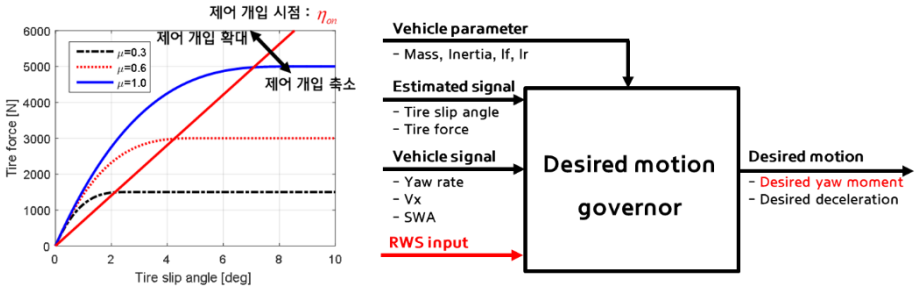

Figure 5.13. ESC algorithm with RWS intervention

The normalized cornering stiffness factor η means the ratio to the cornering stiffness of an area in which the tire characteristics are linear. η_on means the

slope at which the lateral tire forces are saturated. Based on this point, the control intervention of ESC's independent brake system is determined. Based on the concept of ESC algorithm, it is required to construct an integrated control that can consider what effect the intervention of the proposed RWS logic produces by linking with ESC algorithm.

Calculate the desired yaw moment for vehicle lateral stability control through the integration of RWS and ESC. Basically, vehicle lateral dynamics and error dynamics are utilized. The relationship between the tire slip angle and the wheel steer angle is as follows:

$$\alpha_f = \delta_f - \frac{V_y + l_f\gamma}{V_x}$$
$$\alpha_r = \delta_r - \frac{V_y - l_r\gamma}{V_x} \tag{5.20}$$

The time derivative of (5.9) is as follow:

$$\dot{\alpha}_f = \dot{\delta}_f - \frac{\dot{V}_y + l_f\dot{\gamma}}{V_x} + \frac{V_y + l_f\gamma}{V_x^{\,2}} \cdot \dot{V}_x$$
$$\dot{\alpha}_r = \dot{\delta}_r - \frac{\dot{V}_y - l_r\dot{\gamma}}{V_x} + \frac{V_y - l_r\gamma}{V_x^{\,2}} \cdot \dot{V}_x \tag{5.21}$$

In the above expression, an elimination of the deceleration has been conducted. There are two reasons. First, the additional yaw moment results in

the deceleration. Since this system utilizes four brakes to generate the moment, large yaw moment will lead to large deceleration. In other words, the second, both the additional yaw moment and the deceleration are control inputs, free variables. If the elimination of deceleration term does not execute, the additional yaw moment can be generated even when the controller only commands deceleration in the practical application due to model uncertainty and disturbance.

$$\left(V_y - l_r\gamma\right)\dot{\alpha}_f - \left(V_y + l_f\gamma\right)\dot{\alpha}_r = \left(V_y - l_r\gamma\right)\dot{\delta}_f - \left(V_y + l_f\gamma\right)\dot{\delta}_r + \frac{L}{V_x}\left(\gamma\dot{V}_y - \dot{\gamma}V_y\right) \tag{5.22}$$

Vehicle lateral dynamics are as follows:

$$\begin{aligned} F_{yf} + F_{yr} &= ma_y \\ l_f F_{yf} - l_r F_{yr} + M_z &= I_z\dot{\gamma} \end{aligned} \tag{5.23}$$

Where Mz means the yaw moment that occurs through ESC intervention.

Organize lateral dynamics in the form of the tire slip angle by rearranging the above equations.

$$\frac{d}{dt}\begin{pmatrix}\alpha_f\\ \alpha_r\end{pmatrix}=\begin{pmatrix}\left(-\frac{1}{mv_x}-\frac{l_f^2}{I_z v_x}\right)\hat{F}_{yf}+\left(-\frac{1}{mv_x}+\frac{l_f l_r}{I_z v_x}\right)\hat{F}_{yr}+\gamma+\dot{\delta}_f\\ \left(-\frac{1}{mv_x}+\frac{l_f l_r}{I_z v_x}\right)\hat{F}_{yf}+\left(-\frac{1}{mv_x}-\frac{l_r^2}{I_z v_x}\right)\hat{F}_{yr}+\gamma+\dot{\delta}_r\end{pmatrix}+\begin{pmatrix}-\frac{l_f}{I_z v_x}\\ \frac{l_r}{I_z v_x}\end{pmatrix}M_z+\begin{pmatrix}\frac{\delta_f-\alpha_f}{v_x}\\ \frac{\delta_r-\alpha_r}{v_x}\end{pmatrix}\dot{v}_x \tag{5.24}$$

Set the brake intervention point η_{on} using the normalized cornering stiffness factor, which allows for the determination of tire lateral saturation without the road surface friction information. The error dynamics for the tire slip angle is configured as follows:

$$\begin{cases}\dot{e}_{\alpha_f}=-k_f\cdot e_{\alpha_f}\\ \dot{e}_{\alpha_r}=-k_r\cdot e_{\alpha_r}\end{cases} \tag{5.25}$$

Where e_{α_f} and e_{α_r} mean the error of front and rear tire slip angle, respectively. k_f and k_r mean feedback gains.

The yaw moment M_z obtained by aligning vehicle lateral dynamics and error dynamics in the direction of eliminating $\dot{V}_x$ is arranged as follows:

$$M_z = \frac{I_z V_x}{L V_y} \cdot \left[\left(V_y - l_r \gamma \right) \cdot k_f e_{\alpha_f} - \left(V_y + l_f \gamma \right) \cdot k_r e_{\alpha_r} + \left(V_y - l_r \gamma \right) \dot{\delta}_f \right] + \frac{I_z \gamma}{V_y} \cdot \dot{V}_y - l_f F_{yf}$$
$$- \frac{I_z V_x}{L V_y} \cdot \left(V_y + l_f \gamma \right) \dot{\delta}_r + f(V_x, l_f, l_r, \gamma) \cdot \delta_r$$

(5.26)

The red-colored part of the above equation becomes an additional yaw moment through rear-wheel steering interventions. Compared to the independent operation of ESC and RWS systems, the integrated control system reduces the necessary yaw moment for ensuring vehicle lateral stability, thereby reducing brake intervention, which can relieve the driver's feeling of heterogeneity. The overall architecture of the integrated control of the proposed RWS and ESC developed in Joa et al. is illustrated as follows.

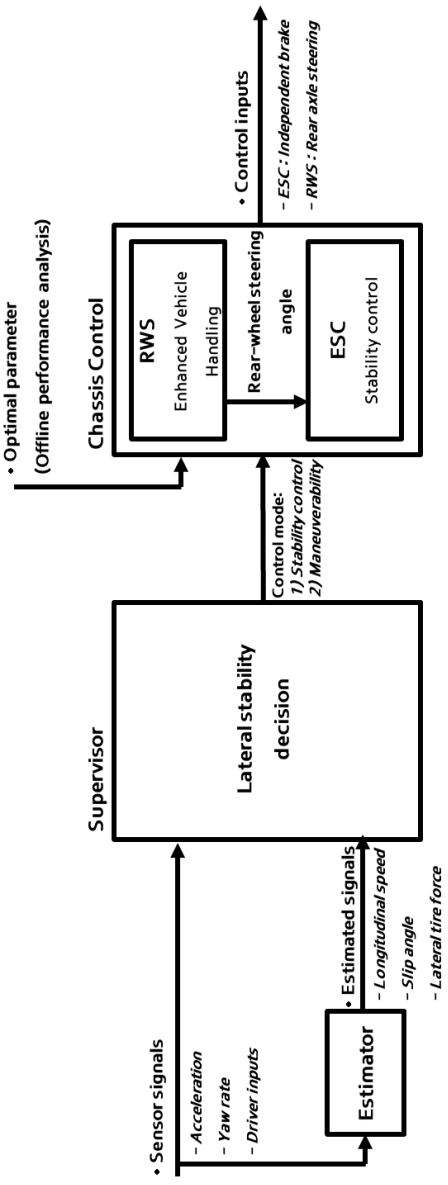

Figure 5.14. Block diagram of the integrated chassis control algorithm with RWS and ESC.

Chapter 6

Performance Evaluation

The simulation results provide analysis and understanding to investigate the performance of the proposed algorithm. Three simulation results were performed in this paper. First, the step steer scenario based-on ISO-7401 was conducted to compare the optimal control results. The comparison results are evaluated whether the proposed control algorithm implements the optimal performance with overshoot, response time, and TB factor as the objective criteria (Fetrati, Kandler, Kärcher, & Schramm, 2016; A. Lee, 1995; Schuller, Haque, & Eckel, 2002; Sivaramakrishnan & Taheri, 2013). Second, the proposed control algorithm is verified in that it performs well even in the sine with dwell scenario. Third, the robustness of the proposed control algorithm is investigated for low friction road conditions. These simulations are compared with three different controllers: 1) Base vehicle, F-segment sedan with Rear-Wheel Drive (RWD); 2) Optimal RWS controller calculated by offline numerical optimization; and 3) Conventional methods, model-based feedforward controls and sliding mode control.

Simulation is investigated via Carsim and MATLAB/Simulink. The vehicle model is configurated by applying the following vehicle body and system data of the target vehicle (F-segment): 1) Vehicle specifications in Table 1; 2) Suspension system; 3) Powertrain system; 4) Tire characteristics; 5) Brake system; 6) Aerodynamics; and 7) Compliances such as steering, suspension, etc.

The vehicle simulator constructed as shown in Figure 6.1 was compared with the actual vehicle data for Double Lane Change (DLC) test. DLC test is conducted based on ISO-3888 under the driving conditions of an initial speed of 55kph (open throttle) on dry asphalt. For the same driver input (SWA, vehicle speed), it can be seen that the simulator shows similar results to the lateral behavior of the actual target vehicle.

We investigate the change in handling performance due to the intervention of the proposed RWS control via the simulator set to be similar to the actual vehicle behavior as you can see in Figure 6.2.

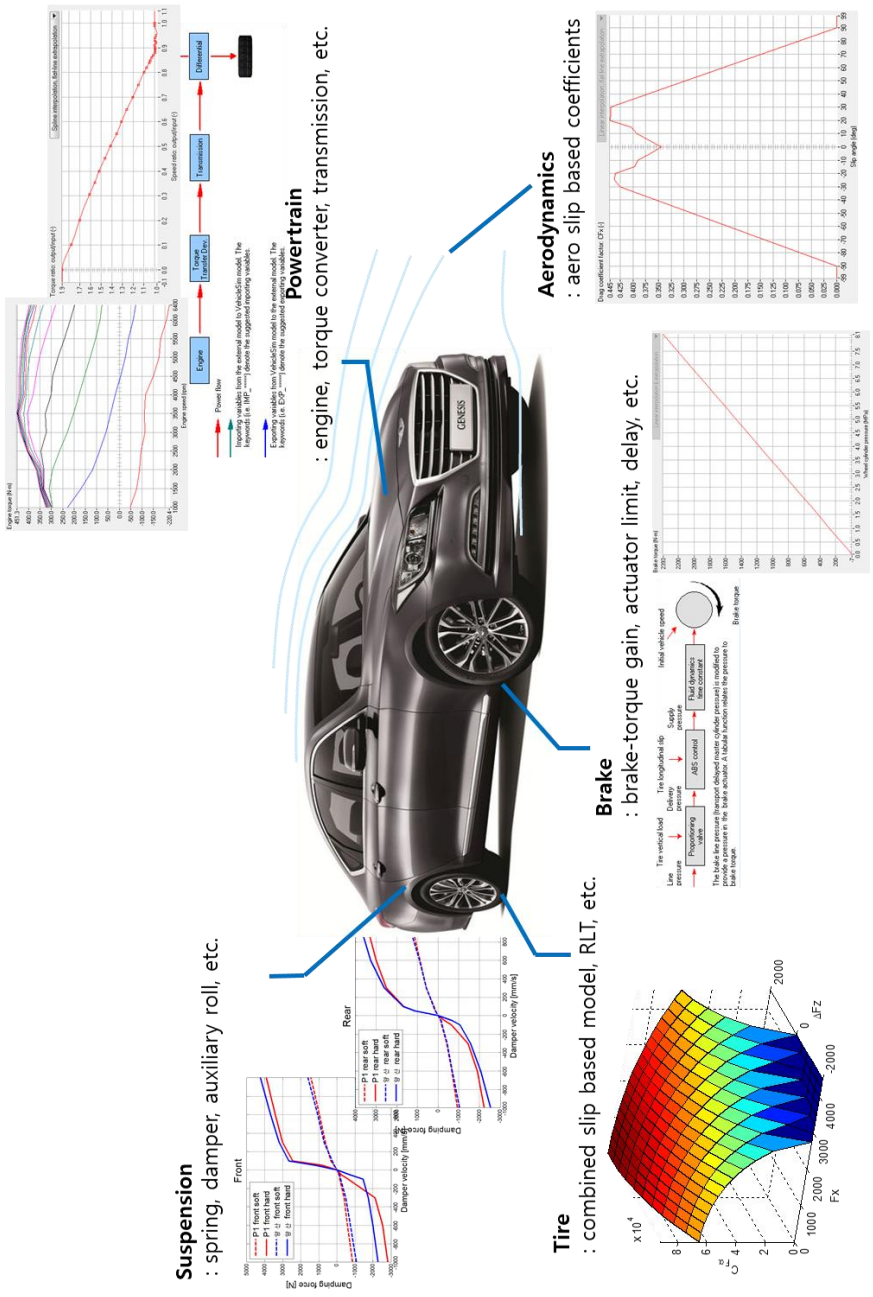

Figure 6.1.Simulator set to implement the lateral behavior of the target vehicle.

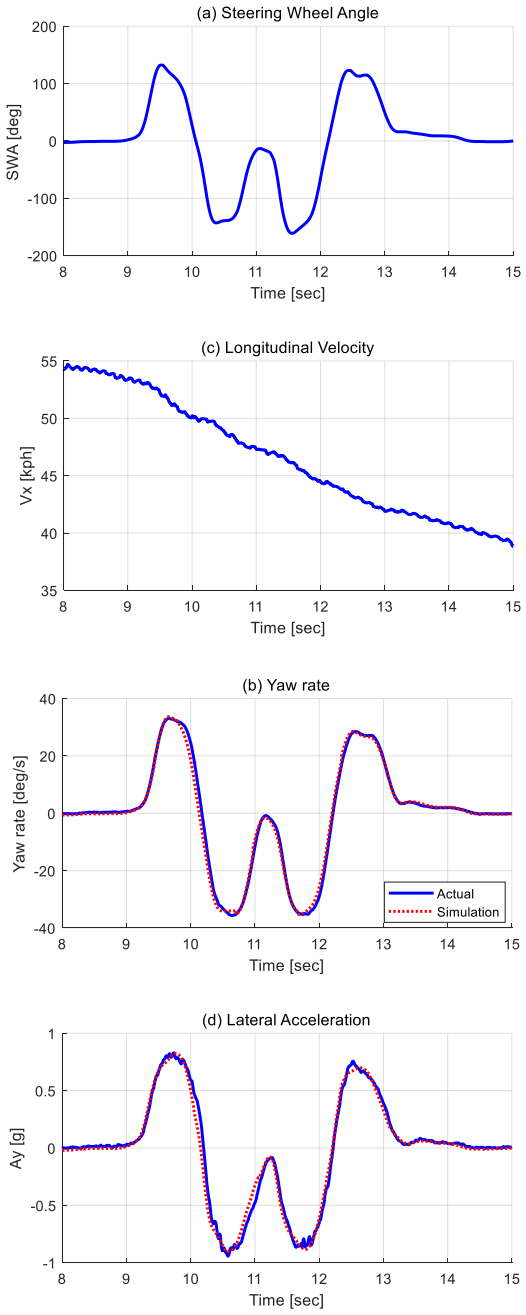

Figure 6.2. Simulation Result of DLC test @ 55 kph (open throttle), dry asphalt.

6.1. Comparison with Optimization Results

The proposed RWS control algorithm is carried out to emulate the lateral behavior of a reference model. The reference model is conducted based on the offline numerical optimization of (S Wagner et al., 2017). The numerical optimization is simulated through open-loop maneuvers that do not involve the driver's intention. In this section, a step steer scenario is adopted that satisfies the ISO-7401 with a 45 deg steering wheel angle and a 300 deg/s steering rate. The optimal control (i.e. RWS^{vy} control) is compared with the passive vehicle (only FWS) through objective criteria such as overshoot, response time, and TB factor of the Table 2.

Figure 6.3 and Figure 6.5 (a) are simulation results and performance assessment graphs at low speeds. Figure 6.3 (a) shows ``SWA/Gear-ratio (15.221)": This means the steering command divided by the gear ratio of vehicle, and it represents the front-wheel steering input by the driver. Steady-state control gain and transient control gains are set for emulating the target behavior of the optimal control. These are designated as (k_δ, η, K_{fb})=(-0.501, 1.3, 0). The performance assessment graph in Figure 6.5 (a) shows that the RWS control at low speeds improves vehicle maneuverability by increasing the steady-state yaw rate gain from 0.16 [1/s] to 0.25 [1/s]. The rear-wheel steering is controlled in the opposite direction to the front-wheels, which increases the yaw rate gain to make the TB factor zero. Vehicles with RWS control input

(proposed, optimal, proportional) reduce the peak response time from 0.31 s to 0.26 s compared to the base vehicle. In terms of overshoot, performance is evaluated as follows: optimal (7.1%) ≤ proposed (7.4%) << proportional (18.5%) < base (20.9%). From an overall perspective, the proposed RWS control algorithm at low speeds shows better performance compared to the proportional control and base, and the proposed algorithm emulates the optimal results very well.

Figure 6.4 and Figure 6.5 (b) illustrate the simulation results and performance assessment at high speed. Steady-state control gain and transient control gains are, set to emulate the target behavior of the optimal control. These values are designated as (k_δ, η, K_{fb})=(0.357, 0.8, 0.016, respectively). The rear-wheel steering is controlled in the same direction to front-wheels, which decreases the yaw rate gain to make the TB factor zero. The proposed algorithm is slightly insufficient to mimic the optimal control's overshoot, but greatly reduces overshoot compared to the proportional and base vehicle. On the other hand, the proposed algorithm shows the fastest response (0.17 s) in terms of peak response time.

The simulation results can be explained in the physical analysis and control design point of view. From the physical analysis viewpoint, one sees a difference in RWS command. Compared to the optimal control, input-delay due to the initial undershoot is similar, but it shows that the proposed algorithm subsequently has an overshoot-shaped control input. This results in greater lateral forces on the rear-axle creating a faster yaw rate response. From the

control design point of view, the feedback control reduces the overshoot and peak response time compared to the feedforward control. Figure 5.6 illustrates that the proposed algorithm has a faster response than the optimal result by further reducing the peak response time using the feedback control. Furthermore, as shown in Figure 6.4 (d), the optimal control and the proposed algorithm has a linear transient response of the lateral acceleration while the proportional control has a nonlinear (stair-shaped) transient response. Additionally, the proposed algorithm converges the side slip angle to zero better than the base and the proportional control.

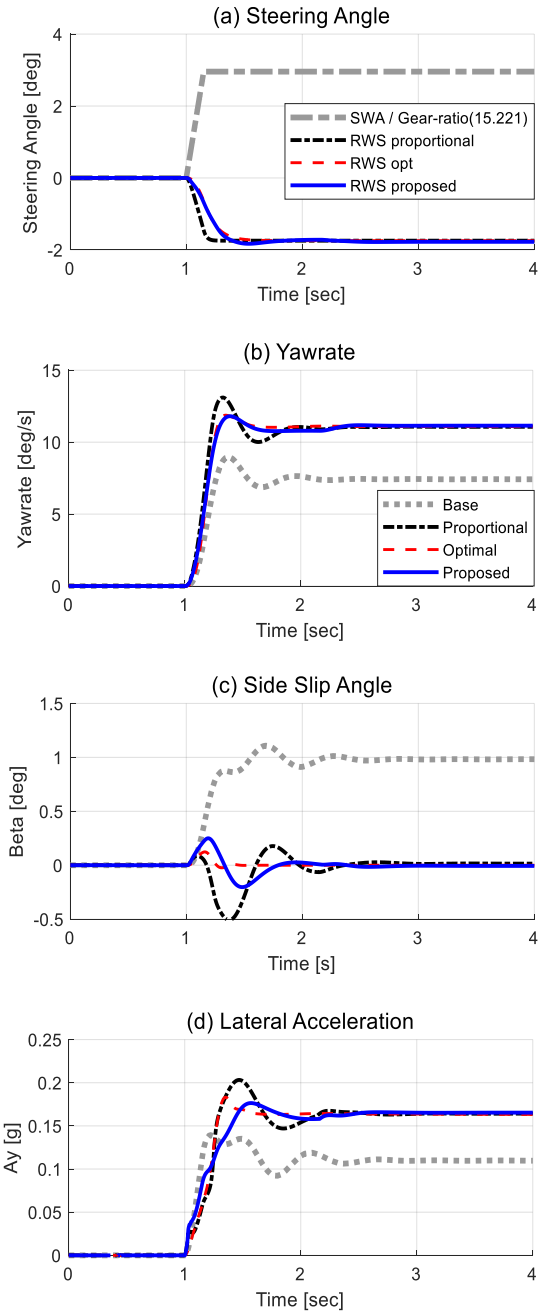

Figure 6.3. Result of step steer at 30 kph, 45 deg (300 deg/s), dry asphalt, with $k_\delta = -0.501$, $\eta = 1.3$, $K_{fb} = 0$.

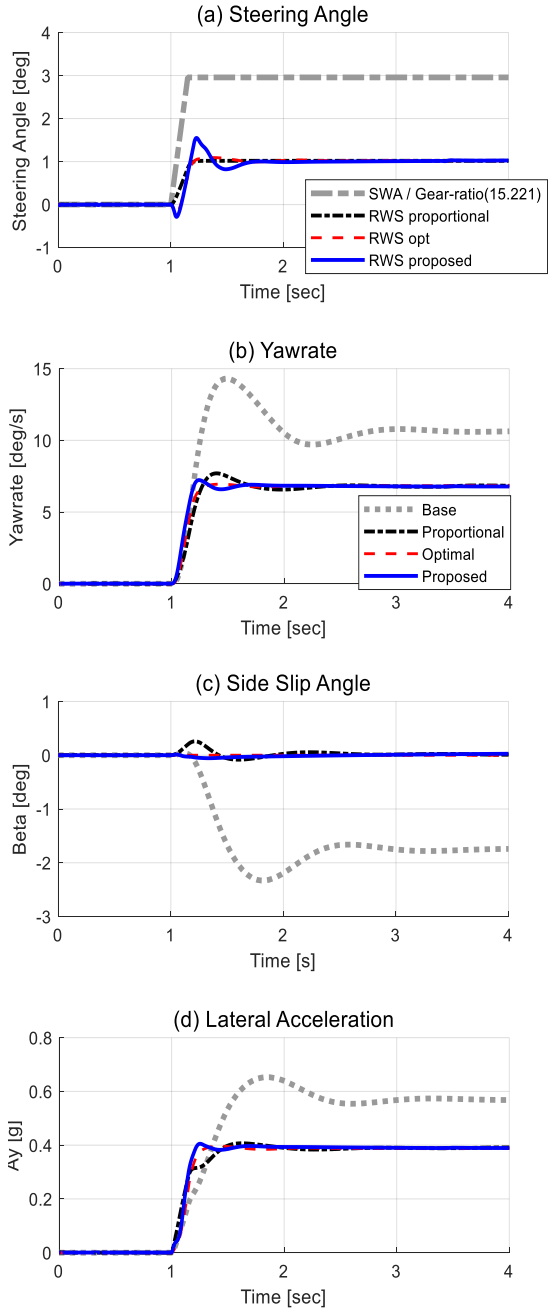

Figure 6.4. Result of step steer at 110 kph, 45 deg (300 deg/s), dry asphalt, with $k_\delta = 0.357$, $\eta = 0.8$, $K_{fb} = 0.016$.

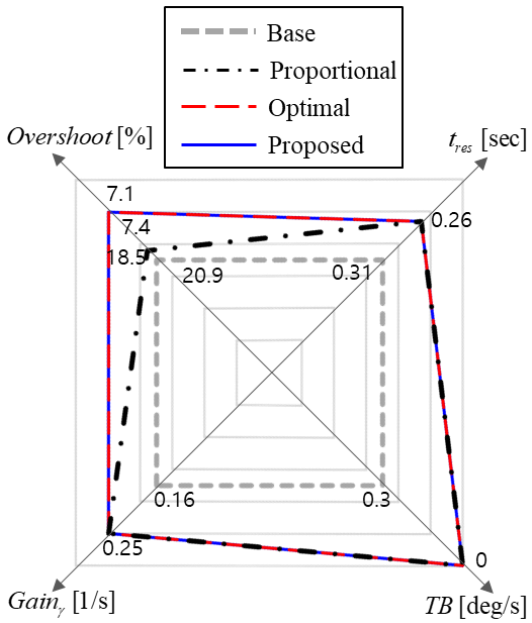

(a) Web Assessment: Step 30 kph

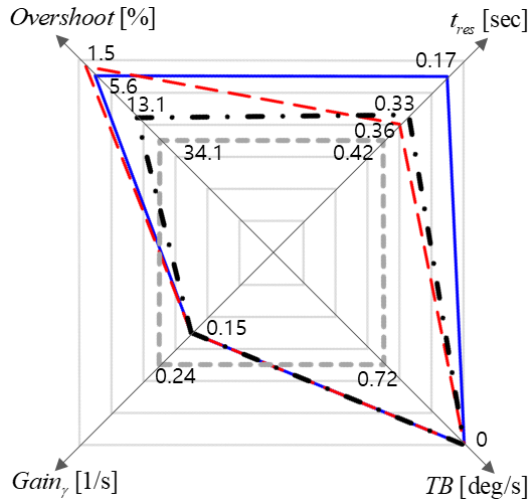

(b) Web Assessment: Step 110 kph

Figure 6.5. Web assessment for comparison with the optimal performance.

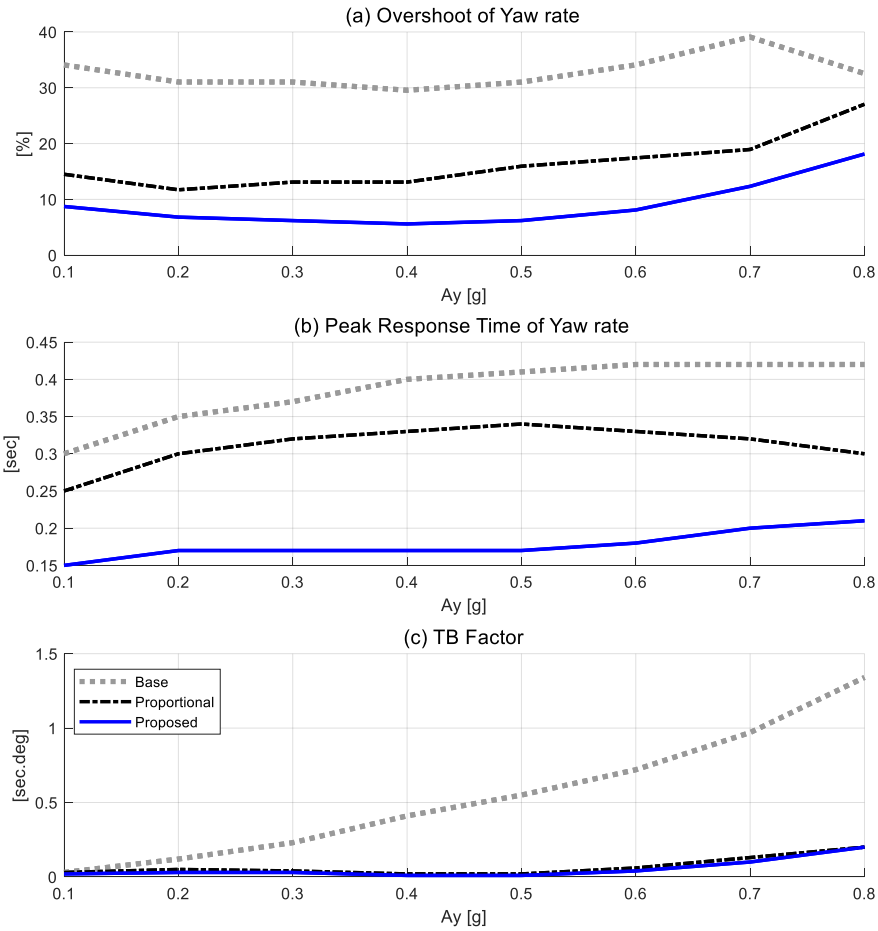

Figure 6.6. Performance indices throughout the driving region: from low to high lateral acceleration.

Figure 6.6 shows the performance indices throughout the driving region: from low to high lateral acceleration. These results are obtained by increasing the amplitude of step steering input at 110 kph. Figure 6.6 (a) shows the changes of the yaw rate overshoot. The base vehicle's overshoot exceeds 30%, and the proportional controller's overshoot rises to 27% as the lateral acceleration

increases. The proposed algorithm also increases the overshoot by more than 10% in limit handling (Ay>0.6g), but it shows good performance in mild driving (Ay<0.6g) by maintaining the overshoot less than 10%. Figure 6.6 (b) represents the peak response time according to the lateral acceleration. Compared to the proportional controller exceeded 0.25 s, the proposed algorithm maintains below 0.2 s from mild driving to limit handling. Figure 6.6 (c) represents the changes in TB factor. In limit handling, the RWS vehicles minimize the side slip angle by maintaining below 0.2 deg·s while the base vehicle increases a TB factor to more than 1 deg·s.

6.2. Effect on Vehicle Lateral Transient Response

This chapter verifies how much the vehicle handling performance of transient area has improved by comparison with conventional practical control methods. Previous studies have shown that the sole proportional rear-wheel steering controller to adjust the steady-state lateral behavior could produce an unnatural response in lateral transient behavior. Representative methods proposed to solve these issues include first-order delay control and phase reversal control. The methods implemented as a comparison target in this study are the HICAS and Super HICAS technology developed by Nissan company.

HICAS delays the rear-wheel steering command by multiplying the conventional proportional controller by the first-order delay term.

$$\delta_r(s) = k_\delta \cdot \delta_f(s) \cdot \frac{1}{\tau s + 1} \tag{6.1}$$

It is known that the yaw rate response can be improved through the time delay of the control input, and the unnatural response of the lateral acceleration can be improved.

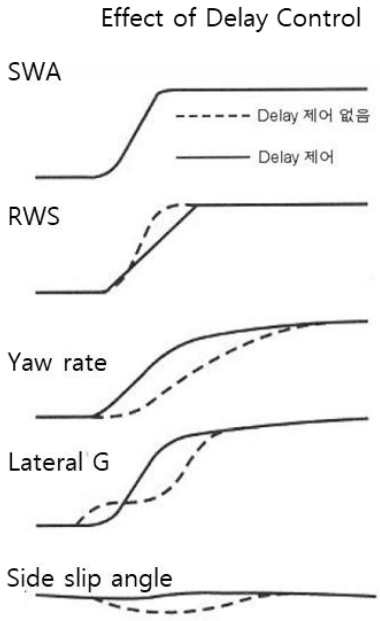

Figure 6.7. Effect of Delay Control.

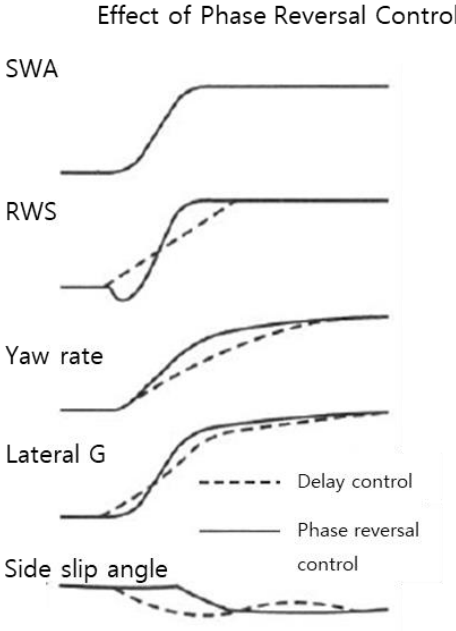

Figure 6.8. Effect of Phase Reversal Control.

Nissan proposed Super HICAS technology as a more improved and advanced rear-wheel steering control. This is a phase reversal control in which the rear-wheel steering is initially inputted in opposite direction to the front-wheels and then controlled in the same direction during high-speed driving. Through the initial reversed-phase, rear-wheel steering command can obtain the effect of a delay control, and its performance is superior to the first-order delay control. The original control method is model-based control using the vehicle suspension dynamics, and it is possible to control that meets the objective by knowing all the vehicle-related specifications accurately. In this paper, we implement the phase reversal control as shown in the following figure, focusing on “the ratio of initial reversed-phase to the in-phase” related to the time delay.

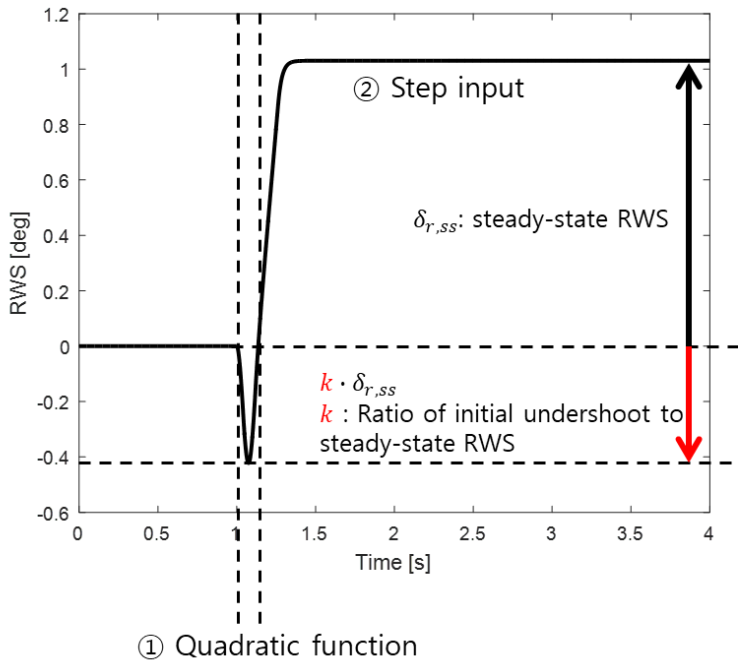

Figure 6.9. Implementation of phase reversal control input

$$
\begin{aligned}
\delta_r &= a\left(t-\tau\right)^2 - b \\
a &= \frac{b}{\left(\tau-1\right)^2} \\
b &= k \cdot \delta_{r,ss} \\
\tau &= \frac{2b}{\dot{\delta}_r} + 1 \\
\delta_{r,ss} &= k_\delta \cdot \delta_f
\end{aligned}
\tag{6.2}
$$

Assuming that the initial reversed-phase is a quadratic function, the form of phase reversal control is determined as the ratio of the magnitude to the local minimum to the steady-state input.

Figure 6.10 and 6.11 proceed to determine the optimal delay control and phase reversal control for the step steer scenario. Figure 6.10 is the results of changing the time delay from 0s to 0.1s. as the time delay increases, it can be seen that the linearity of the transient response of the lateral acceleration is improved. Along with this, it can be shown that the response time of yaw rate is reduced, but the amplitude of overshoot and sideslip angle is increased. As a compromise point for features having such a trade-off relationship, the first-order delay control with 0.06s is selected as the optimal delay control for this scenario.

Likewise, in the phase reversal control, in order to select the optimal control for this scenario, the ratio of the initial reversed-phase to the in-phase is different to find a suitable ratio for the control purpose. Figure 6.11 is the results of changing the ratio from 0% to 10%. As the ratio is increases, the initial

reversed-phased of the rear-wheel steering increases, and the effect of the input delay increases. As the ratio increases, the linearity of the lateral acceleration becomes stronger, but it can be seen that the yaw rate overshoot and vibration of the sideslip angle worsen as in the previous delay control. Therefore, 8% is selected as the optimal phase reversal control ratio, and performance comparison is conducted with the proposed algorithm.

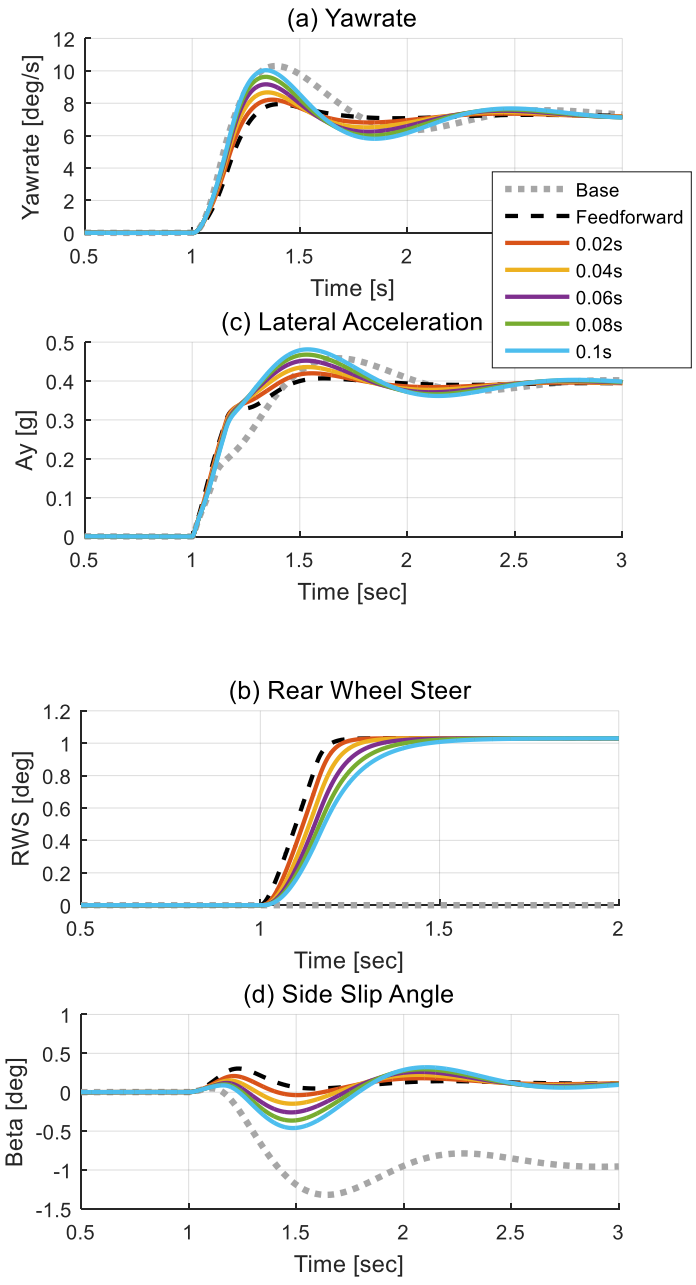

Figure 6.10. Effect of first-order delay control according to time constant change

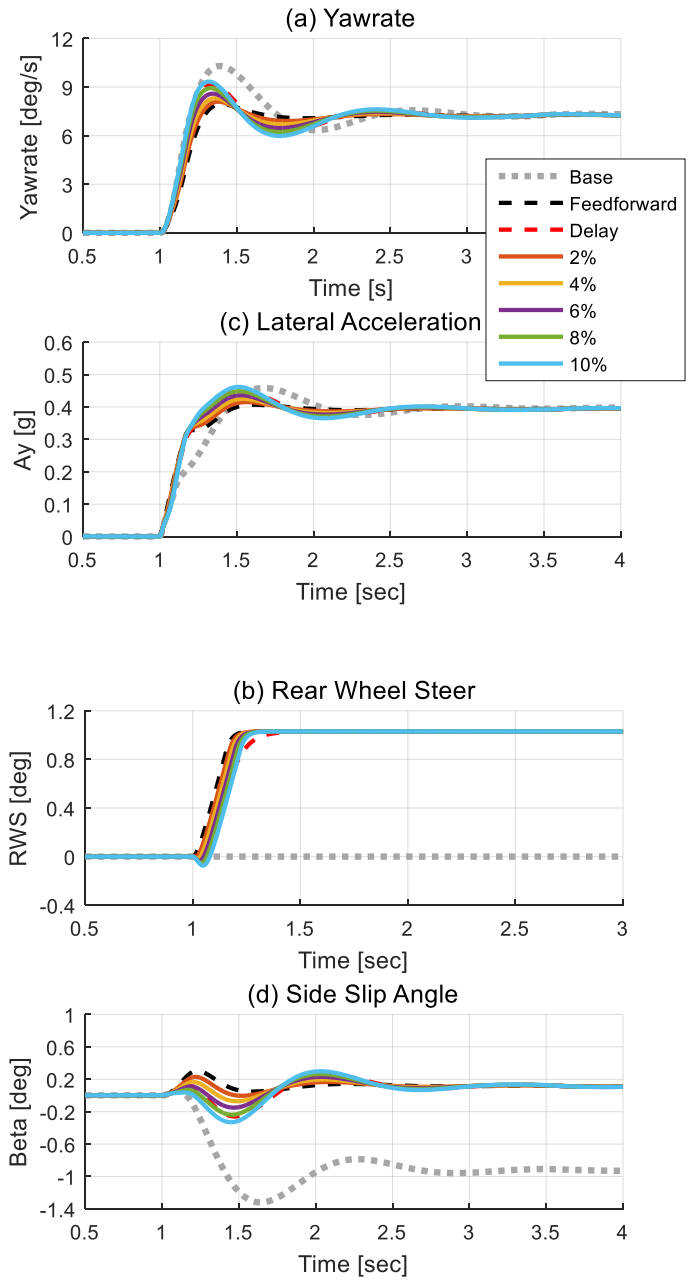

Figure 6.11. Effect of phase reversal control according to the reversal ratio changes

The proposed RWS control algorithm is compared to sole proportional control, first-order delay control with 0.06s time delay, and phase reversal control with 8% ratio for step steer scenario @ high speed 110kph, steering speed 300deg/s, and lateral acceleration 0.4g level. This is a scenario set to have the same steady-state, and a clear comparison of lateral transient response is possible. The rear-wheel steering in high-speed driving quickly generates the rear-wheel lateral force, causing a lateral jerk behavior. As a control to improve this point, we implemented HICAS (first-order delay control) and Super HICAS (phase reversal control) proposed by Nissan. Like the conclusion of (Eguchi et al., 1989), it can be shown that the phase reversal control has improved handling performance compared to the delay control. In addition, when comparing the proposed RWS algorithm, the response time of yaw rate is reduced to a similar level by controlled in-phase after initial reversed-phase input at a level similar to that of Super HICAS control. However, in terms of overshoot, the proposed algorithm achieves the smallest overshoot (15%), while sole proportional control 20%, delay control 26%, and phase reversal control 23%. At the same time, it can be shown that the proposed RWS algorithm improves noticeably the linearity of lateral acceleration.

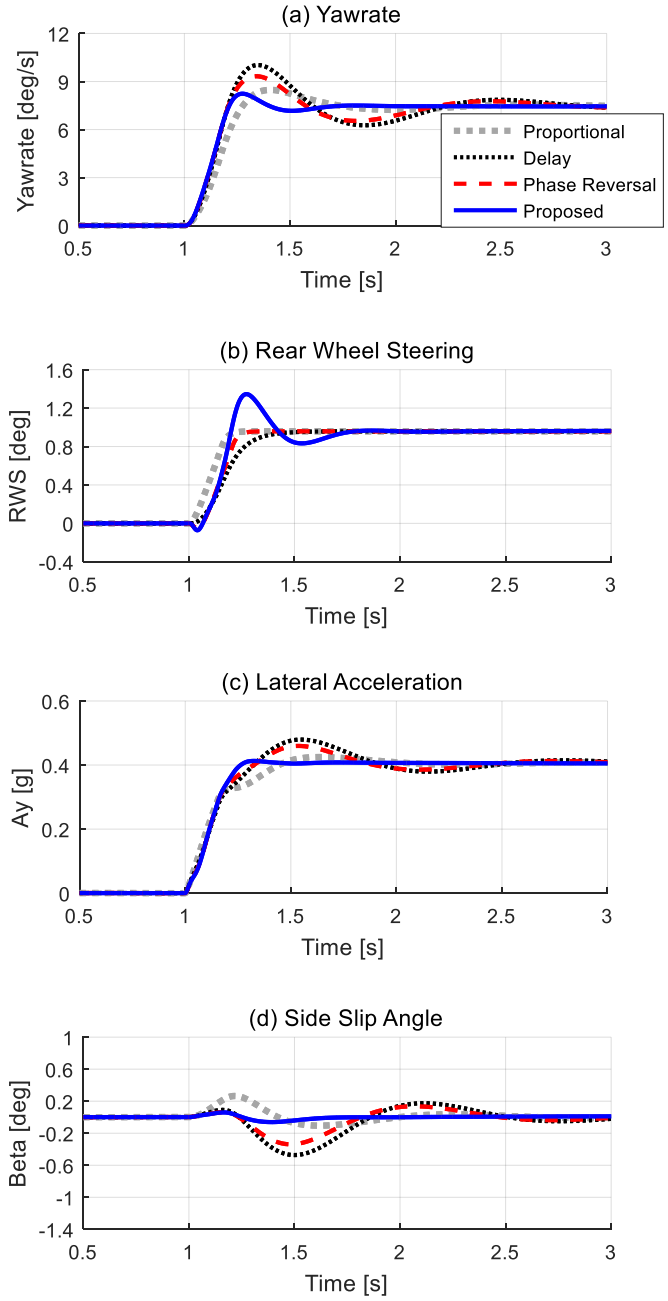

Figure 6.12. Comparison of control methods to improve lateral transient response.

In addition to the practical methods, comparisons were made with the conventional model-based feedforward and sliding mode control (SMC) to make the sideslip angle zero. In the case of feedforward controller, it was constructed for two versions: reducing the steady-state sideslip angle to zero, and always reducing the sideslip angle to zero (Abe, 1999). In the case of sliding mode control, it is constructed with the aim of tracking a reference model with RWS that does not produce the sideslip angle (Abe, 1999; Yim et al., 2016).

The results of the step steering scenario at low speed (30kph) show that SMC and the proposed control occur less sideslip angle than the feedforward control. However, sideslip angle error-based SMC delays the generation of rear-wheel steering by feedback control. As a result, it can be seen that severe oscillation has occurred in the transient area of yaw rate and lateral acceleration. On the other hand, the proposed algorithm has decreased fluctuation, showing improvements in terms of overshoot/undershoot and settling time.

Similarly, in the case of the step steering scenario at high speed (110kph), the proposed algorithm shows that overshoot/undershoot of lateral behavior are reduced and settling in steady-state rapidly.

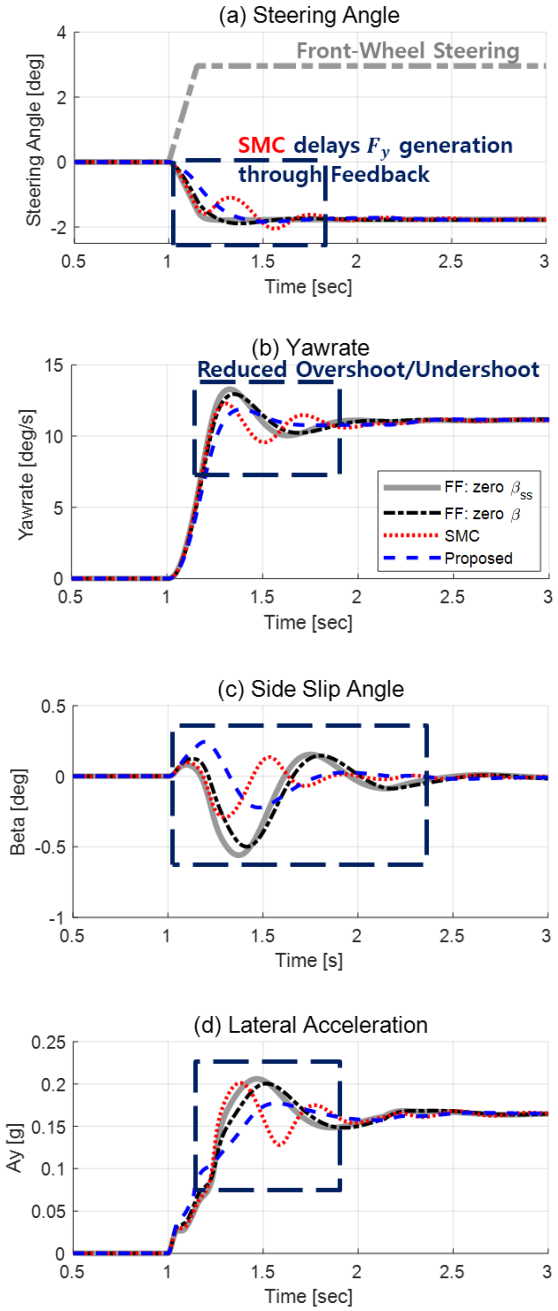

Figure 6.13. Comparison with conventional methods: step steer @ 30kph, dry asphalt.

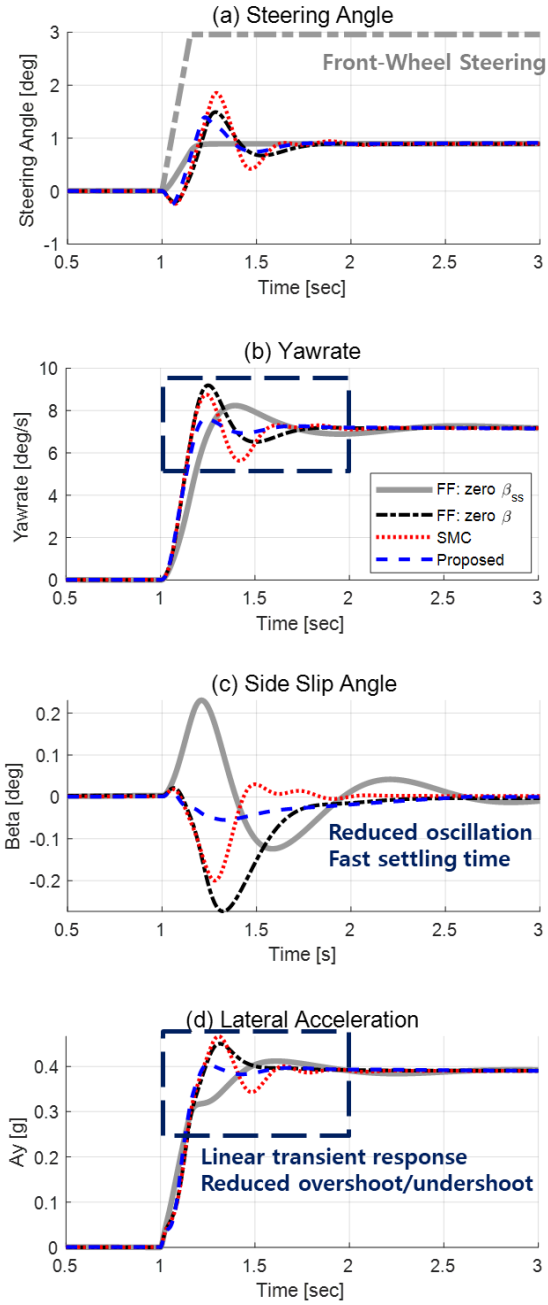

Figure 6.14. Comparison with conventional methods: step steer @ 110kph, dry asphalt.

6.3. Effect on Vehicle Lateral Stability

In this chapter, we verify whether the proposed RWS algorithm set up for the step steer scenario of high friction road shows robust performance for other road friction conditions and steering scenarios. Also, check how the integrated control with ESC and RWS improves performance compared to individual independent control.

6.3.1. Individual Rear-Wheel Steering Control

The proposed control algorithm has been simulated to verify whether it performs well for the sine with dwell scenario (Administration, 2007). The steering input is configured as 0.4 g/0.8 g Ay level in the first peak. This is based-on ISO-19365 (sine wave of 0.7 Hz frequency, 500 ms delay at the dwelling zone). The performance test is conducted with the previously set η and K_{fb}. This result comparison was conducted for the following four controlled vehicles: base, feedforward, sliding mode control, and proposed control. The purpose of this section is to identify the effect of RWS intervention and transient controller on vehicle stability.

Figure 6.15 shows the simulation results for the sine dwell test with Ay 0.4 g level. The vehicle speed is 110 kph, and SWA for a 0.4g level of Ay requires about 25 deg for the base vehicle and about 45 deg for the RWS vehicles. Figure

6.15 (b) shows that the proposed algorithm has a linearity yaw rate response to the driver's steering input in the dwelling area (2.5 s - 4 s). The proposed algorithm then shows a quick convergence and a smaller overshoot compared to other vehicles. Comparing the side slip angle in Figure 6.15 (c), one sees that the proposed algorithm significantly reduces below 0.09 deg while the base vehicle produces a side slip angle of up to 1.2 deg; the feedforward controller produces a value up to 0.24 deg; the sliding mode controller produces a value up to 0.15deg. Additionally, the proposed algorithm has the smallest rate of change in the side slip angle. This can be seen in the graphs of yaw rate and lateral acceleration. The proposed algorithm shows that the first peak time of yaw rate and lateral acceleration are almost the same, while the base and feedforward control have a time gap. This result is explained by the effect of the feedback control in (5.10).

Figure 6.16 represents the simulation results for the sine dwell test at Ay 0.8g level where the base vehicle spins out. The vehicle speed is 110 kph and SWA for 0.8g level of Ay requires about 55 deg for the base vehicle and about 100 deg for RWS vehicles. For a mild maneuver (Ay 0.4g level), the proposed algorithm has a similar performance in limit handling maneuver (Ay 0.8g level). Thus, it can be seen that the proposed algorithm, tuned to emulate the optimal control to minimize side slip angle for step steer, performs the control objective well for other steering inputs.

The robustness of the proposed RWS algorithm has been investigated for low tire-road friction cases. In contrast to the results in chapter 6.1, where the RWS controlled vehicle performs the optimal performance on high friction roads

(μ=1), this section shows what happens to RWS performance when the road surface condition is changed to low friction roads (μ=0.3). The performance of the proposed RWS control algorithm has been compared to the base vehicle and the conventional RWS controller. The simulation was conducted to investigate the performance of the proposed algorithm for the following scenarios: step steer (45 deg, 300 deg/s) and sine with dwell (0.3g level of the first peak Ay).

Figure 6.17 illustrates the performance changes of RWS controllers when driving on a low friction road. The base vehicle spins out and has a loss of stability. In the case of the conventional controllers tuned on high friction roads, the vehicles also spin out and lose its stability. In the case of the proposed algorithm, the algorithm tuned on dry asphalt has a 0.5 deg offset in side slip angle, but it converges fast. Versus the dry asphalt results (Figure 6.3 – 6.5), the proposed algorithm has the following features: slightly increased overshoot (7.4% to 10.5%) and peak response time (0.26 s to 0.28 s); this is superior to other controllers. In terms of lateral acceleration, the proposed algorithm maintains the linear shape response in the transition area, while the feedforward control has a nonlinear shape.

Figure 6.18 shows the results of sine with dwell scenario on the icy asphalt driving condition. The base vehicle and the conventional controllers (feedforward, sliding mode control) tuned on high friction roads lead to spin out and loss of lateral stability. The proposed RWS algorithm does not diverge. Compared to dry asphalt results (Figure 6.15 – 6.16), the RWS input of the proposed algorithm on the low friction road differs remarkably from RWS input of the conventional controllers.

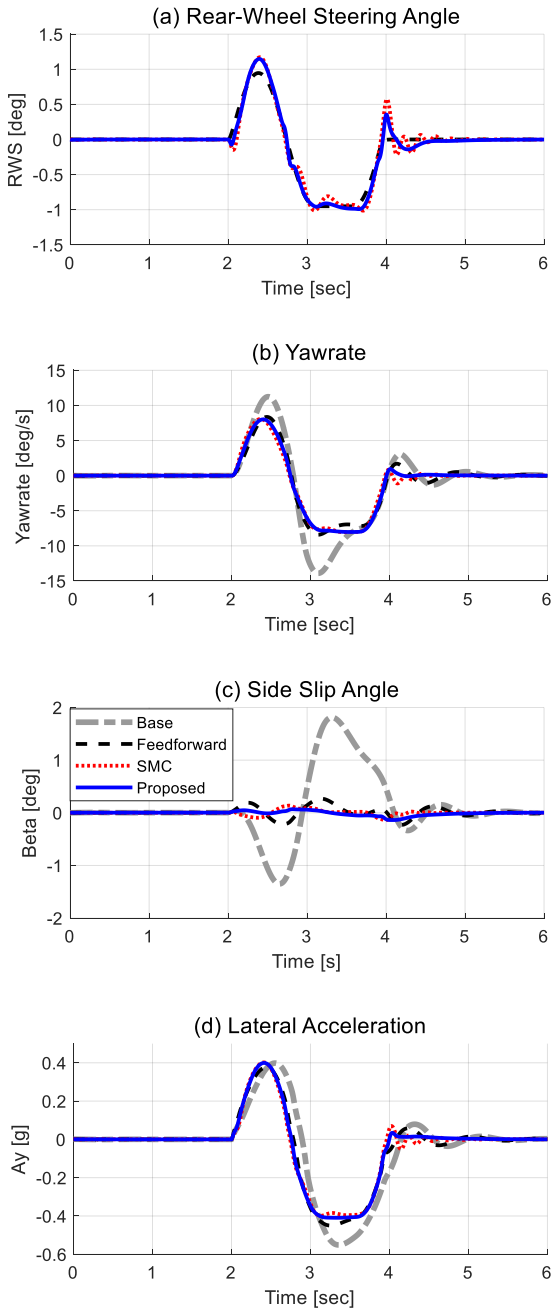

Figure 6.15. Result of sine with dwell test at 110 kph, Peak Ay 0.4g, dry asphalt, with $k_\delta = 0.357$, $\eta = 0.8$, $K_{fb} = 0.016$.

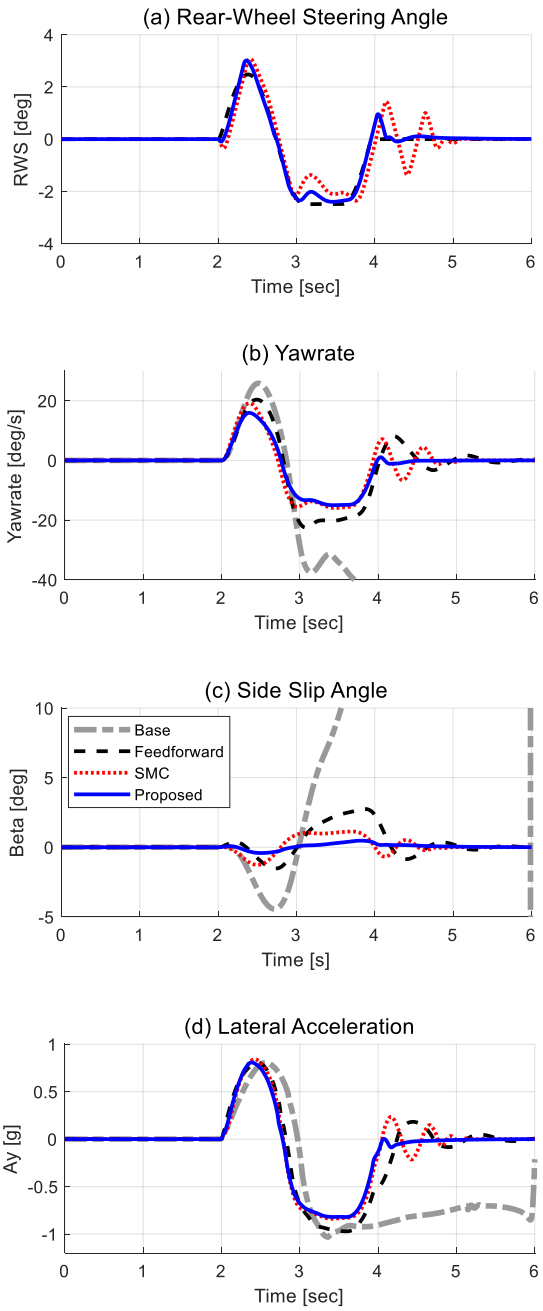

Figure 6.16. Result of sine with dwell test at 110 kph, Peak Ay 0.8g, dry asphalt, with $k_\delta = 0.357$, $\eta = 0.8$, $K_{fb} = 0.016$.

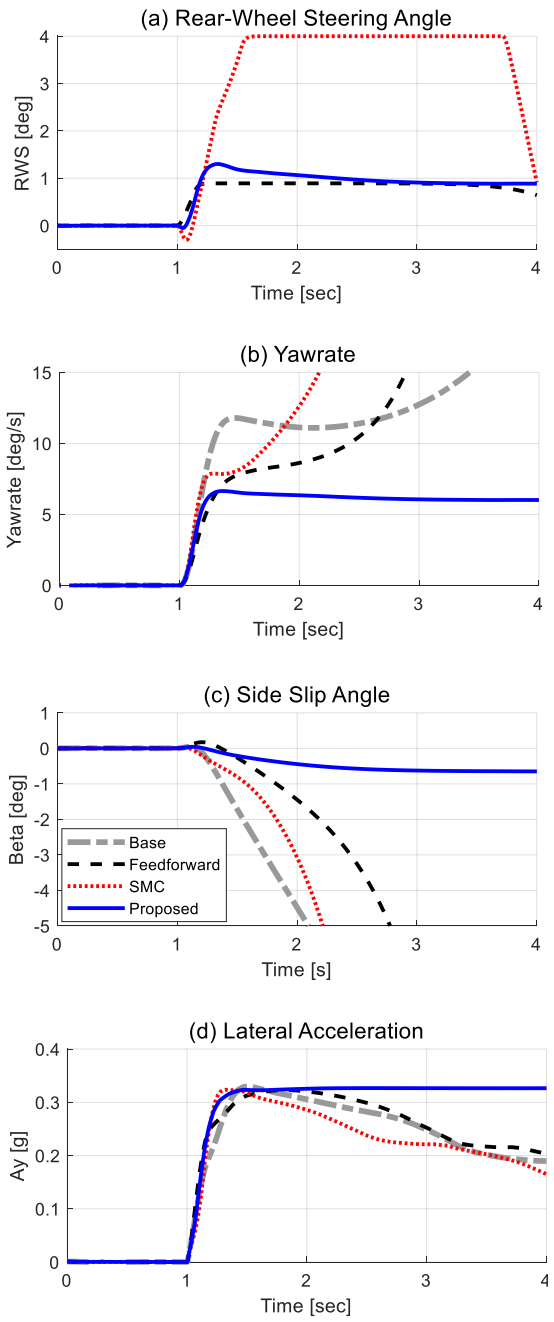

Figure 6.17. Step steer at 110 kph, 45deg(300deg/s), icy asphalt, with $k_\delta = 0.357$, $\eta = 0.8$, $K_{fb} = 0.016$.

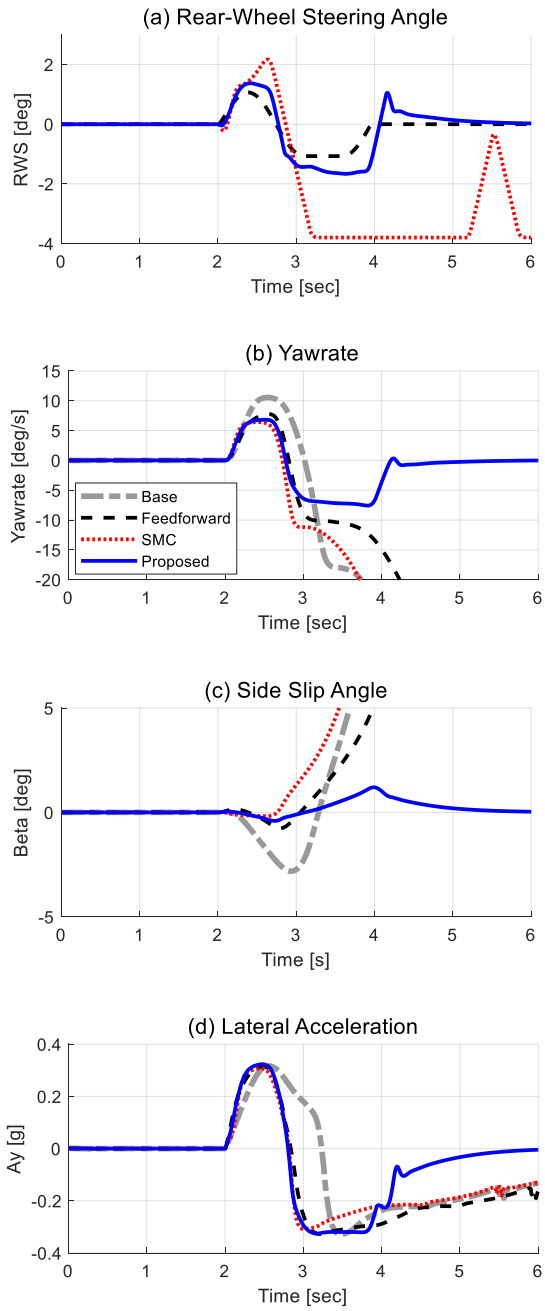

Figure 6.18. Sine with dwell test at 110 kph, Peak Ay 0.3g, icy asphalt, with $k_\delta = 0.357$, $\eta = 0.8$, $K_{fb} = 0.016$.

6.3.2. Integrated with Electronic Stability Control

This chapter validates how the integrated chassis control of the proposed RWS and ESC algorithm improve vehicle lateral stability. Compared to the proposed RWS logic and independent control with RWS/ESC, performance is analyzed in terms of vehicle states and actuator interventions.

The scenario for evaluating vehicle stability control performance is the sine with dwell test based on ISO-19365, and is conducted with a steering input of 120deg and 0.7Hz.

Under the dry asphalt conditions, the initial vehicle speed is 125kph and zero throttle (without stepping on the excel pedal), and as a result of the simulation, it is a limit handling scenario with a lateral acceleration of up to 0.9g level. By comparing the vehicle states of the stability control simulation conducted on the high friction road, it can be seen that the vehicle sideslip angle decreases and the settling time of yaw rate is slightly improved as the ESC intervention is performed rather than the rear-wheel steering control. Comparing the actuator intervention in the same situation, it can be seen that the amount of brake usage decreases in realizing the similar performance of the integrated control than the independent control of RWS/ESC. As a result, it can be seen that the proper reduction of vehicle speed has an advantage in improving the escape speed.

Under the wet asphalt conditions, the initial vehicle speed is 100kph and zero throttle (without stepping on the excel pedal), and as a result of the simulation, it is a limit handling scenario with a lateral acceleration of up to 0.65g level. In

the vehicle states results of Figure 6.21, it can be shown that the proposed rear-wheel steering loses lateral stability against changes in road surface friction, while the stability is ensured by adding ESC. In addition, when comparing the independent control and integrated control, the integrated control improves in yaw rate settling time, and reduces the sideslip angle from 7.5deg to 5.5deg, and increases the escape speed. At the same time, in terms of actuator operation of Figure 6.22, the rear-wheel steering is limited to 4deg, which is the actuator constraint, in the case of RWS only and independent control with ESC. As a result, RWS cannot ensure the stability. So, brake intervention of ESC is strongly required. On the other hand, the integrated control, which is considering the effect of RWS intervention, decreases the total required brake usage, and does not saturate RWS. So, it can be seen that the actuator efficiency has increased.

Figure 6.23 shows the results of comparing vehicle stability performance against road surface condition changes; from base vehicle (without any chassis control module) to the proposed integrated chassis control system with ESC/RWS. The stability performance is expressed by measuring the maximum lateral acceleration and vehicle speed within the range of the maximum sideslip angle not exceeding 8deg. Based on the strong stability performance of the proposed RWS control algorithm, it can be shown that the vehicle lateral stability is improved by integrating with ESC against the road condition changes.

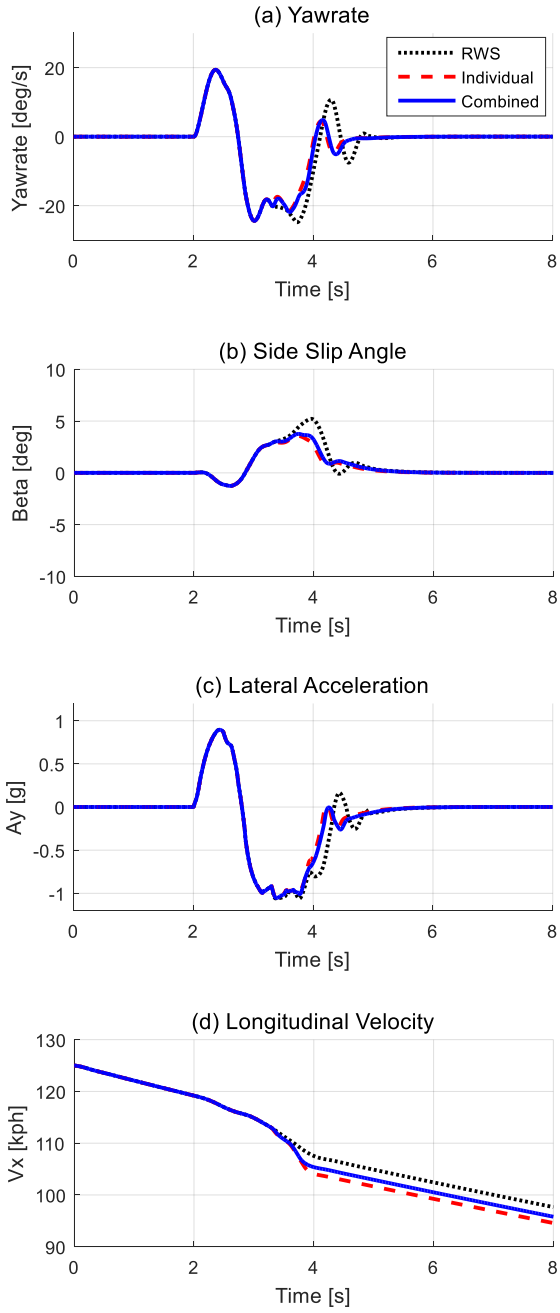

Figure 6.19. Vehicle states of Sine with dwell test at 125 kph, Peak Ay 0.9g, dry asphalt.

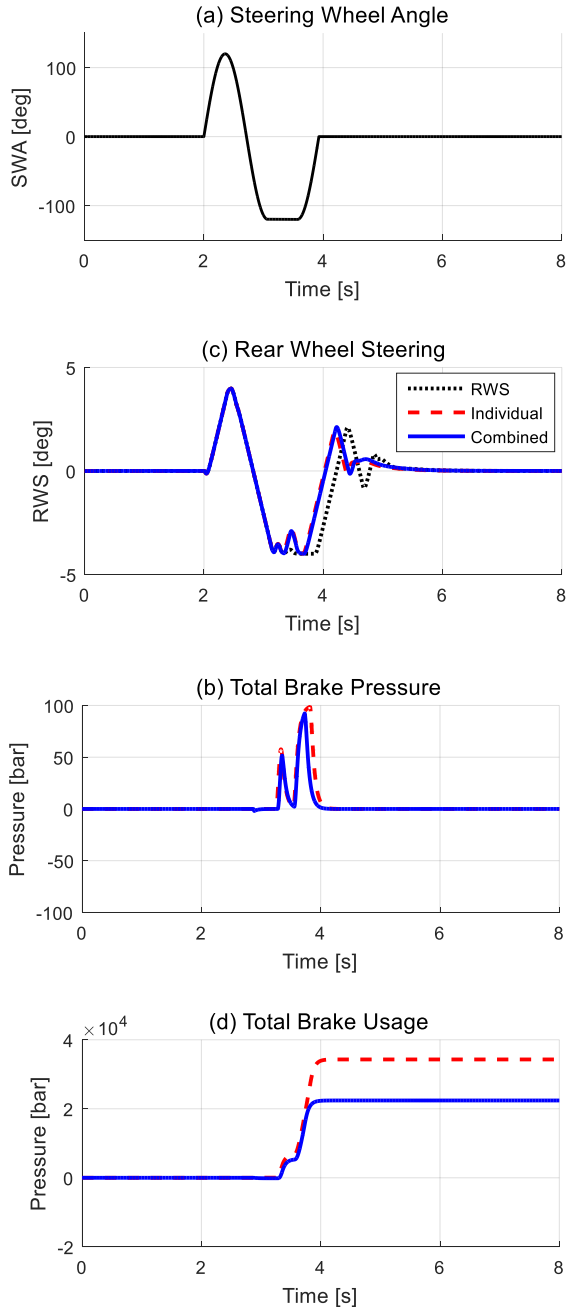

Figure 6.20. Actuator intervention of Sine with dwell test at 125 kph, Peak Ay 0.9g, dry asphalt.

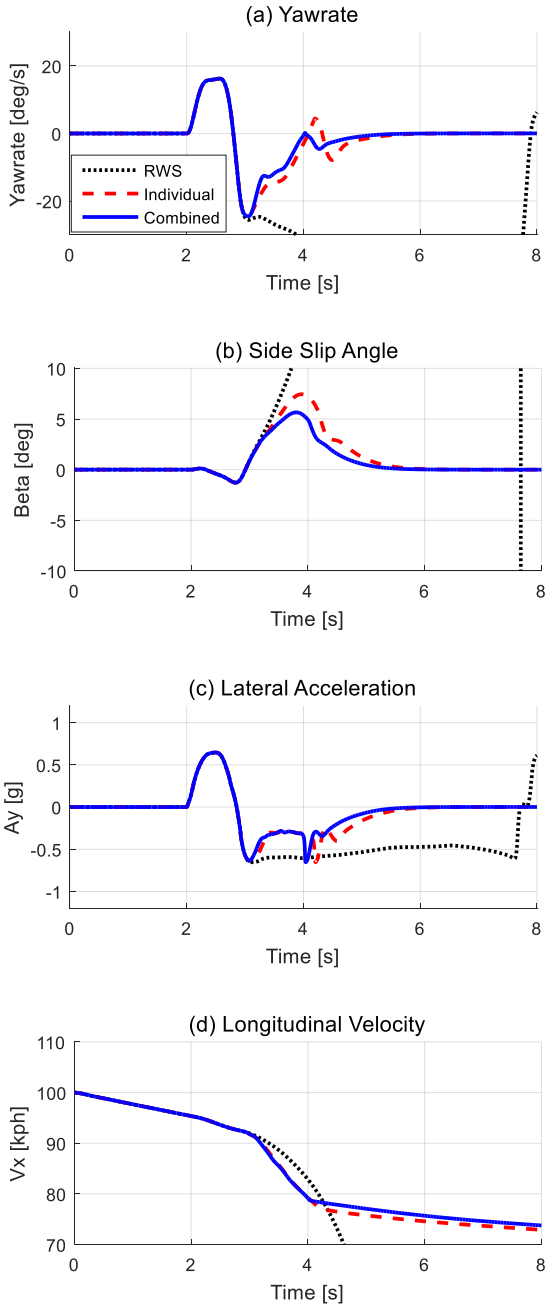

Figure 6.21. Vehicle states of Sine with dwell test at 100 kph, Peak Ay 0.65g, wet asphalt.

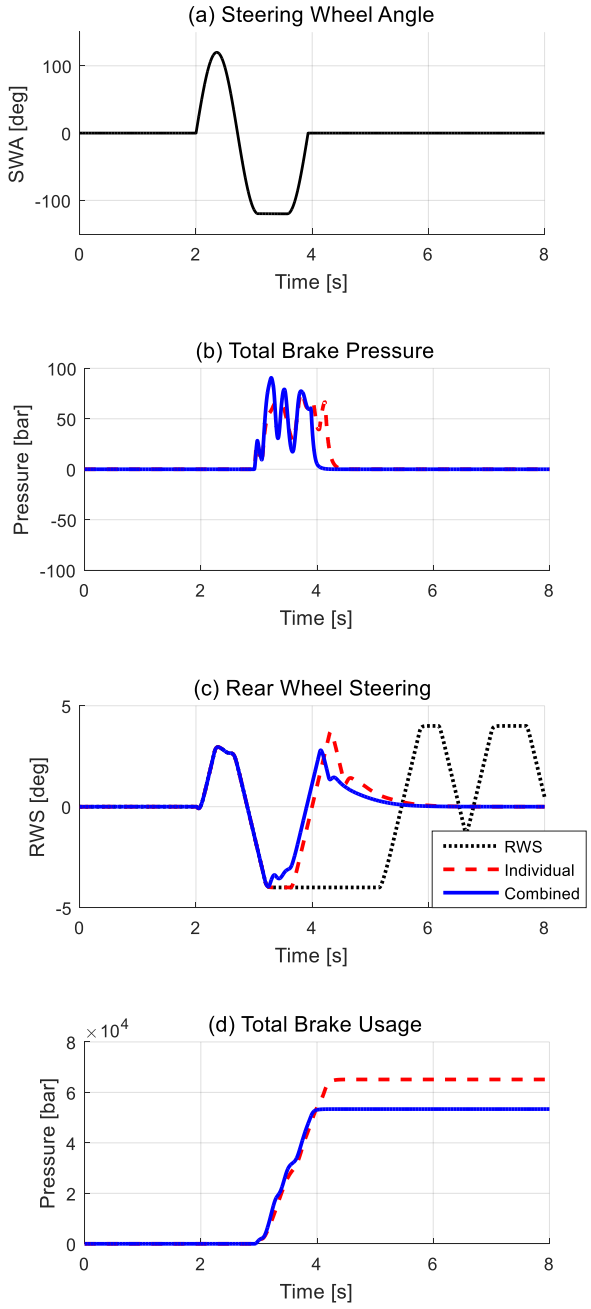

Figure 6.22. Actuator intervention of Sine with dwell test at 100 kph, Peak Ay 0.65g, wet asphalt.

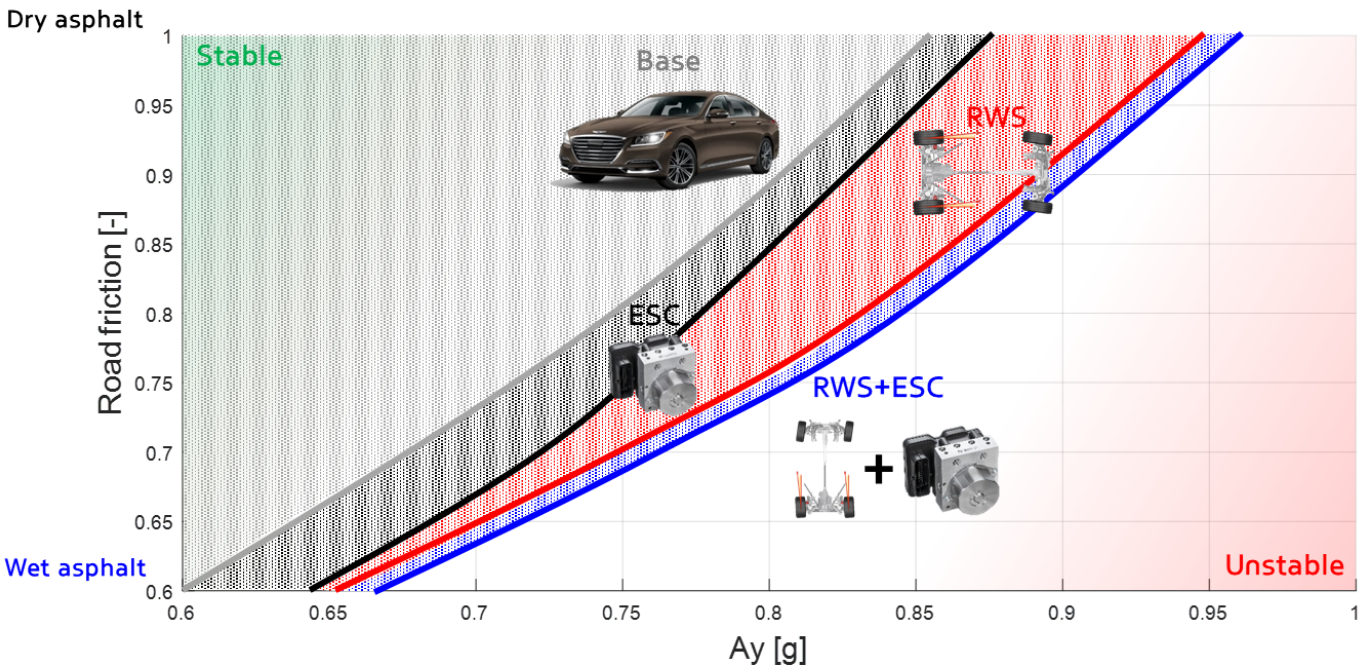
Dry asphalt
Stable
Base
RWS
ESC
RWS+ESC
Unstable
Wet asphalt
Road friction [-]
Ay [g]
1
0.95
0.9
0.85
0.8
0.75
0.7
0.65
0.6
0.6
0.65
0.7
0.75
0.8
0.85
0.9
0.95
1

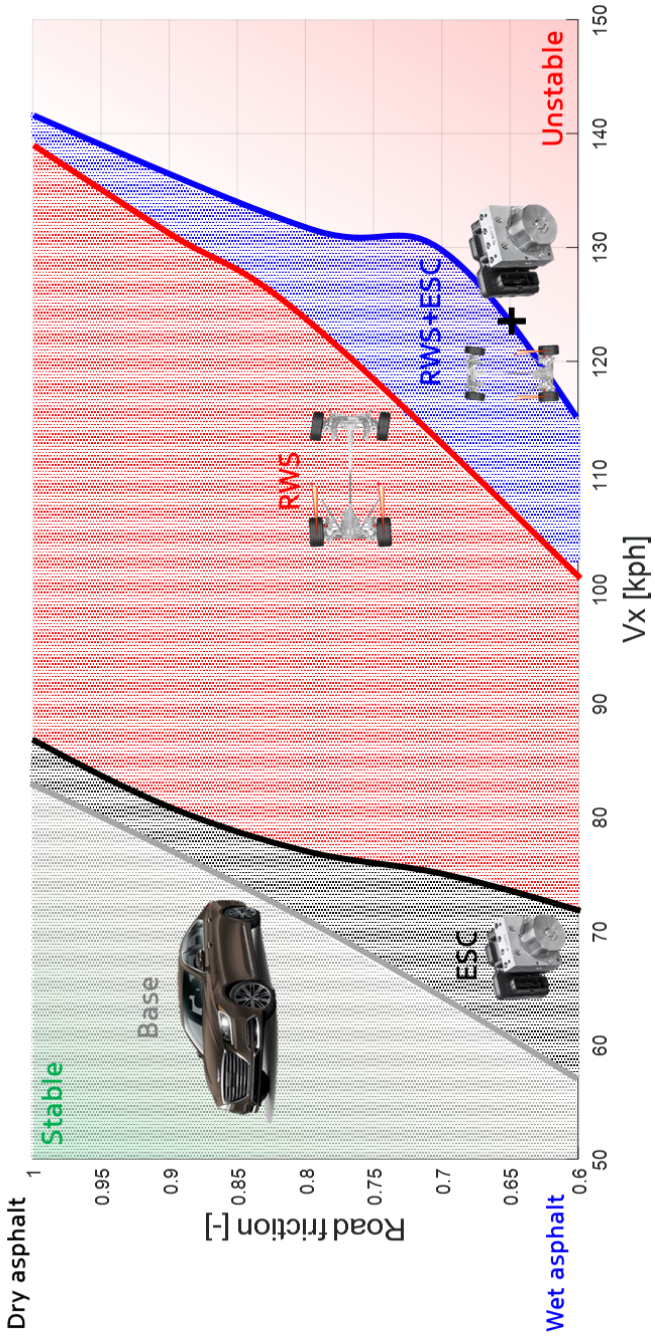

Figure 6.23. Comparison of stability performance against changes in road surface and driving conditions

Chapter 7

Conclusion and Future Work

A new rear-wheel steering control method to enhance the vehicle handling characteristics without any information on tire characteristics parameters has been presented. The proposed algorithm consists of the steady-state and transient control input. The steady-state control input is proportional to the driver's front-wheel steering. The proportional gain is pre-determined as a function of vehicle speed using the offline optimization results, which is designed to minimize sideslip angle. The transient control input enhances the lateral transient response of the vehicle's yaw rate and lateral acceleration, and is designed as a combination of the feedforward and feedback inputs. In the feedforward input, a new feedforward gain is introduced to shape the transient response of vehicle's yaw rate. The feedback input significantly reduces the yaw rate overshoot via the first- time derivative of the vehicle side slip angle.

Computer simulations were used to evaluate the proposed control algorithm and were compared with three different control systems: (1) base (passive)

vehicle; (2) proportional RWS system with the pre-determined rear-to-front steering ratio that is a function of the vehicle speed; and (3) optimal RWS system obtained by offline numerical optimization. The simulation results show that the proposed algorithm nicely emulates the optimal handling performance for step steer scenarios without any information on tire parameters. Moreover, compared to the conventional RWS control algorithms, the proposed control algorithm shows superior performance in the vehicle's lateral stability and maneuverability even under various steering and road surface conditions.

Since the proposed RWS control algorithm exhibits good performance at the simulation level, rear-wheel steering control algorithm for the target vehicle could be developed via a real-time software tool. Real-time implementation and vehicle tests for the evaluation of this algorithm are the topics of our future research.

Bibliography

Abe, M. (1999). Vehicle dynamics and control for improving handling and active safety: from four-wheel steering to direct yaw moment control. *Proceedings of the Institution of Mechanical Engineers, Part K: Journal of Multi-body Dynamics, 213*(2), 87-101.

Abe, M. (2015). *Vehicle handling dynamics: theory and application*: Butterworth-Heinemann.

Abe, M., Ohkubo, N., & Kano, Y. (1996). A direct yaw moment control for improving limit performance of vehicle handling-comparison and cooperation with 4WS. *Vehicle System Dynamics, 25*(S1), 3-23.

Ackermann, J., & Sienel, W. (1993). Robust yaw damping of cars with front and rear wheel steering. *IEEE Transactions on Control Systems Technology, 1*(1), 15-20.

Administration, N. H. T. S. (2007). Federal motor vehicle safety standards; electronic stability control systems; controls and displays. *Federal Rule, FMVSS, 126*.

Akar, M. (2006). *Yaw rate and sideslip tracking for 4-wheel steering cars using sliding mode control.* Paper presented at the 2006 IEEE Conference on Computer Aided Control System Design, 2006 IEEE International Conference on Control Applications, 2006 IEEE International Symposium on Intelligent Control.

Akita, M. (2019). *The chassis of the all-new LS/LC–Lexus luxury prestige Sedan/Coupé.* Paper presented at the 9th International Munich Chassis Symposium 2018.

Bedner, E., Fulk, D., & Hac, A. (2007). *Exploring the trade-off of handling stability and responsiveness with advanced control systems* (0148-7191). Retrieved from

Bredthauer, L., & Lynch, D. (2018). *Use of Active Rear Steering to Achieve Desired Vehicle Transient Lateral Dynamics* (0148-7191). Retrieved from

Byrnes, C. I., Gilliam, D. S., & He, J. (1994). Root-locus and boundary feedback design for a class of distributed parameter systems. *SIAM journal on control and optimization, 32*(5), 1364-1427.

Byrnes, C. I., Isidori, A., & Willems, J. C. (1991). Passivity, feedback equivalence, and the global stabilization of minimum phase nonlinear systems. *IEEE Transactions on Automatic Control, 36*(11), 1228-1240.

Cho, Y. H., & Kim, J. (1995). Design of optimal four-wheel steering system. *Vehicle System Dynamics, 24*(9), 661-682.

Dai, L., & Han, Q. (2004). Stability and Hopf bifurcation of a nonlinear model for a four-wheel-steering vehicle system. *Communications in Nonlinear Science and Numerical Simulation, 9*(3), 331-341.

Eguchi, T. (1991). Rear wheel steering control system for vehicle. In: Google Patents.

Eguchi, T., Sakita, Y., Kawagoe, K., Kaneko, S., Mori, K., & Matsumoto, T. (1989). Development of" Super Hicas", a New Rear Wheel Steering System with Phasereversal Control. *SAE transactions, 98*, 1495-1504.

Fetrati, S. R., Kandler, C., Kärcher, C., & Schramm, D. (2016). Inversion based feedforward design to improve the lateral dynamics of high performance sports cars. In *Advanced Vehicle Control* (pp. 625-629): CRC Press.

Furukawa, Y., Yuhara, N., Sano, S., Takeda, H., & Matsushita, Y. (1989). A review of four-wheel steering studies from the viewpoint of vehicle dynamics and control. *Vehicle System Dynamics, 18*(1-3), 151-186.

Gottmann, F., Böhm, M., & Sawodny, O. (2017). *Integrated trajectory and path tracking of under-actuated and over-actuated cars up to the handling limits.* Paper presented at the 2017 American Control Conference (ACC).

Gu, G., Chen, X., Sparks, A. G., & Banda, S. S. (1999). Bifurcation stabilization with local output feedback. *SIAM journal on control and optimization, 37*(3), 934-956.

Harada, H. (1995). Control strategy of active rear wheel steering in consideration of system delay and dead times. *JSAE review, 16*(2), 171-177.

Harrer, M., Görich, H.-J., Reuter, U., & Wahl, G. (2013). 50 Years of the Porsche 911 Optimisation of Chassis Control and Brake Systems. *ATZ worldwide, 115*(12), 14-19.

Her, H., Koh, Y., Joa, E., Yi, K., & Kim, K. (2015). An integrated control of differential braking, front/rear traction, and active roll moment for limit handling performance. *IEEE Transactions on Vehicular Technology, 65*(6), 4288-4300.

Irie, N., & Kuroki, J. (1990). *4WS technology and the prospects for improvement of vehicle dynamics* (0148-7191). Retrieved from

Joa, E., Yi, K., Sohn, K., & Bae, H. (2018). Four-wheel independent brake control to limit tire slip under unknown road conditions. *Control Engineering Practice, 76*, 79-95.

Jones, E. W. (1989). Adjustable, proportionally steerable auxiliary wheel asemblies for trucks. In: Google Patents.

Lee, A. (1995). Performance of four-wheel-steering vehicles in lane change maneuvers.

Lee, S.-H., Lee, U.-K., Ha, S.-K., & Han, C.-S. (1999). Four-wheel independent steering (4WIS) system for vehicle handling improvement by active rear toe control. *JSME International Journal Series C Mechanical Systems, Machine Elements and Manufacturing, 42*(4), 947-956.

Liberzon, D., Morse, A. S., & Sontag, E. D. (2002). Output-input stability and minimum-phase nonlinear systems. *IEEE Transactions on Automatic Control, 47*(3), 422-436.

Lv, H., Chen, N., & Li, P. (2004). Multi-objective H^{∞} optimal control for four-wheel steering vehicle based on yaw rate tracking. *Proceedings of the Institution of Mechanical Engineers, Part D: Journal of Automobile Engineering, 218*(10), 1117-1123.

Manning, W., & Crolla, D. (2007). A review of yaw rate and sideslip controllers for passenger vehicles. *Transactions of the Institute of Measurement and Control, 29*(2), 117-135.

Marino, R., Scalzi, S., & Cinili, F. (2007). Nonlinear PI front and rear steering control in four wheel steering vehicles. *Vehicle System Dynamics, 45*(12), 1149-1168.

Miki, K., Sumi, K., Fukui, K., Hayashi, Y., & Ishiguro, M. (1988). Apparatus for controlling steer angle of rear wheels of vehicle. In: Google Patents.

Moiola, J. L., Colantonio, M. C., & Doñate, P. D. (1997). Analysis of static and dynamic bifurcations from a feedback systems perspective. *Dynamics and Stability of Systems*, *12*(4), 293-317.

Montani, M., Favilli, T., Berzi, L., Capitani, R., Pierini, M., Pugi, L., & Annicchiarico, C. (2020). *ESC on In-Wheel Motors Driven Electric Vehicle: Handling and Stability Performances Assessment.* Paper presented at the 2020 IEEE International Conference on Environment and Electrical Engineering and 2020 IEEE Industrial and Commercial Power Systems Europe (EEEIC/I&CPS Europe).

Mori, K. (1993). Rear wheel steering system for automotive vehicle. In: Google Patents.

Nagai, M., Hirano, Y., & Yamanaka, S. (1997). Integrated control of active rear wheel steering and direct yaw moment control. *Vehicle System Dynamics*, *27*(5-6), 357-370.

Nah, J., & Yim, S. (2019). Optimization of control allocation with ESC, AFS, ARS and TVD in integrated chassis control. *Journal of Mechanical Science and Technology*, *33*(6), 2941-2948.

Ogaji, S., Sampath, S., Singh, R., & Probert, S. (2002). Parameter selection for diagnosing a gas-turbine's performance-deterioration. *Applied Energy*, *73*(1), 25-46.

Ogata, K., & Yang, Y. (2002). *Modern control engineering* (Vol. 4): Prentice hall India.

Ono, E., Hosoe, S., Tuan, H. D., & Doi, S. i. (1996). *Robust stabilization of vehicle dynamics by active front wheel steering control.* Paper presented at the Proceedings of 35th IEEE Conference on Decision and Control.

Pacejka, H., & Besselink, I. (1997). Magic formula tyre model with transient properties. *Vehicle System Dynamics*, *27*(S1), 234-249.

Pacejka, H. B., & Bakker, E. (1992). The magic formula tyre model. *Vehicle System Dynamics*, *21*(S1), 1-18.

Patterson, M. A., & Rao, A. V. (2014). GPOPS-II: A MATLAB software for solving multiple-phase optimal control problems using hp-adaptive Gaussian quadrature collocation methods and sparse nonlinear programming. *ACM Transactions on Mathematical Software (TOMS), 41*(1), 1-37.

Peng, J., He, H., & Feng, N. (2013). Simulation research on an electric vehicle chassis system based on a collaborative control system. *Energies, 6*(1), 312-328.

Phillips, C. L., & Habor, R. D. (1995). *Feedback control systems*: Simon & Schuster, Inc.

Qiu, L., & Davison, E. J. (1993). Performance limitations of non-minimum phase systems in the servomechanism problem. *Automatica, 29*(2), 337-349.

Rajamani, R. (2011). *Vehicle dynamics and control*: Springer Science & Business Media.

Rasof, B. (1962). The initial-and final-value theorems in Laplace transform theory. *Journal of the Franklin Institute, 274*(3), 165-177.

Rill, G. (2006). *First order tire dynamics.* Paper presented at the Proceedings of the III European Conference on Computational Mechanics Solids, Structures and Coupled Problems in Engineering, Lisbon, Portugal.

Rissanen, J. (1966). Performance deterioration of optimum systems. *IEEE Transactions on Automatic Control, 11*(3), 530-532.

Russell, H. E., & Gerdes, J. C. (2015). Design of variable vehicle handling characteristics using four-wheel steer-by-wire. *IEEE Transactions on Control Systems Technology, 24*(5), 1529-1540.

Sano, S., Furukawa, Y., & Shiraishi, S. (1986). *Four Wheel Steering System with Rear Wheel Steer Angle Controlled as a Function of Steering Wheel Angle* (0148-7191). Retrieved from

Schäfer, P., Wahl, G., & Harrer, M. (2012). The chassis of the Porsche 911. *ATZ worldwide, 114*(6), 4-8.

Schuller, J., Haque, I., & Eckel, M. (2002). An approach for optimisation of vehicle handling behaviour in simulation. *Vehicle System Dynamics, 37*(sup1), 24-37.

Setiawan, J. D., Safarudin, M., & Singh, A. (2009). *Modeling, simulation and validation of 14 DOF full vehicle model.* Paper presented at the International Conference on Instrumentation, Communication, Information Technology, and Biomedical Engineering 2009.

Sivaramakrishnan, S., & Taheri, S. (2013). Using Objective Vehicle-Handling Metrics for Tire Performance Evaluation and Selection. *SAE International Journal of Passenger Cars-Mechanical Systems, 6*(2013-01-0743), 732-740.

Smith, E., Tavernini, D., Claret, C., Velenis, E., & Cao, D. (2016). *Optimal yaw-rate target for electric vehicle torque vectoring system.* Paper presented at the The Dynamics of Vehicles on Roads and Tracks: Proceedings of the 24th Symposium of the International Association for Vehicle System Dynamics (IAVSD 2015), Graz, Austria, 17-21 August 2015.

Song, J. G., & Yoon, Y. S. (1998). Feedback control of four–wheel steering using time delay control. *International Journal of Vehicle Design, 19*(3), 282-298.

Tanelli, M., Savaresi, S. M., & Cantoni, C. (2006). *Longitudinal vehicle speed estimation for traction and braking control systems.* Paper presented at the 2006 IEEE Conference on Computer Aided Control System Design, 2006 IEEE International Conference on Control Applications, 2006 IEEE International Symposium on Intelligent Control.

Treichel, A. (2016). Model Archive for BMW models· The new BMW Alpina B7 Bi-Turbo· Monday, 8th February 2016· bmwarchive. org.

Uys, P., Els, P., & Thoresson, M. (2006). Criteria for handling measurement. *Journal of Terramechanics, 43*(1), 43-67.

Wagner, S., Schilling, J., Braun, J., & Prokop, G. (2017). Design and assessment of optimal feedforward control for active steering configurations in passenger vehicles. *Vehicle System Dynamics, 55*(8), 1123-1142.

Wagner, S., Weiskircher, T., Ammon, D., & Prokop, G. (2018). Pivot point-based control for active rear-wheel steering in passenger vehicles. *Vehicle System Dynamics, 56*(8), 1139-1161.

Wang, J.-S., Zhang, Y., & Wang, W. (2006). Optimal design of PI/PD controller for non-minimum phase system. *Transactions of the Institute of Measurement and Control, 28*(1), 27-35.

Wang, X. F., Chen, G., & Man, K. F. (2001). Making a continuous-time minimum-phase system chaotic by using time-delay feedback. *IEEE Transactions on Circuits and Systems I: Fundamental Theory and Applications, 48*(5), 641-645.

Wimmer, M., Meurle, J., Sacher, H., & Siedersberger, K.-H. (2015). Motor vehicle having a driver assistance device and method for operating a motor vehicle. In: Google Patents.

Xu, X., Chen, D., Zhang, L., & Chen, N. (2019). Hopf bifurcation characteristics of the vehicle with rear axle compliance steering. *Shock and Vibration, 2019*.

Yim, S. (2015). Coordinated control with electronic stability control and active steering devices. *Journal of Mechanical Science and Technology, 29*(12), 5409-5416.

Yim, S. (2020). Comparison among Active Front, Front Independent, 4-Wheel and 4-Wheel Independent Steering Systems for Vehicle Stability Control. *Electronics, 9*(5), 798.

Yim, S., Kim, S., & Yun, H. (2016). Coordinated control with electronic stability control and active front steering using the optimum yaw moment distribution under a lateral force constraint on the active front steering. *Proceedings of the Institution of Mechanical Engineers, Part D: Journal of Automobile Engineering, 230*(5), 581-592.

Zarco, P., & Exposito, A. G. (2000). Power system parameter estimation: a survey. *IEEE Transactions on power systems, 15*(1), 216-222.

Zhang, B., Khajepour, A., & Goodarzi, A. (2017). Vehicle yaw stability control using active rear steering: Development and experimental validation. *Proceedings of the Institution of Mechanical Engineers, Part K: Journal of Multi-body Dynamics, 231*(2), 333-345.

Zhao, J., Wong, P. K., Ma, X., & Xie, Z. (2017). Chassis integrated control for active suspension, active front steering and direct yaw moment systems using hierarchical strategy. *Vehicle System Dynamics, 55*(1), 72-103.

Zhao, S.-e., Li, Y., & Qu, X. (2014). Vehicle chassis integrated control based on multimodel and multilevel hierarchical control. *Mathematical Problems in Engineering, 2014*.

Zheng, B., & Anwar, S. (2009). Yaw stability control of a steer-by-wire equipped vehicle via active front wheel steering. *Mechatronics, 19*(6), 799-804.

초 록

차량 조종성과 횡방향 안정성 향상을 위한 타이어-노면 정보 독립적 후륜 조향 제어

후륜조향 시스템은 차량의 핸들링 성능과 안정성 향상을 목표로 지난 몇 십년간 개발되었다. 후륜의 직접적인 조향을 통해 후방 타이어의 횡력에 영향을 주며, 이는 차량의 도심주행 상황과 고속도로 주행 상황에서 모두 이점을 가져다준다. 좁은 골목과 같은 도심 주행 상황에서는 전륜과 반대방향으로 후륜조향을 입력함으로써 차량을 보다 민첩한 거동이 가능하게 한다. 고속도로 주행 상황에서는 전륜과 같은 방향으로 후륜조향을 입력함으로써 차량의 횡방향 안정성을 향상시킨다.

후륜조향 시스템은 목표 거동을 추종하기 위한 모델 기반 제어로 설계되는 것이 일반적이다. 하지만, 실제 차량 적용에 있어서 타이어 모델에 필요한 타이어-노면 마찰 계수와 강성 계수를 정확히 알아내는 것은 어려운 일이다. 위와 같은 이유로, 본 논문에서는 어떠한 타이어-노면 정보도 사용하지 않고 측정 가능한 센서 신호만을 이용하여 설계된 후륜조향 제어 알고리즘을 제안한다.

먼저 3D 차량 모델에 대한 오프라인 수치 최적화를 진행함으로써, 후륜조향 시스템이 탑재된 차량의 횡거동을 분석하고 물리적 통찰력을 얻는다. 이렇게 얻어진 최적화 결과를 매개변수화하여 제어에 직접적으로 반영하였다.

제안된 후륜조향 제어 알고리즘은 정상상태영역과 과도영역에서의 핸들링 특성을 향상시키는데 목적을 둔 제어 입력의 합으로써 설계되었다. 우선, 정상상태 영역에서의 후륜조향 제어 입력은 목표 요레이트 게인을 얻기 위해 운전자의 조향 입력에 비례하는 형태로 설계되었다. 목표 요레이트 게인은 오프라인 최적화를 통해 얻어진 차량의 요레이트 반응이다. 저속에서는 전륜조향과 반대 방향으로 조향됨으로써 요레이트 게인을 증가시켜 차량 민첩성을 향상시킨다. 고속에서는 전륜조향과 같은 방향으로 조향됨으로써 요레이트 게인을 감소시켜 차량의 안정성을 향상시킨다. 과도 영역에서의 후륜조향 제어 입력은 타이어 관한 어떠한 사전 정보를 요구하지 않고 차량의 횡방향 과도 반응을 조정할 수 있도록 설계되었다. 그러한 과도 제어 입력을 설계하기 위해, 타이어 모델 파라미터를 대체하여 과도 반응을 조정할 수 있는 새로운 설계 파라미터를 고안하여 피드포워드 제어 입력을 설계하였다. 이와 함께, 요레이트의 오버슈트와 반응 시간이 가지는 트레이드 오프 관계를 보완하기 위해 요레이트 댐핑 계수를 높여주는 효과를 가지는 피드백 제어 입력을 추가 고안함으로써 최종 후륜조향 제어 알고리즘을 구성하였다.

제안된 후륜조향 제어 알고리즘의 성능은 다양한 시나리오에서

시뮬레이션을 통해 검증되었다. 운전자의 의도가 개입되지 않는 상황에서의 차량 성능을 정량화하여 비교하기 위해 ISO에 기반한 개루프 조향 시나리오를 사용한 시뮬레이션이 수행되었다. 제어 성능의 정량화를 위한 객관적 지표를 선정하여, 오프라인 최적화 결과와 비교를 통해 성능 평가가 이루어졌으며 타이어-노면 마찰과 관련한 계수 정보없이 최적 성능을 잘 모방할 수 있음을 확인하였다. 또한, 차량 안정성 확인을 위해 저마찰로에서 동일한 조건의 시뮬레이션을 수행하였다. 이를 통해, 제안된 후륜조향 제어 알고리즘이 타이어 모델 정보없이 기존의 제어 알고리즘에 비해 차량 횡방향 안정성과 조종성을 향상시킬 수 있는 실용적인 방법임이 검증되었다.

주요어: 후륜조향 제어, 차량 핸들링 성능, 차량 조종성, 횡방향 안정성, 횡방향 과도 반응, 오프라인 수치 최적화, 매개변수화, 성능 평가

학 번: 2017-35813